PURDUE UNIVERSITY
SCHOOL OF AERONAUTICS AND ASTRONAUTICS

A FEASIBILITY STUDY REGARDING THE ADDITION OF A FIFTH CONTROL TO A ROTORCRAFT IN-FLIGHT SIMULATOR

by

Simon Turner and Dominick Andrisani, II

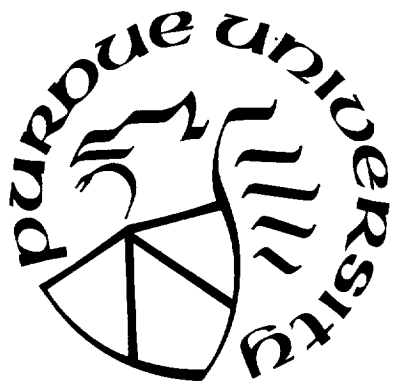

1282 Grissom Hall
West Lafayette, Indiana 47907-1282

A FEASIBILITY STUDY REGARDING THE ADDITION OF A FIFTH CONTROL TO A ROTORCRAFT IN-FLIGHT SIMULATOR

by

Simon Turner and Dominick Andrisani, II

School of Aeronautics and Astronautics

Purdue University

West Lafayette, Indiana 47907

Final Report

NASA- Ames Cooperative Agreement No. NCC 2-671

Title: "Multivariable Control System Design Techniques for Piloted Rotorcraft"

Principle Investigator: Dominick Andrisani, II

Period Of Performance: June 1, 1990 - May 31, 1991

Purdue DSP No. 520-1282-0492

July 1992

ACKNOWLEDGEMENTS

The authors would like to thank Mr. William S. Hindson, Dr. J. Victor Lebacqz and everyone else in the Flight Dynamics and Controls Branch of the NASA Ames Research Center whose assistance and encouragement was greatly appreciated.

TABLE OF CONTENTS

Page

APPENDICES

LIST OF TABLES

LIST OF FIGURES

Figure Page

Figure Page

Appendix
Figure

Appendix Figure

ABSTRACT

Turner, Simon. M.S.A.A., Purdue University, December 1992. A Feasibility Study Regarding the Addition of a Fifth Control to a Rotorcraft In-Flight Simulator. Major Professor: Dominick Andrisani, II.

This thesis evaluates the addition of a large movable horizontal tail surface to the control system of a rotorcraft in-flight simulator being developed from a Sikorsky UH-60A Black Hawk Helicopter. The capabilities of the control surface as a trim control and as an active control are explored. The helicopter dynamics are modelled using the Generic Helicopter simulation program developed by Sikorsky Aircraft. The effect of the horizontal tail on the helicopter trim envelope is examined by plotting trim maps of the aircraft attitude and controls as a function of the flight speed and horizontal tail incidence. The control power of the tail surface relative to that of the other controls is examined by comparing control derivatives extracted from the simulation program over the flight speed envelope. The horizontal tail's contribution as an active control is evaluated using an explicit model following control synthesis involving a linear model of the helicopter in steady, level flight at a flight speed of eighty knots.

The horizontal tail is found to provide additional control flexibility in the longitudinal axis. As a trim control, it provides effective control of the trim pitch attitude at mid to high forward speeds. As an active control, the horizontal tail provides useful pitching moment generating capabilities at mid to high forward speeds.

CHAPTER 1.

INTRODUCTION

To support investigations regarding advanced rotorcraft dynamics and control concepts in the next decade, NASA and the U.S. Army are currently developing a new flight research vehicle, the Rotorcraft-Aircrew Systems Concepts Airborne Laboratory (RASCAL) [1]. This aircraft will be utilized by programs such as the Superaugmented Controls for Agile Maneuvering Performance (SCAMP) program, the Automated Nap-of-the-Earth Flight (ANOE) program and the Rotorcraft Agility and Pilotage Improvement Demonstration (RAPID) program. In addition to supporting these and other future research programs, the RASCAL will also play an important role as a rotorcraft in-flight simulator. This investigation is primarily concerned with the RASCAL's performance in the role of an in-flight simulator.

Variable stability aircraft and in-flight simulation have been in existence for over forty years. In 1976, NASA selected the Ames Research Center as its lead center for rotorcraft research and development. In 1977, in cooperation with the U.S. Army, NASA began operation of a UH-1H V/STOLAND variable stability helicopter for investigations into guidance and control concepts as well as handling qualities specifications. In 1979, the Ames Research Center acquired a CH-47B helicopter which was used extensively as a variable stability aircraft and in-flight simulator until 1989. As a variable stability aircraft, desired dynamics of the CH-47B could be selected and the resulting in-flight performance could be evaluated. As an in-flight simulator, the CH-47B could be forced to behave like another aircraft, with some restrictions, and the resulting in-flight performance of the desired aircraft could be assessed using the CH-47B. The RASCAL is to be the next in-flight simulation and experimentation platform with greater capabilities than its predecessors.

In addition to the efforts of NASA and the U.S. Army, other organizations have

also been active in the field of rotorcraft in-flight simulation [2]. The National Aeronautical Establishment of Canada has operated variable stability helicopters since 1961 [3,4]. The German Aerospace Research Establishment is also active in the area of rotorcraft in-flight simulation. This organization is currently operating a BO-105 helicopter as an in-flight simulator for the investigation of areas such as rotorcraft handling qualities and rotorcraft flight control and guidance system concepts [5,6].

In rotorcraft research, the in-flight simulator plays a necessary role. It is used for applications which require the high level of realism and pilot-in-the-loop characteristics unique to an in-flight simulator, as opposed to a ground based simulation or unmanned computer simulation. Some of the applications requiring in-flight simulation include validation of ground based simulators, development of handling qualities specifications and support of new rotorcraft designs.

In-flight simulation is required to validate and compliment ground-based simulation due to the uncertainty involved in rotorcraft modelling and the inherent limitations of ground-based simulators. It is frequently important that simulators accurately reproduce pilot cues, including aural and visual cues, vehicle accelerations and environmental effects such as turbulence and ground effect. In-flight simulators can be used to verify the accuracy of ground-based simulator performance in these and other areas. Another important consideration in simulation is the psychological effect on the pilot. The ground-based simulator environment is less stressful than the in-flight environment. This factor can cause the pilot to operate at a lower gain than he normally would, making critical flight control problems difficult to detect.

In-flight simulators also play an important role in supporting the design and development of new rotorcraft concepts by allowing designs to be tested and revised without requiring manufacture of a prototype. The use of in-flight simulation reduces the expense in the development stage by allowing design concepts to be tested in a highly realistic environment through the use of the in-flight simulator. Otherwise, a prototype incorporating the desired concepts would have to be built and flown when it became necessary to evaluate the system in a more realistic environment than ground based simulators are capable of providing.

The usefulness of any in-flight simulator is limited by certain characteristics of the host vehicle [5]. The number of independent controls available on the host aircraft limits

the number of degrees of freedom that can be independently controlled. Since an aircraft has six rigid body degrees of freedom, six independent controls are desirable. However, a typical helicopter possesses only four independent controls: longitudinal cyclic pitch, lateral cyclic pitch, collective pitch, tail rotor collective pitch. Control of all six degrees of freedom would require additional longitudinal and lateral force or moment generating capabilities. The Flight Research Department of the Calspan Corporation overcame this limitation with its fixed wing Total In-Flight Simulator (TIFS) by adding direct lateral force control surfaces and throttle control to the simulator control system [7,8]. The control power available in each degree of freedom is also an important limitation since it limits the amount of force and moment that the simulator can generate in each axis. The speed of the control response in each axis is an important limitation because it places a limit on the speed of response of the simulator in each axis. Finally, the flight envelope of the host aircraft is important because it limits the operational flight envelope of the simulator. For the RASCAL to be an effective in-flight simulator, each of these issues must be addressed during its development.

The baseline vehicle for the RASCAL is the Sikorsky UH-60A Black Hawk helicopter. This helicopter was selected because it best satisfied the criteria set by NASA and the U.S. Army [1]. For example, it is more agile and maneuverable than its predecessor, the CH-47B, and also more receptive to high bandwidth flight control due to a stiffer rotor head. In the development of the UH-60A into the RASCAL platform, the helicopter will be equipped with a high quality data acquisition system, a programmable flight control computer and high-performance actuators. The physical components of the aircraft which provide control of its motion are its main rotor, tail rotor and movable horizontal tail.

The principle interest of this thesis is the Black Hawk's movable horizontal tail, or stabilator. The stabilator is a large aerodynamic tail surface commanded by a flight control computer and is currently automatically programmed to improve the aircraft's static and dynamic stability in forward flight. However, in an in-flight simulator application, the stabilator could be incorporated into the flight control system as a fifth independent control. At mid to high forward speeds, this large aerodynamic surface can generate significant lift and drag forces and substantial pitching moments. This capability could conceivably provide the flight control system with additional control of the aircraft's trim characteristics as well as provide a greater degree of control of the aircraft motion in its six degrees of

freedom. The extent to which this extra capability can safely be exploited, as well as the attendant design issues, is of interest in the development of the RASCAL.

The objective of this thesis is to examine the capabilities of the horizontal stabilator over the flight envelope of the UH-60A and to evaluate some of the benefits and limitations involved in adding it to the RASCAL's flight control system. The following sections include a brief statement of purpose, a description of the approach taken in this investigation, a discussion of the results obtained and a summary of the conclusions.

CHAPTER 2.

STATEMENT OF PURPOSE

The objective of this investigation is to evaluate the capabilities and limitations of the Black Hawk's horizontal stabilator and to determine how the stabilator can be exploited to expand the in-flight simulation capabilities of the Rotorcraft-Aircrew Systems Concepts Airborne Laboratory (RASCAL) being developed at the Ames Research Center. Fundamentally, the addition of the stabilator can enhance the performance of the in-flight simulator by making a fifth control available to the simulator. This fifth control can be exploited in two roles: an additional trim control and an additional active control.

The stabilator affects the trim state of the aircraft by generating aerodynamic lift and drag forces which depend on the stabilator's incidence and the flight speed of the aircraft. Due to the distance between the stabilator and the aircraft center of gravity, the aerodynamic forces acting on the stabilator will also result in torques on the aircraft about its center of gravity. The effect of the stabilator on the trim conditions of the aircraft over its flight envelope is one of the primary areas of interest in this research. This thesis investigates the effect of the stabilator on the trim conditions of the aircraft and shows how the stabilator could be used to provide increased control over the trim conditions of the aircraft.

Due to its ability to generate aerodynamic forces and moments about the center of gravity, the stabilator also offers some additional control over the aircraft's dynamics. As an active control, the stabilator could enhance the active control system of the aircraft by providing an additional independent control input. The current aircraft offers four independent controls but the addition of the stabilator to the flight control system could offer a fifth independent control. If the stabilator has sufficient force and moment generating capabilities, it could be used together with the other four controls to provide a wider range of control over the aircraft's six rigid body degrees of freedom. This thesis evaluates the force and moment generating capabilities of the stabilator through a

comparison with the other controls. The degree of improvement in dynamic simulation fidelity that the stabilator could offer the in-flight simulator is examined through a control system application representative of the kind of control system that would be used by an in-flight simulator.

CHAPTER 3.

BACKGROUND

The purpose of this investigation is to study the potential contribution of the Black Hawk's movable horizontal tail, or stabilator, to the flight control system of the RASCAL. The first step in this analysis was to obtain a suitable representation of the UH-60A Black Hawk helicopter. As a result, this investigation was carried out in a non-real time computational environment using two different mathematical models of the Black Hawk: a non-linear FORTRAN simulation program and a linear state space model.

The non-linear, full flight envelope FORTRAN simulation program [10,11], referred to as GENHEL (GENeral HELicopter Simulation Program), was used to examine the effect of the stabilator on the trim properties of the helicopter and to estimate the stabilator's force and moment generating capabilities over its flight speed envelope in level flight. The effect of the stabilator on the trim state of the aircraft was evaluated by using GENHEL to trim the aircraft over a range of stabilator settings and flight speeds. To estimate the stabilator's force and moment generating capabilities over the flight speed range, GENHEL was used to extract first order derivatives of the aircraft forces and moments with respect to the stabilator and pilot controls over the flight speed range. Taking into account the maximum travel of the different controls, this provided a method to compare the force and moment generating capabilities of the stabilator to the capabilities of the other available controls.

The linear, state space model, derived from GENHEL, was used to study the influence of the stabilator on the stability properties of the helicopter and was also used in a model following flight control application. To evaluate the influence of the stabilator on the vehicle's stability characteristics, linear models were used to study the linear stability properties of the aircraft about a particular trim state over the range of stabilator settings. Incorporating the stabilator into an active control design allowed the demand on the stabilator, in an active role, to be assessed. The effect of the speed of response of the

stabilator on the performance of the model following system was also studied by varying the stabilator's speed of response and evaluating the resulting performance.

3.1 The UH-60A Black Hawk

The aircraft being studied in this investigation is the Sikorsky UH-60A Black Hawk helicopter developed for the U.S. Army under the Utility Tactical Transport Aircraft System (UTTAS) program. The Black Hawk is a medium sized, single main rotor helicopter as illustrated in Figure 3.1. Reference 9 provides a more complete description of the aircraft. Table 3.1 presents the nominal configuration used in this study. The reference frames for the measurement of the center of gravity location are illustrated in Appendix A.

Table 3.1. Inertia Properties of the UH-60A Black Hawk

Weight (in flight)	16825.0	Lb.
Fuselage Station CG	355.0	In.
Waterline Station CG	248.2	In.
Buttline Station CG	0.0	In.
Ixx	4659.0	Slug ft^2
Iyy	38512.0	Slug ft^2
Izz	36796.0	Slug ft^2
Ixz	1882.0	Slug ft^2

Of interest to this investigation is the flight control system of the aircraft. The primary pilot controls are the longitudinal cyclic stick, lateral cyclic stick, collective lever and pedals. The longitudinal and lateral cyclic stick allow the pilot to control the orientation of the main rotor thrust vector with respect to the fuselage by allowing the pilot to control the pitch of the rotor blades cyclically. The collective lever allows the pilot to control the magnitude of the main rotor thrust by allowing the pitch of the rotor blades to be controlled collectively. The pedals allow the pilot to command yawing moment by allowing control of the collective pitch of the tail rotor blades. The pilot controls are linked to the control boost actuators which assist the pilot in manipulating the control linkages. The boost actuators are linked to the mixing box where the controls are mechanically mixed together in an effort to reduce inter-axis coupling of the aircraft responses. It should be noted that the mixing

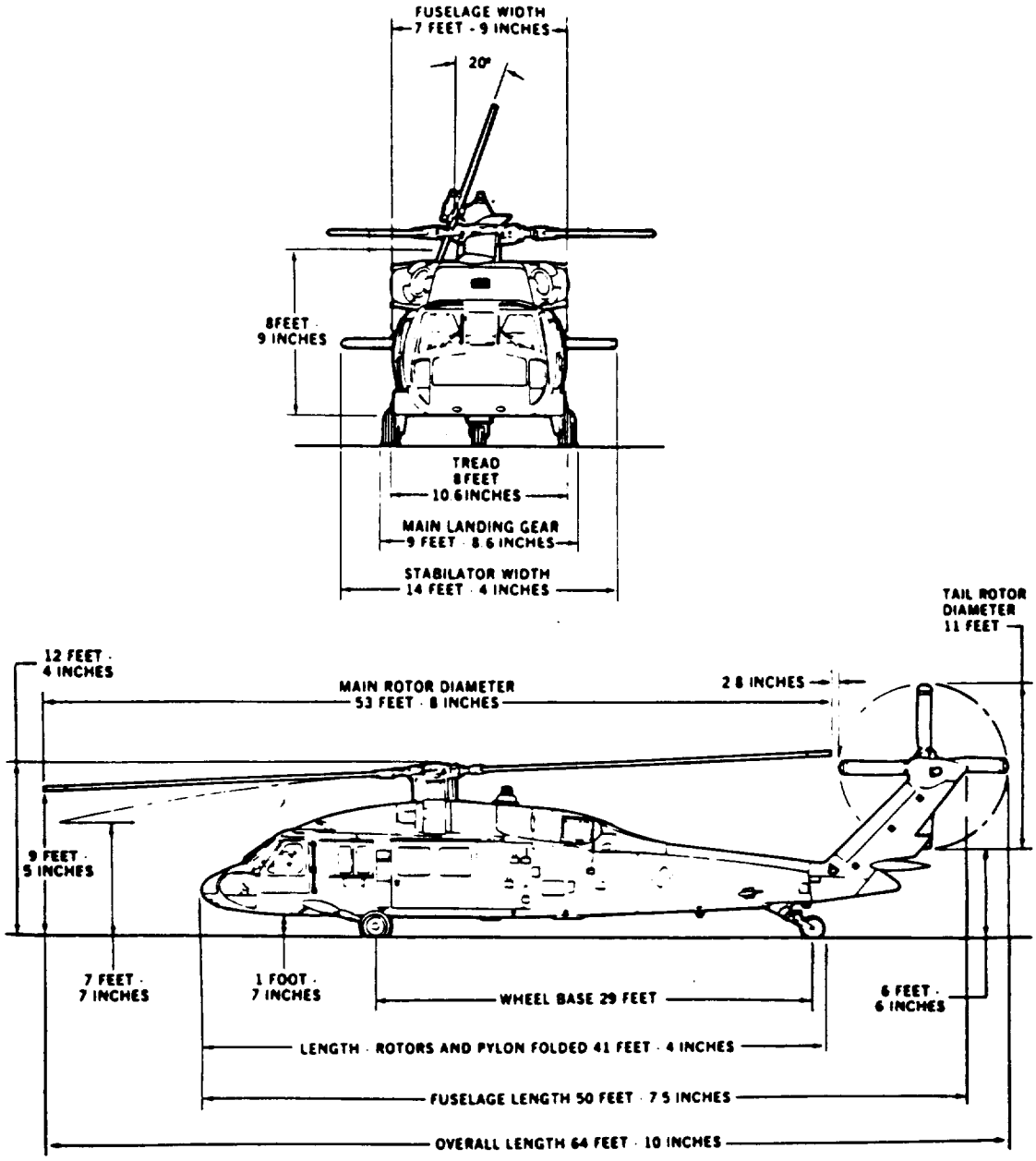

Figure 3.1 Sikorsky UH-60A Black Hawk Helicopter

box is a mechanical device with a fixed schedule so the control mixing is fixed and independent of any variables such as airspeed. The mixing box outputs are linked to the primary servos which control the pitch of the main rotor and tail rotor blades. The pilot control limits are presented in Table 3.2.

Unlike the main rotor and tail rotor systems, the stabilator does not respond directly to pilot control inputs. The stabilator is a large horizontal tail, hinged by its leading edge to the helicopter and driven by dual electric screwjack actuators. On the standard helicopter, the stabilator system is automatically programmed to serve several purposes [9]. At low speeds, the stabilator is aligned with the main rotor downwash to minimize nose up attitude that would result from downwash. At higher speeds, the stabilator incidence is decreased to provide improved longitudinal static stability. In forward flight, the stabilator is programmed to improve dynamic stability by providing pitch rate feedback to the stabilator, it is programmed to minimize pitch excursions due to collective inputs by feeding collective lever position back to the stabilator and it is programmed to reduce the pitching motion induced by the tail rotor in a lateral gust by feeding back lateral acceleration to the stabilator. The stabilator control limits are also presented in Table 3.2.

Table 3.2. UH-60A Control Deflection Conventions

Longitudinal Cyclic Stick	Forward	0.0	Inches
	Aft	10.0	Inches
Collective Lever	Down	0.0	Inches
	Up	10.0	Inches
Lateral Cyclic Stick	Left	0.0	Inches
	Right	10.0	Inches
Pedals	Left	0.0	Inches
	Right	5.37	Inches
Stabilator	Up	-8.0	Degrees
	Down	40.0	Degrees

In this investigation, the actuators between the pilot controls and the main and tail rotor have been modelled using only constant gains. The mixing box was included in the model of the flight control system and has also been modelled using constant gains. The stabilator control laws were removed and the stabilator control system has been modelled as

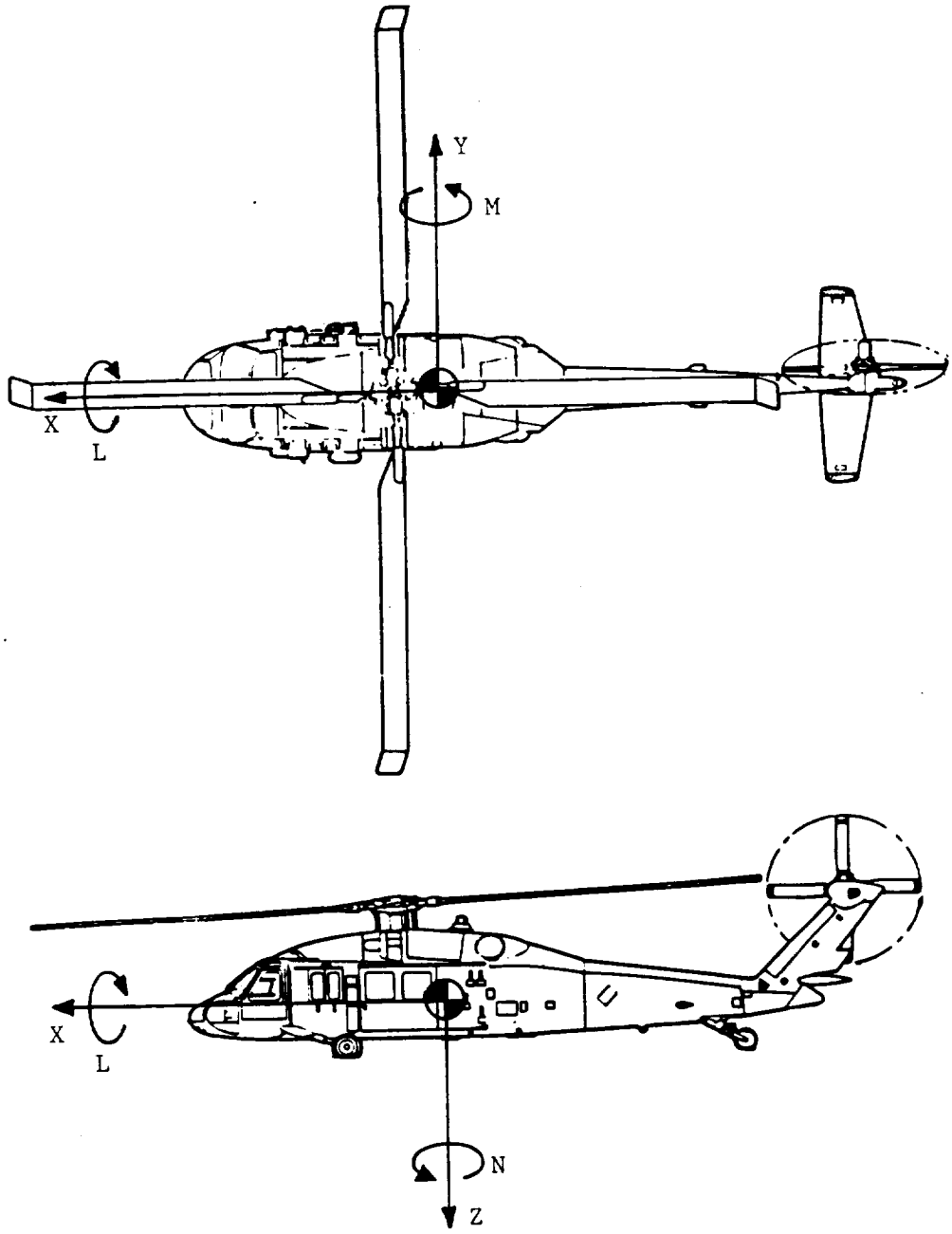

Figure 3.2 Body Fixed Axis System

a first order actuator, the production hardware having a time constant of 0.113 seconds.

The axis system used in this investigation is a body fixed coordinate system with its origin at the aircraft's center of gravity and is illustrated in Figure 3.2. The X axis points toward the nose of the aircraft and is parallel to the centerline of the aircraft, the Z axispoints toward the bottom of the aircraft and, consequently, the Y axis points toward the starboard side of the aircraft. All forces (X,Y,Z) and moments (L,M,N) are referred to this axis system. All translational and rotational accelerations, velocities and displacements are also referred to in this axis system.

3.2 Full Flight Envelope, Non-Linear Model

The non-linear model of the UH-60A used in this analysis to provide trim conditions and force and moment derivatives is a non-real time computer simulation model based on the Sikorsky Aircraft General Helicopter Flight Dynamics Simulation (GENHEL) and modified at NASA Ames [10,11]. As part of a continuing program conducted by NASA and the Army Aeroflightdynamics Directorate to improve rotorcraft flight simulation, GENHEL has been developed as a simulation program with the fidelity necessary for handling qualities research and for research into advanced control concepts. GENHEL is a non-linear, full flight envelope, blade element model of the single main rotor UH-60A Black Hawk helicopter and is valid for a full range of angle of attack, sideslip and rotor inflow. The model includes six rigid body degrees of freedom, and also main rotor flapping, lagging, air-mass and hub-rotational degrees of freedom.

GENHEL is based on a group of modularized FORTRAN subroutines which are mathematical representations of the major force and moment producing subsystems of the aircraft. These modules include the main rotor dynamics, engine and gearbox dynamics, tail rotor dynamics, fuselage and empennage aerodynamics, and the flight control system dynamics including sensors and actuators. All aerodynamics are modelled using wind tunnel test data. Appendix B presents more details about the model of the stabilator used in the simulation model particularly its aerodynamic characteristics.

To investigate the effectiveness of the stabilator as a trim control, trim conditions were generated for the aircraft using the GENHEL program. To trim the aircraft, once the mass of the vehicle and its center of gravity location are fixed, the desired airspeed, flight

path angle, heading angle and stabilator incidence must be specified. The program then uses an iterative procedure to trim the aircraft by reducing the linear and angular accelerations of the aircraft to a specified convergence criteria. This is achieved by manipulating six independent variables to balance the forces and moments acting in the six degrees of freedom. The independent variables used by the program are the longitudinal cyclic stick, lateral cyclic stick, collective lever, pedals, pitch attitude and either roll angle or horizontal flight path angle. At low speeds, roll angle is used and at speeds greater than sixty knots, horizontal flight path angle is used. The trim procedure was limited by the control travel limits of the pilot's controls, which are listed in Table 3.2.

To investigate the control power of the stabilator relative to the other controls, GENHEL was used to generate force and moment derivatives with respect to the pilot controls. The program uses a double sided, small perturbation linear extraction method. One control is perturbed by a small amount, while all others are held fixed, and the rotor dynamics are given a few rotor cycles to reach steady state. The resulting changes in the forces and moments are recorded and then the aircraft is retrimmed and the process is repeated except that the control is perturbed in the opposite direction. The average of the resulting change in each force and moment is divided by the magnitude of the perturbation to yield the appropriate derivative. After each derivative extraction, the aircraft is retrimmed before extracting the next derivative.

3.3 Linear, Small Perturbation Model

To study the stabilator's role as an active control, as well as its effect on the stability of the helicopter, a linear model of the helicopter was required. The model used in this study was a thirty state, small perturbation, linear model provided by a computer program which was developed at the University of Maryland for NASA to provide high order linear models of the Black Hawk [12,13]. This computer program was based on the code from the GENHEL simulation program. The linear model states and inputs represent small perturbations from the trim values of the variables describing the dynamics of the aircraft and the control inputs. The linear model state vector (x) includes states representing the rigid body dynamics, rotor flapping and lead-lag dynamics and the air mass and rotor blade twist dynamics. The linear model input vector (δ_a) includes the input to the stabilator actuator and the inputs from the cockpit controls to the pilot boost actuators which send the pilot commands to the control linkages and servos responsible for changing the pitch of the

main rotor and tail rotor blades.

The trim state chosen for this analysis was steady, level, forward flight at eighty knots. A complete summary of the trim state of the aircraft is presented in Appendix C. The trim stabilator incidence was chosen to be ten degrees trailing edge down. This results in a trim pitch attitude of 0.2 degrees and allows approximately twenty degrees of stabilator travel in either direction before the stabilator deflection reaches the physical limits on the aircraft. However, the stabilator aerodynamic data presented in Appendix B indicate that the stabilator's lift generating capability is only linear for stabilator deflections of up to fifteen degrees from the zero lift position. The pilot controls are also trimmed approximately at the center of their allowable travel.

The resulting thirty state linear model is presented in Appendix D. It should be pointed out that the linear model results from a linearization procedure about the chosen trim conditions. Due to the small perturbation assumption associated with the linearization procedure, the linear model is only valid for small state and control perturbations about the trim values. Large perturbations will excite non-linear behavior in the actual aircraft which the linear model cannot predict. In this investigation, only small amplitude motion was examined and so the linear model was assumed to be sufficiently accurate.

3.3.1 Linear Model Reduction

The thirty state model is useful for examining the behavior of the helicopter over a large frequency range but is too cumbersome for control law design. Therefore, for the purposes of control law design, the thirty state model was reduced to an eight state linear model which models only the six rigid body degrees of freedom. The linear model was reduced from thirty states to eight states as follows. The thirty state model is first partitioned into the states to be kept (x_1) and the states to be discarded (x_2).

$$\begin{Bmatrix} \dot{x}_1 \\ \dot{x}_2 \end{Bmatrix} = \begin{bmatrix} F_{11} & F_{12} \\ F_{21} & F_{22} \end{bmatrix} \begin{Bmatrix} x_1 \\ x_2 \end{Bmatrix} + \begin{bmatrix} G_1 \\ G_2 \end{bmatrix} \{\delta_a\}$$

The states to be discarded (x_2) are the rotor states, the structural twist states, and the rotor inflow states. These states correspond to high frequency dynamics and are not necessary when studying the low frequency, rigid body behavior of the aircraft. To eliminate these states they are assumed to be constant which is equivalent to setting their derivatives equal

to zero. The second equation now provides the states to be discarded (x_2) in terms of the desired states (x_1) and the inputs (δ_a).

$$\{x_2\} = -\left[F_{22}^{-1}F_{21}\right]\{x_1\} - \left[F_{22}^{-1}G_2\right]\{\delta_a\}$$

This approach assumes that the F_{22} matrix has full rank. This equation is then substituted into the first equation to obtain a new state equation for the desired states (x_1) only. The resulting linear model is of the form

$$\{\dot{x}_1\} = [F_8]\{x_1\} - [G_8]\{\delta_a\}$$

where the F_8 and G_8 matrices are given by the equations

$$F_8 = F_{11} - F_{12}F_{22}^{-1}F_{21}$$
$$G_8 = G_1 - F_{12}F_{22}^{-1}G_2$$

In this investigation, vertical velocity (w) was replaced with flight path angle (γ) and all angular units were converted from radians to degrees. The states and controls of the linear model are given by the vectors .

$$x_1 = [\, u \;\; \gamma \;\; q \;\; \theta \;\; v \;\; p \;\; \phi \;\; r \,]^T$$
$$\delta_a = [\, \delta_{lon} \;\; \delta_{col} \;\; \delta_{lat} \;\; \delta_{ped} \;\; i_{ht} \,]^T$$

The resulting eight state linear model is also presented in Appendix D.

It must be pointed out that this reduced model is 'quasi-steady' with respect to the rotor degrees of freedom. In the model reduction process, the discarded, higher order states, including the rotor dynamics, are assumed to be constant. Since the rotor dynamics are assumed to be constant, the eight state model only accounts for the rigid body dynamics. Frequency responses comparing the higher order model with the reduced model are presented in Appendix E. From the frequency responses, it can be seen that the responses of the two models to main rotor inputs match for frequencies below 2-3 radians per second. At and above 2-3 radians per second, the higher frequency dynamics introduce additional phase lag that is not predicted by the eight state model. The additional phase lag introduced by the rotor degrees of freedom is not included in the eight state model so it only matches the high order model at frequencies below the natural frequencies of the rotor dynamics. It is interesting to note that the response to the tail rotor and stabilator show no

difference between the thirty state model and the eight state model at higher frequencies. This is due to the fact that the higher frequency dynamics in the thirty state model represent main rotor dynamics only.

Since the eight state model excludes the rotor dynamics, it is sufficient for the study of rigid body motion but is inappropriate for high bandwidth flight control design. It has been shown in the past that the design of high bandwidth rotorcraft flight control systems using models that exclude the rotor dynamics can result in feedback control laws which have a tendency to destabilize the rotor dynamics [14-15]. In this investigation, the primary interest is the stabilator's contribution to the in-flight simulation of rigid body dynamics. The eight state model will be used for control law design but the thirty state model will be used to insure that the feedback gains are within reason and to provide a more realistic prediction of the aircraft's response to control inputs.

3.3.2 Linear Stability Analysis

Once the linear model was obtained, the eight state dynamics matrix (F_8) was decomposed into its eigenvalues and eigenvectors to gain insight into the natural modes of motion of the unaugmented aircraft. The eigenvalues of the eight state model are listed in Table 3.3. The eigenvalues reveal that there is one unstable mode contained in the eight state model which is primarily longitudinal motion consisting of forward speed and pitching motion. This is a forward speed divergence mode caused by aerodynamic loads on the aircraft [16]. The rotor response to an increase in forward speed will cause the rotor to "blow back" causing the helicopter to pitch up and decrease the forward speed and return to its trim state. While the rotor encourages a stable response, fuselage aerodynamics, particularly the stabilator, may not. If the stabilator is carrying an upward load, an increase in airspeed will cause an increase in the aerodynamic force and, therefore, an increase in nose down pitching moment causing the aircraft to diverge from its trim state. If, as a result of a perturbation, the magnitude of the nose down pitching moment generated by the fuselage and stabilator is greater than the nose up pitching moment generated by the main rotor, the aircraft will pitch down causing a further speed increase and result in a divergence in speed and pitch attitude. Since the stabilator was trimmed at ten degrees trailing edge down, and since the trim pitch attitude is only 0.2 degrees nose down, the stabilator local angle of attack is positive. This results in an upward load on the stabilator and so, at this trim state, the stabilator contributes to this instability.

Table 3.3 Eigenvalues of the Eight State Model of the Unaugmented Aircraft Trimmed at Eighty Knots with the Stabilator Ten Degrees Trailing Edge Down

Eigenvalues	Mode Characteristics
+ 0.4758	Forward Speed and Pitching
- 0.1754	Yawing
- 0.0683 ± 0.2867	Forward and Lateral Velocity
- 0.4219 ± 1.5228	Pitching, Rolling and Yawing
-2.0178	Pitching and Rolling
-2.9196	Rolling

To appreciate the effect of the trim incidence of the stabilator on the natural modes of motion of the aircraft, linear models were derived over a range of trim values of stabilator incidence, from forty degrees down to eight degrees up in increments of five degrees. A locus of the eigenvalues of the different models are presented in Figure 3.3. This locus indicates that when the aircraft is trimmed in steady, level flight at eighty knots, it possesses the divergent speed stability mode regardless of the stabilator incidence though the stabilator setting does have a significant impact on the unstable pole. The unstable pole is largest when the stabilator is at its maximum positive incidence of forty degrees, however the divergence pole is closest to the origin when the the aircraft's pitch attitude is near zero. This shows that the stabilator incidence is not exclusively responsible for the instability since the pole corresponding to the instability is in the right half plane regardless of the position of the stabilator.

Since the thirty state linear model will be used to represent the actual aircraft in the evaluation of the a control laws designed using the eight state model, the effect of the model reduction procedure on the unstable pole needs to be addressed. Using residualization to reduce the order of the linear model preserves the accuracy of the model at low frequency, which was pointed out in Section 3.3.1 and illustrated by the frequency response comparisons contained in Appendix E. To evaluate the effect of the model reduction procedure on the locations of the low frequency eigenvalues of the model, the low frequency eigenvalues of the thirty state linear model were compared to the eigenvalues of the eight state model by plotting them on the complex plane. This comparison is presented in Figure 3.4 and shows that the eigenvalues within one radian per second are virtually unchanged by the model reduction procedure. This includes the unstable eigenvalue which

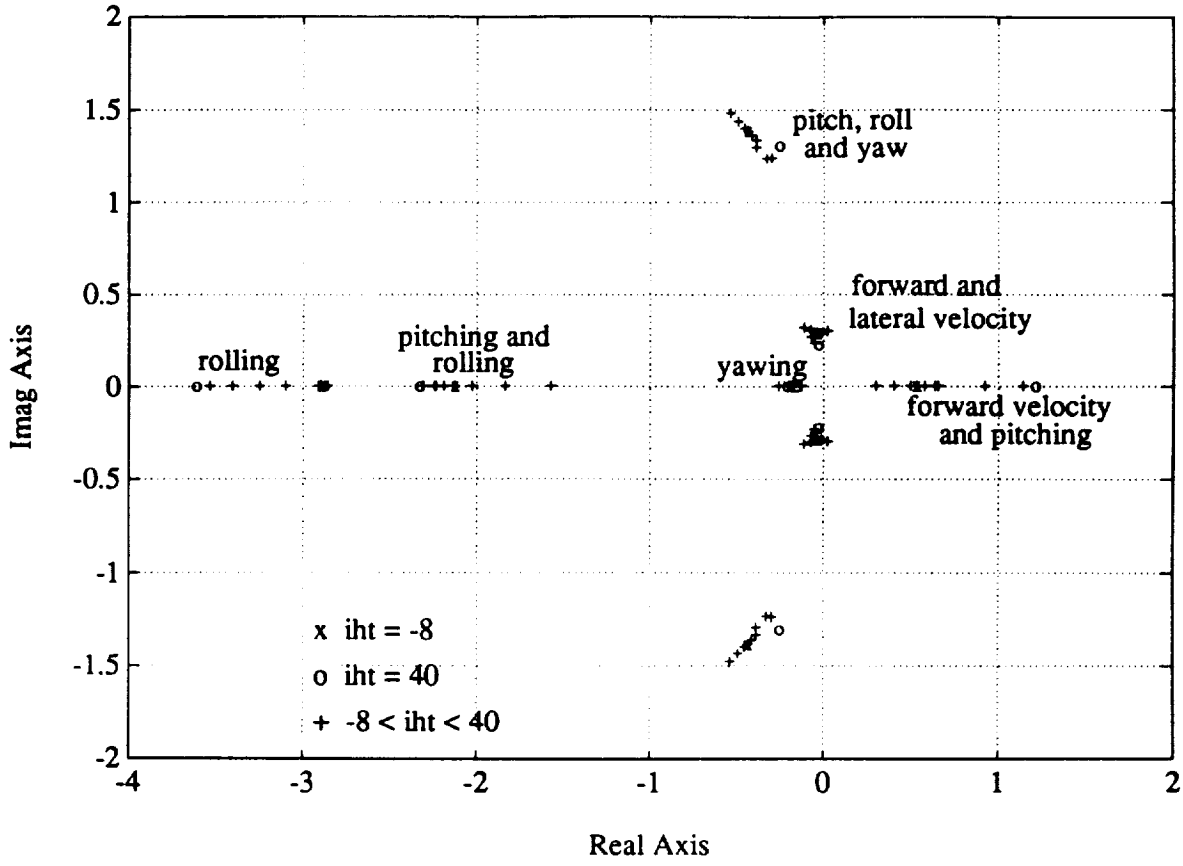

Figure 3.3 Influence of the Stabilator on the Eigenvalues of the Eight State Linear Model

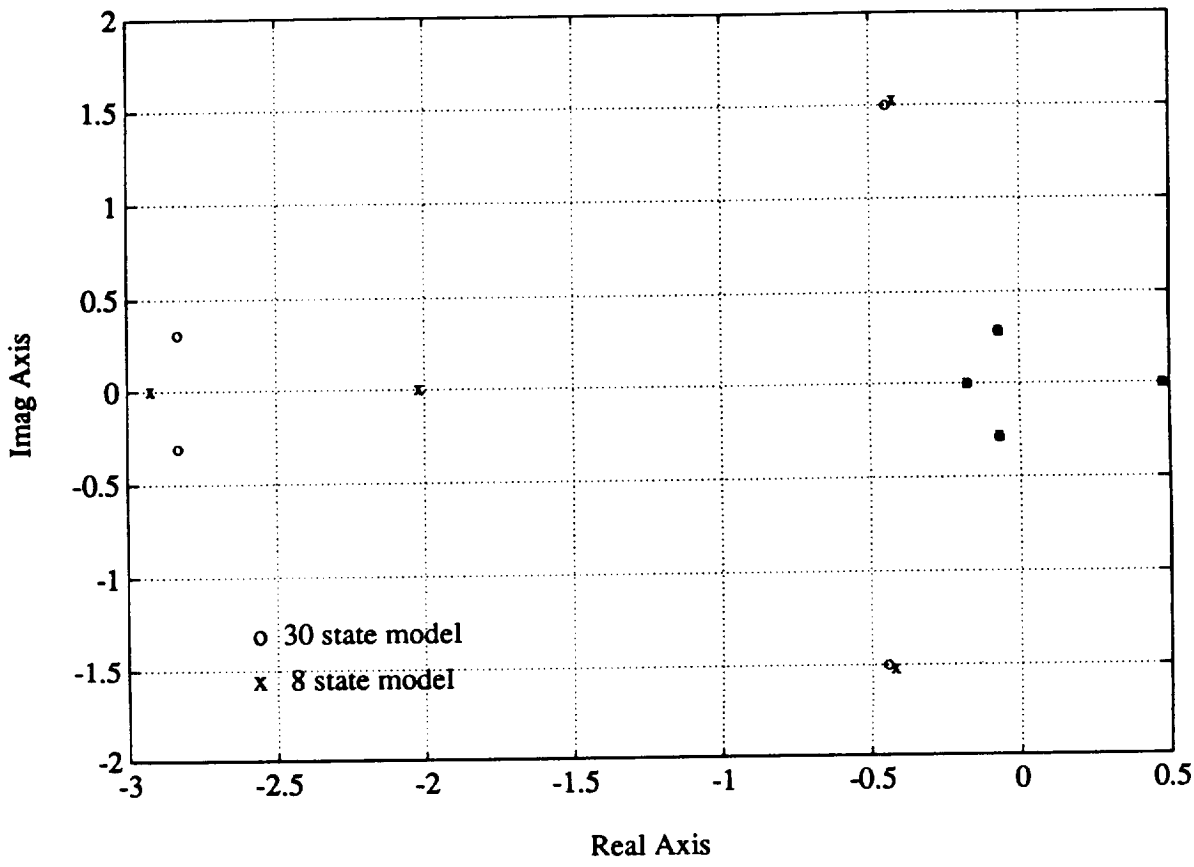

Figure 3.4 Comparison of the Low Frequency Eigenvalues of the Thirty State Model with the Eigenvalues of the Eight State Model

only moves from a value of 0.4772 radians per second to 0.4758 radians per second when the model is reduced.

3.4 Model Following Control Synthesis

An explicit model following control law was used to evaluate the stabilator in an in-flight simulation application. Using the explicit model following methodology, control laws with and without the stabilator were designed using the eight state linear model described in Section 3.3.1. The control laws were applied to the thirty state model and the resulting systems were used to evaluate the contribution of the stabilator by comparing the performance of a design including the stabilator with one that excluded the stabilator. This application was also used to evaluate the effect that a stabilator actuator pole has on the performance of the system. The control law design is described in Reference [7].

The control law used in this investigation consists of three components which include feedback gains to provide stability and sensitivity reduction, a linear model of the desired dynamics and feedforward gains to provide model following. Figure 3.5 presents a diagram of the control synthesis. The command inputs (δ_c), which would be input by the research pilot flying the in-flight simulator, pass through the model of the desired dynamics generating the desired responses (x_m). To produce the control inputs to the actuators (δ_a), the command inputs and the model states pass through the feedforward gains (K_δ and K_x) and are summed with the feedback signal which results from feeding back the aircraft states through the feedback gains (K_{fb}). The purpose of the resulting control inputs is to cause the aircraft to duplicate the response of the model to the command inputs. If the aircraft possesses an independent control input for every degree of freedom, it is theoretically possible to cause the aircraft to duplicate the response of the model exactly [17]. If there are fewer control inputs than degrees of freedom, it will generally not be possible to provide perfect model following since the degrees of freedom of the aircraft can not be controlled independently.

The feedback component consists of a constant feedback gain matrix (K_{fb}) through which the states of the aircraft are fed back to the aircraft control inputs (δ_a) to stabilize the aircraft and reduce the sensitivity of the lateral-directional degrees of freedom. The values of the feedback gains were determined by closing one feedback loop at a time beginning with the fastest loop. To suppress the lateral-directional response to longitudinal inputs,

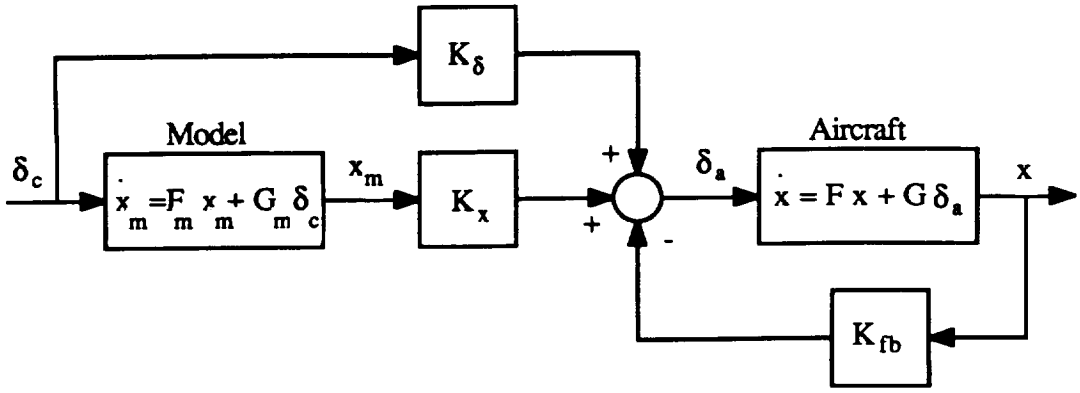

Figure 3.5 Explicit Model Following Control Design

roll rate (p) and roll attitude (ϕ) were first fed back to the lateral cyclic (δ_{lat}) and then yaw rate (r) and the integral of the yaw rate ($\int r$) were fed back to the pedals (δ_{ped}). To feed back the integral of the yaw rate, it was necessary to add an additional state to the system representing the integral of the yaw rate ($\int r$). This increased the number of states of the linear model to nine. After the roll and yaw loops were closed, the pitch rate (q) and pitch attitude (θ) were fed back to the longitudinal cyclic (δ_{lon}) to stabilize the unstable longitudinal mode. Appendix F presents a more detailed description of the feedback control law design.

The feedforward component consists of the model of the desired dynamics and the feedforward gain matrices (K_δ, K_x) needed to feed the commands (δ_c) and model states (x_m) forward to the aircraft control inputs (δ_a) to cause the aircraft to follow the model. Once the linear model of the aircraft and the linear model of the desired dynamics were obtained and the feedback loops were closed, the feedforward gains required for model following (K_δ, K_x) could be determined. Before computing the feedforward gains, the state vectors of the linear models representing the aircraft dynamics and the desired dynamics were divided into the longitudinal states and the lateral-directional states and the matrices were partitioned as follows:

$$\text{Aircraft:} \quad \begin{Bmatrix} \dot{x}_1 \\ \dot{x}_2 \end{Bmatrix} = \begin{bmatrix} F_{11} - G_1 K_{fb1} & F_{12} - G_1 K_{fb2} \\ F_{21} - G_2 K_{fb1} & F_{22} - G_2 K_{fb2} \end{bmatrix} \begin{Bmatrix} x_1 \\ x_2 \end{Bmatrix} + \begin{bmatrix} G_1 \\ G_2 \end{bmatrix} \{\delta_a\}$$

$$x_1 = [\, u \;\; \gamma \;\; q \;\; \theta \,]^T$$

$$x_2 = [\, v \;\; p \;\; \phi \;\; r \;\; \int r \,]^T$$

$$\delta_a = [\, \delta_{lon} \;\; \delta_{col} \;\; \delta_{lat} \;\; \delta_{ped} \;\; i_{ht} \,]^T$$

$$K_{fb} = [\, K_{fb1} \;\; K_{fb2} \,]$$

Model:
$$\dot{x}_{m1} = F_{m11}x_{m1} + G_{m1}\delta_c$$
$$\dot{x}_{m2}(t) = x_{m2}(t) = 0 \quad \forall t$$
$$x_{m1} = [\, u_m \;\; \gamma_m \;\; q_m \;\; \theta_m \,]^T$$
$$x_{m2} = [\, v_m \;\; p_m \;\; \phi_m \;\; r_m \;\; \int r_m \,]^T$$
$$\delta_c = [\, u_c \;\; \gamma_c \;\; \theta_c \,]^T$$

Since the stabilator generates forces and moments which are primarily in the longitudinal plane of the aircraft, its contribution to the longitudinal dynamics was of primary interest. The model of the longitudinal dynamics was chosen to be fairly representative of the kind of demands placed on an in-flight simulator and is presented in Appendix G. The states of the model of the desired longitudinal dynamics include the forward velocity (u_m), flight path angle (γ_m), pitch rate (q_m) and pitch attitude (θ_m). The inputs to the system are the commanded forward velocity (u_c), flight path angle (γ_c) and pitch attitude (θ_c). Each degree of freedom is to be controlled exclusively by one input, which is indicated by the decoupled control matrix (G_{m1}). Coupling between the longitudinal degrees of freedom is also undesirable, which is indicated by the decoupled longitudinal dynamics matrix (F_{m11}). In this study, the lateral-directional responses of the in-flight simulator were desired to be as small as possible. This is specified in the model of the desired dynamics by setting the lateral-directional model states and state rates equal to zero for all time.

The feedforward gains were computed by specifying that the states of the aircraft match the states of the model. This results in the following requirements:

$$x = x_m$$
$$\dot{x} = \dot{x}_m$$

While only the three longitudinal control inputs (δ_{lon}, δ_{col}, i_{ht}) are required to cause the three longitudinal degrees of freedom to follow the model, the two lateral-directional controls (δ_{lat}, δ_{ped}) were also utilized in the feedforward control to improve the model following performance by reducing the coupling from the command inputs (δ_c) and the longitudinal states (x_1) to the lateral-directional states (x_2). The required control law was determined in terms of the model states (x_m) and the command inputs (δ_c) by substituting the model states into the state equation of the aircraft and then setting the state equation of the aircraft equal to the state equation of the model. This provides the resulting equality:

$$\begin{bmatrix} F_{11}-G_1K_{fb1} & F_{12}-G_1K_{fb2} \\ F_{21}-G_2K_{fb1} & F_{22}-G_2K_{fb2} \end{bmatrix}\begin{Bmatrix} x_{m1} \\ 0 \end{Bmatrix}+\begin{bmatrix} G_1 \\ G_2 \end{bmatrix}\{\delta_a\}=\begin{bmatrix} F_{m11}x_{m1}+G_{m1}\delta_c \\ 0 \end{bmatrix}$$

Solving for the required control inputs to the actuators (δ_a) yields the control law required to approximately achieve the model following requirements. The resulting control law is given by the expression

$$\{\delta_a\} = G^+\begin{bmatrix} F_{m11}-(F_{11}-G_1K_{fb1}) \\ -(F_{21}-G_2K_{fb1}) \end{bmatrix}\{x_{m1}\} + G^+\begin{bmatrix} G_{m1} \\ 0 \end{bmatrix}\{\delta_c\}$$

As a result, the feedforward gain matrices are given by the expressions:

$$K_x = G^+\begin{bmatrix} F_{m11}-(F_{11}-G_1K_{fb1}) \\ -(F_{21}-G_2K_{fb1}) \end{bmatrix}$$

$$K_\delta = G^+\begin{bmatrix} G_{m1} \\ 0 \end{bmatrix}$$

The feedforward control, including the feedforward gains and the model of the desired dynamics, can be combined with the aircraft model to yield the total system equations which are given by:

$$\begin{Bmatrix} \dot{x}_1 \\ \dot{x}_2 \\ \dot{x}_{m1} \end{Bmatrix} = \begin{bmatrix} F_{11}-G_1K_{fb1} & F_{12}-G_1K_{fb2} & G_1K_x \\ F_{21}-G_2K_{fb1} & F_{22}-G_2K_{fb2} & G_2K_x \\ 0 & 0 & F_{m11} \end{bmatrix}\begin{Bmatrix} x_1 \\ x_2 \\ x_{m1} \end{Bmatrix}+\begin{bmatrix} G_1K_\delta \\ G_2K_\delta \\ G_{m1} \end{bmatrix}\{\delta_c\}$$

To cause the longitudinal states to follow the model states the G_1K_δ and G_1K_X terms feed the commanded inputs and the states of the model of the desired response into the longitudinal equations. To minimize the lateral-directional response, the G_2K_δ term is used to reduce the coupling from the commanded inputs (δ_c) to the lateral-directional states while the G_2K_X term is used to reduce the coupling from the longitudinal states to the lateral-directional states.

Since the G matrix has more columns than rows, it cannot have a true inverse and the left inverse must be used to determine the feedforward gains. The G^+ term represents the left inverse of the aircraft G matrix. There are a number of ways to determine G^+ and the method used depends on the design goals. The left inverse was computed as follows:

$$G^+ = (G^T G)^{-1} G^T$$

If there were as many controls inputs as degrees of freedom, the product GG^+ in the feedforward terms would be diagonal. This would allow perfect model following in all degrees of freedom. If there are fewer control inputs than degrees of freedom, the product GG^+ will not be diagonal and perfect model following will not be achieved. However, if it is acceptable to attempt to achieve model following in only as many degrees of freedom as there are control inputs, then G^+ can be computed such that the product GG^+ will be diagonal except for the rows corresponding to the unconstrained degrees of freedom. To compute the left inverse which will achieve this goal, the rows in the G matrix corresponding the equations representing the degrees of freedom to be left unconstrained are set to zero. This is accomplished by multiplying the G matrix by a diagonal weighting matrix (W) which is an identity matrix that may have one or more of its diagonal elements equal to zero. Premultiplying the G matrix by this weighting matrix allows selected rows of the G matrix to be set equal to zero as desired. The weighted G matrix is defined as follows:

$$\hat{G} = WG$$

This weighted G matrix is used to determine the left inverse as follows:

$$G^+ = (\hat{G}^T \hat{G})^{-1} \hat{G}^T$$

Using this left inverse will cause the rows of GG^+ corresponding to the degrees of freedom to be controlled to be equal to rows of an identity matrix of the same dimension as GG^+. With this approach, the model following error will come from coupling from the uncontrolled degrees of freedom. In this investigation, when five controls were available, the lateral velocity (v) was left uncontrolled due to its relatively small effect on the longitudinal states. When only four controls are available, the forward velocity (u) and the lateral velocity (v) were left uncontrolled so the flight path angle (γ) and the angular rates (p, q, r) could be controlled.

To examine the performance of the stabilator using a more realistic model, the control laws were applied to the thirty state linear model. Though the control gains were designed using the eight state linear model, they were evaluated using the thirty state model to allow the higher order dynamics of the main rotor to be taken into account in the

examination of the performance of the model following system. The control laws designed using the rigid body linear model cannot account for the coupling introduced by the higher order states. As a result, the coupling from the uncontrolled, higher order states to the rigid body states will also introduce error into the model following performance of the in-flight simulator.

CHAPTER 4.

RESULTS AND DISCUSSION

This chapter presents the results of the investigations into the stabilator's trim effectiveness, its force and moment generating capabilities and its usefulness as an active control. The results of the trim investigation are presented in the form of trim maps of the six independent variables used to trim the aircraft over the flight speed range. The trim maps are used to show the effect of the stabilator on the trim variables. The results of the control power investigation are presented in the form of a comparison of the stabilator's control power with the control power of the pilot controls over the flight speed range. The effectiveness of the stabilator as an active control is evaluated using a model following flight control synthesis. A control system is designed with and without the stabilator as a fifth control and the performance of the resulting systems is compared. The impact of the stabilator's actuator speed is also examined using the model following control synthesis.

4.1 Trim Analysis

The influence of the stabilator on the trim properties of the aircraft was evaluated by trimming the aircraft in steady, level flight over a range of flight speeds and stabilator settings. As described in Section 3.2, the aircraft is in trim when the forces and moments acting in the six different degrees of freedom of the aircraft are balanced. All forces and moments are referred to using the axis system described in Section 3.1. In this investigation, the airspeed was varied between zero and 120 knots in increments of ten knots. The trim routine had difficulty converging at flight speeds at and above 120 knots so this was chosen to be the maximum airspeed. The stabilator incidence was varied between its stops, forty degrees trailing edge down to eight degrees trailing edge up in increments of five degrees. At higher airspeeds, where the stabilator is more effective, the demand on the longitudinal cyclic control exceeded its aft limit in the trim routine when the stabilator was at extreme positive incidences and so only the trim conditions where all

dependent variables were between the appropriate limits are presented. The control limits consistent with this investigation are presented in Table 3.2.

Given a constant rotor speed of 27.0 radians per second and a fixed center of gravity location, the trim flight conditions are uniquely selected by choosing the aircraft's mass (m), flight speed (V), flight path angle (γ_v) and stabilator incidence (i_{ht}). The forces and moments in the six degrees of freedom are simultaneously balanced by manipulating six independent variables. In this investigation, the six variables used to trim the aircraft were the longitudinal cyclic stick (δ_{lon}), collective lever (δ_{col}), pitch attitude (Θ), lateral cyclic stick (δ_{lat}), pedals (δ_{ped}) and either roll attitude (Φ) or horizontal flight path angle (γ_h), depending on the flight speed. Three of the trim equations result from balancing the aerodynamic forces (X,Y,Z) and gravitational forces acting along each of the axes. The other three result from balancing the aerodynamic moments (L,M,N) acting about the center of gravity. The resulting six equations must be solved simultaneously to determine the necessary values of the six trim variables. The trim equations can be represented by the following six equations:

X-Force:	$\Sigma X(\delta_{lon}, \delta_{col}, \Theta, \delta_{lat}, \delta_{ped}, \phi/\gamma_h; V, \gamma_v, i_{ht}) - mg \sin\Theta = 0$
Y-Force:	$\Sigma Y(\delta_{lon}, \delta_{col}, \Theta, \delta_{lat}, \delta_{ped}, \phi/\gamma_h; V, \gamma_v, i_{ht}) + mg \sin\Phi = 0$
Z-Force:	$\Sigma Z(\delta_{lon}, \delta_{col}, \Theta, \delta_{lat}, \delta_{ped}, \phi/\gamma_h; V, \gamma_v, i_{ht}) + mg \cos\Theta = 0$
Rolling Moment:	$\Sigma L(\delta_{lon}, \delta_{col}, \Theta, \delta_{lat}, \delta_{ped}, \phi/\gamma_h; V, \gamma_v, i_{ht}) = 0$
Pitching Moment:	$\Sigma M(\delta_{lon}, \delta_{col}, \Theta, \delta_{lat}, \delta_{ped}, \phi/\gamma_h; V, \gamma_v, i_{ht}) = 0$
Yawing Moment:	$\Sigma N(\delta_{lon}, \delta_{col}, \Theta, \delta_{lat}, \delta_{ped}, \phi/\gamma_h; V, \gamma_v, i_{ht}) = 0$

In this investigation, the trim conditions were determined numerically using the GENHEL program. As described in Section 3.2, an iterative procedure was used to reduce the three linear and three rotational accelerations below a predetermined convergence criterion.

Since the stabilator is a large horizontal aerodynamic surface, it generates forces and moments that are directly dependent on both the airspeed and the local angle of attack of the stabilator. The local angle of attack of the stabilator is composed of the stabilator incidence with respect to the fuselage (i_{ht}), the trim pitch attitude (Θ) and the downwash from the main rotor (ε_{mr}) and fuselage (ε_{fus}) and is given by the expression

$$\alpha_{ht} = \Theta + i_{ht} + \varepsilon_{mr} + \varepsilon_{fus}$$

Since the forces and moments produced by the stabilator depend on the stabilator incidence,

so will the trim values of the six variables required to balance the forces and moments acting on the aircraft. Of particular interest is the sensitivity of the six independent trim variables to the stabilator incidence over the flight speed range.

4.1.1 Longitudinal Trim

Longitudinal trim is achieved by causing the forces along the X-axis (horizontal forces), the forces along the Z-axis (vertical forces) and the moments about Y-axis (pitching moments) to be balanced resulting in zero net linear and rotational acceleration in the longitudinal plane of the aircraft. This is primarily achieved through the use of the longitudinal cyclic and collective controls and the pitch attitude. In the longitudinal plane of the aircraft, defined by the X and Z axes, the longitudinal cyclic and collective controls determine the orientation of the main rotor with respect to the fuselage while the pitch attitude determines the orientation of the fuselage with respect to the flight path. By manipulating these three variables, the fuselage and main rotor can be oriented in such a way that the horizontal and vertical forces and pitching moments acting on the aircraft are roughly balanced. To be rigorous, the lateral cyclic, pedals and roll attitude/horizontal flight path angle also play a role in trimming the longitudinal forces and moments due to coupling between the degrees of freedom.

The stabilator, as an aerodynamic surface, will add components of vertical and horizontal force to the force summations and, due to the moment arm between the stabilator and the center of gravity, it will also add a component of pitching moment to the pitching moment summation. Different stabilator settings will require different trim values of longitudinal cyclic, collective and pitch attitude to balance the longitudinal forces and moment acting on the aircraft. Since the loads on the stabilator also depend on the local dynamic pressure, the stabilator will generate larger forces and moments at higher speeds and so variation in the stabilator incidence at higher flight speeds should cause greater variations in the trim values of the variables used to trim the aircraft.

The pitch attitude trim map, presented in Figure 4.1, shows that the trim pitch attitude exhibits a strong dependence on flight speed and stabilator incidence. At flight speeds below twenty knots, the trim pitch attitude is positive, or nose up, at about five degrees and shows little dependence on the stabilator setting. This is due to the low dynamic pressure acting on the stabilator resulting in negligible aerodynamic forces. The

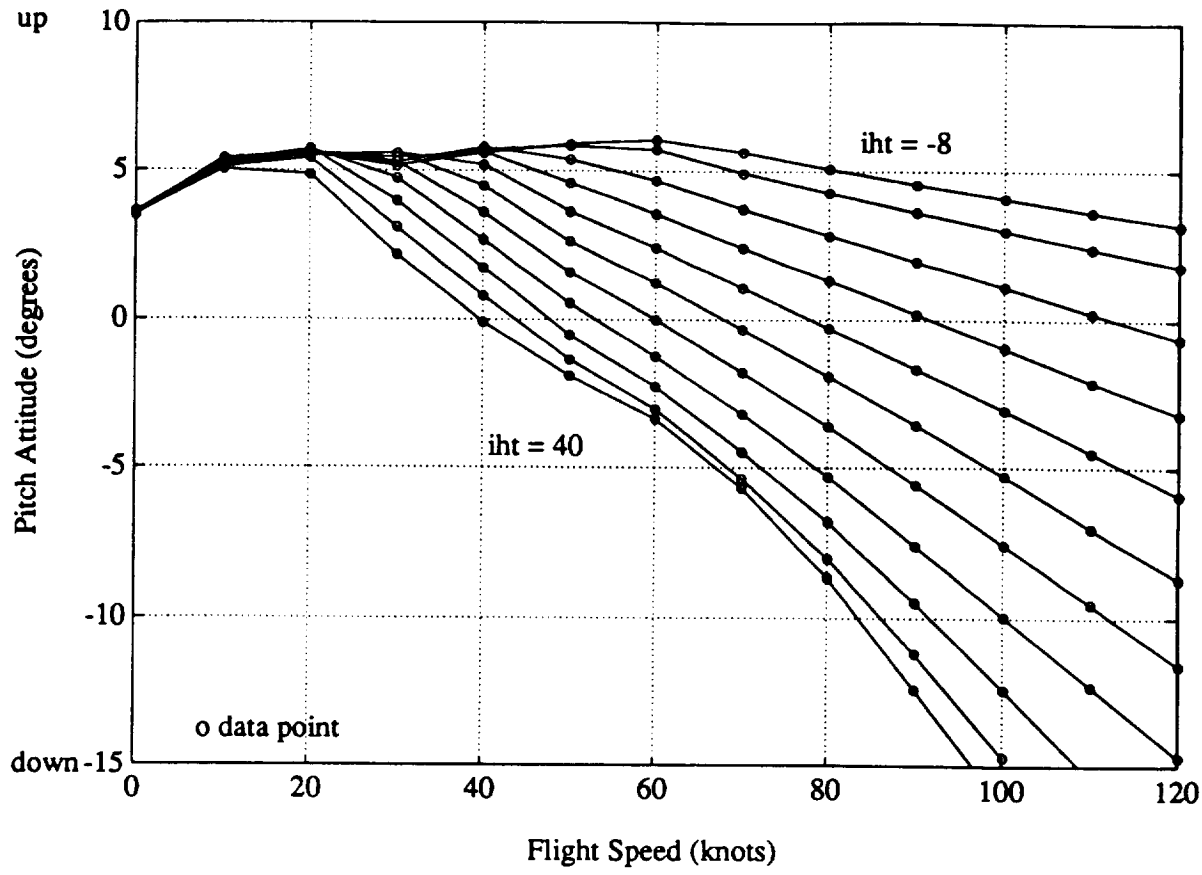

Figure 4.1 Pitch Attitude Trim Map Parameterized by Stabilator Incidence

reason the aircraft trims nose up at low speeds is that the main rotor is located forward of the center of gravity in the configuration chosen in this investigation. Since, at low speeds, the main rotor produces the most significant pitching moment about the center of gravity, the trim pitch attitude and longitudinal cyclic are used to balance the pitching moment acting about the center of gravity by reducing the moment arm between the main rotor thrust and the center of gravity. This causes the aircraft to hang below the rotor in a slightly nose up attitude.

As the flight speed increases, the pitch attitude trim map indicates that the effect of the stabilator on the trim pitch attitude also increases. At higher airspeeds, the increments in trim pitch attitude, corresponding to the five degree increments in stabilator, are larger than at lower speeds. This indicates that the stabilator setting has a greater effect on the trim pitch attitude at higher flight speeds. The trim map also shows that as the stabilator incidence becomes more positive, the trim pitch attitude becomes more nose down. Increasing the stabilator incidence will increase the aerodynamic forces that it generates and consequently, the pitching moment that it generates about the center of gravity. The results indicate that as the stabilator incidence is increased, the pitch attitude must be decreased to help balance the forces and moments acting on the aircraft.

The pitch attitude trim map also indicates that, when the stabilator is set at incidences exceeding thirty degrees, the increments in trim pitch attitude are smaller than the rest at a given flight speed. This indicates that the stabilator is not as effective at extreme incidences. This observation can be explained by the stabilator's aerodynamic characteristics (Appendix B). The plot of stabilator lift coefficient vs. local angle of attack (Figure B.1) shows that the stabilator will stall at local angles of attack above sixteen degrees. When the stabilator is at extreme positive incidences, its local angle of attack may be beyond the stall point of the airfoil resulting in a loss in lift causing a loss in pitching moment capability.

The longitudinal cyclic trim map, presented in Figure 4.2, shows that the longitudinal cyclic also exhibits a strong dependence on flight speed and stabilator setting. The longitudinal cyclic is sensitive to the stabilator setting since the fuselage pitch attitude is sensitive to the stabilator setting. The main rotor thrust is required to balance the vertical and horizontal forces on the aircraft. This requires a particular orientation of the main rotor thrust with respect to the flight path. Since the orientation of the main rotor with respect to the flight path is the sum of the attitude of the main rotor with respect to the fuselage and

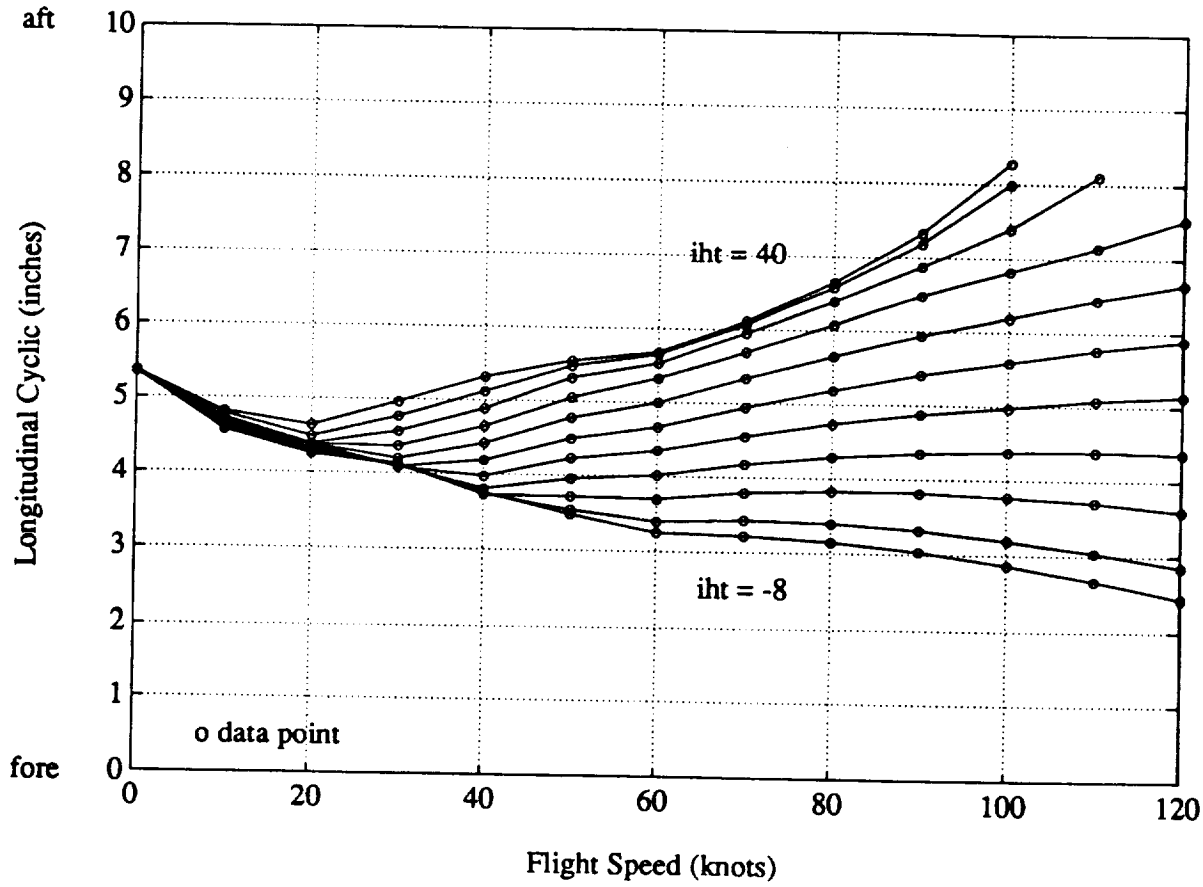

Figure 4.2 Longitudinal Cyclic Control Trim Map Parameterized by Stabilator Incidence

the pitch attitude of the fuselage, and since the longitudinal cyclic controls the orientation of the main rotor with respect to the fuselage, the longitudinal cyclic must be used to compensate for the change in pitch attitude. The results show that at low speeds, the longitudinal cyclic is trimmed near the center of its travel and shows little dependence on the stabilator setting. This is, again, due to the stabilator's negligible force generating capability at low speeds resulting in little change in the trim pitch attitude. The results show that at higher airspeeds, the longitudinal cyclic becomes more sensitive to the stabilator setting. This indicates that as the airspeed increases, greater deflections of the longitudinal cyclic are required to compensate for the pitch attitude. The results also show that as the stabilator incidence becomes more positive, causing the pitch attitude of the aircraft to become increasingly nose down, a greater amount of aft longitudinal cyclic is required to tip the main rotor tip path plane aft in order to maintain the orientation of the main rotor thrust with respect to the flight path.

The collective trim map, presented in Figure 4.3, shows that the trim stabilator incidence has little effect on the collective control trim setting over the flight speed range, particularly at flight speeds below forty knots. At higher flight speeds, the results show that the stabilator incidence does have a small effect on the trim collective position. As the stabilator incidence becomes more positive, the results indicate that there is an increase in the collective pitch of the rotor blades required to provide the thrust necessary to trim the aircraft.

These results point to a number of conclusions about the stabilator's effect on the longitudinal trim state of the aircraft. The stabilator does not produce any significant changes at low speeds due to the lack of sufficient dynamic pressure. At higher forward speeds, the stabilator incidence has a significant effect on the trim pitch attitude and trim longitudinal cyclic position. Because of its effect on the trim pitch attitude, the stabilator could be used to set the trim pitch attitude. The pitch attitude trim map illustrates that the range of trim pitch attitudes that could be selected using the stabilator depends on the flight speed of the aircraft. At low flight speeds, the stabilator has little effect on the trim pitch attitude, but at higher speeds, the stabilator can command a trim pitch attitude range of nearly twenty degrees. It is important to recognize the effect of the trim pitch attitude on the longitudinal cyclic in this type of application. A nose down pitch attitude will require aft cyclic to maintain the main rotor orientation required for steady, level flight. A margin of longitudinal cyclic must be held in reserve to control the vehicle. In this study, at speeds

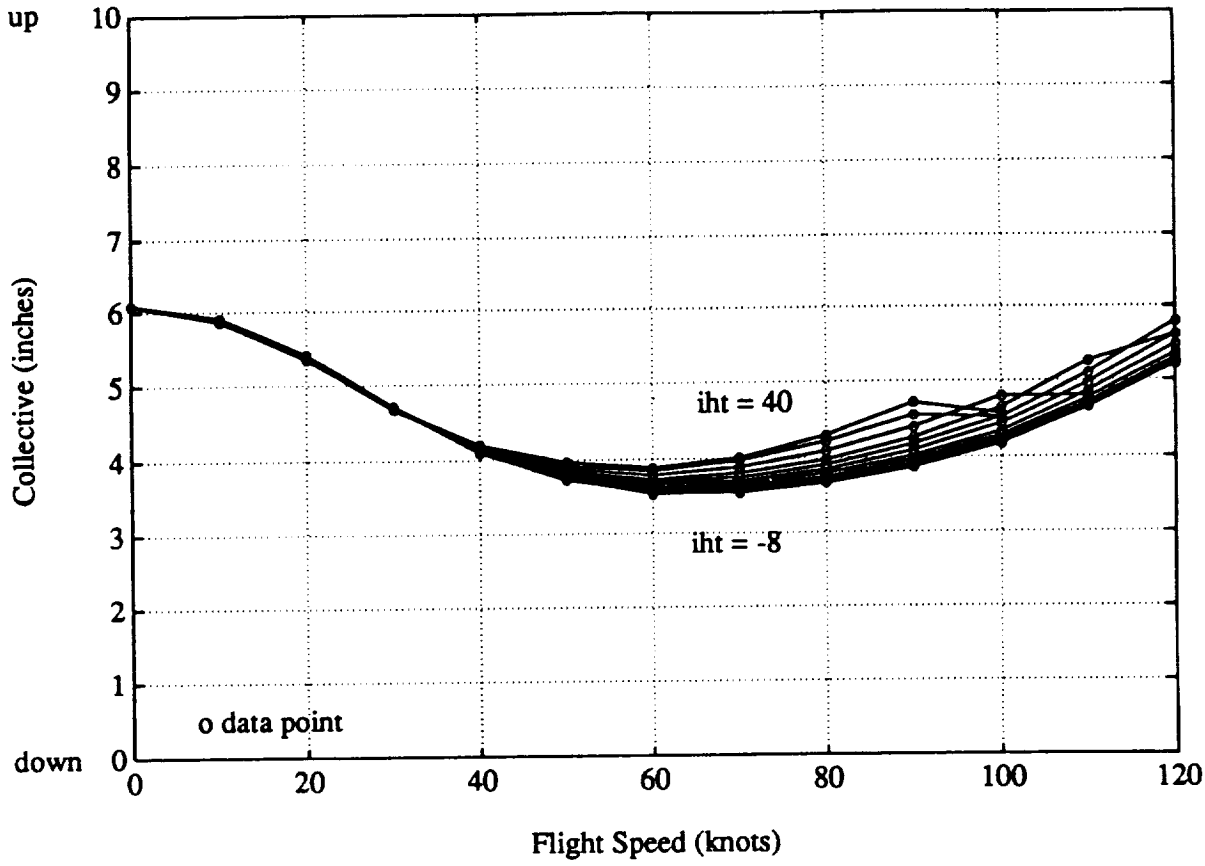

Figure 4.3 Collective Control Trim Map Parameterized By Stabilator Incidence

exceeding 100 knots, extreme positive incidences of the stabilator caused the longitudinal cyclic control to exceed its aft limit. At these conditions, very little aft longitudinal cyclic control is left to the pilot. This is potentially dangerous because it may not leave the pilot and the control system sufficient control power to control the aircraft.

4.1.2 Lateral-Directional Trim

Lateral-directional trim is primarily achieved by manipulating the lateral cyclic and pedal controls and either the roll attitude or the horizontal flight path angle in order to balance the lateral forces and the rolling and yawing moments acting on the aircraft. At low speeds, below sixty knots, roll attitude is used as one of the trim controls and at speeds above sixty knots, horizontal flight path angle is used. This convention was adopted due to pilots' preference when flying the helicopter. The lateral cyclic is used to control the lateral component of the main rotor thrust while the pedals control the tail rotor thrust. The roll attitude or horizontal flight path angle is used as the third trim control necessary to balance the lateral forces and rolling and yawing moments acting on the aircraft.

Since the stabilator is a horizontal tail surface, it produces aerodynamic forces and moments that are primarily in the longitudinal plane of the aircraft so the influence of the stabilator incidence on the lateral-directional trim controls should be minimal. The lateral cyclic trim map, presented in Figure 4.4, indicates very little effect on the lateral cyclic. The pedal trim map, presented in Figure 4.5, shows that at speeds above forty knots, increasing the trim stabilator incidence requires more left pedal to achieve trim. Since the pedals control the tail rotor thrust which is primarily responsible for balancing the yawing moment induced by the drag torque on the main rotor, this variation in pedal demand is correlated to the variation in collective lever position. A comparison of Figures 4.3 and 4.5 shows that both collective and pedals show no variation at flight speeds below forty knots but show similar variation at higher airspeeds. The trim maps of roll attitude and horizontal flight path angle are presented in Figure 4.6. The roll attitude trim map illustrates that while the roll attitude required to trim the aircraft does vary by about two degrees between zero and fifty knot flight speeds, the dependence on stabilator incidence is negligible. This is due to the fact that the stabilator is less effective at low speeds and produces forces and moments in the longitudinal plane of the aircraft. The trim map of horizontal flight path angle shows that when the flight speed is in excess of sixty knots and the horizontal flight path angle is used as one of the trim controls, there is a small variation of about half a

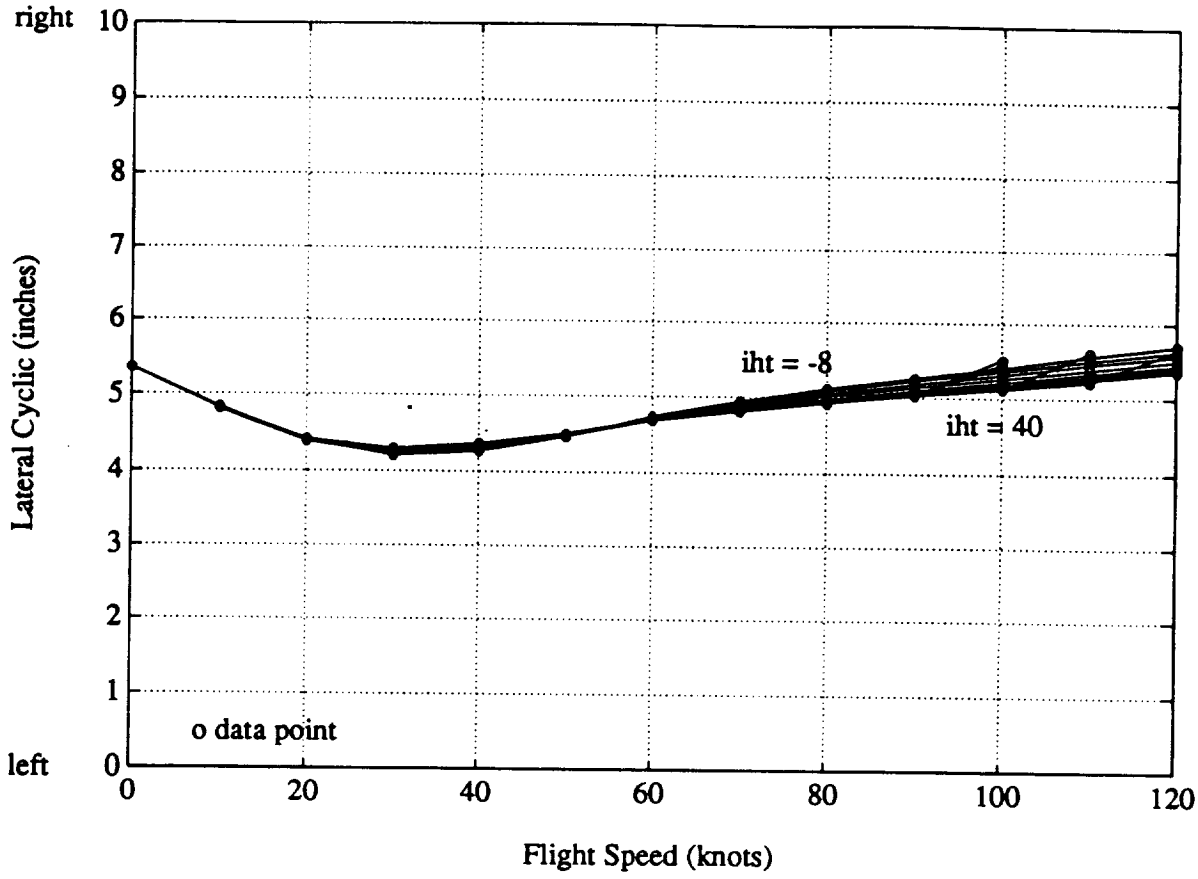

Figure 4.4 Lateral Cyclic Control Trim Map Parameterized by Stabilator Incidence

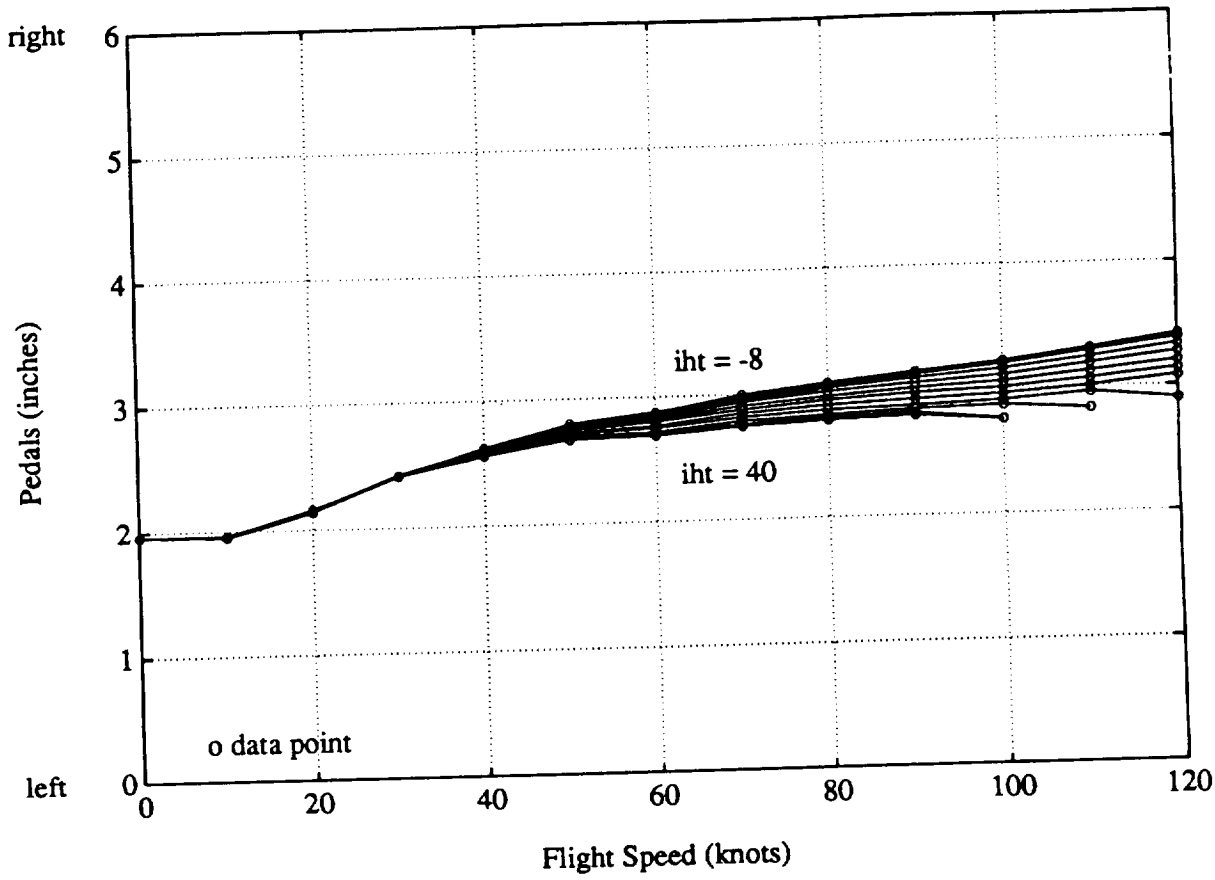

Figure 4.5 Pedal Control Trim Map Parameterized by Stabilator Incidence

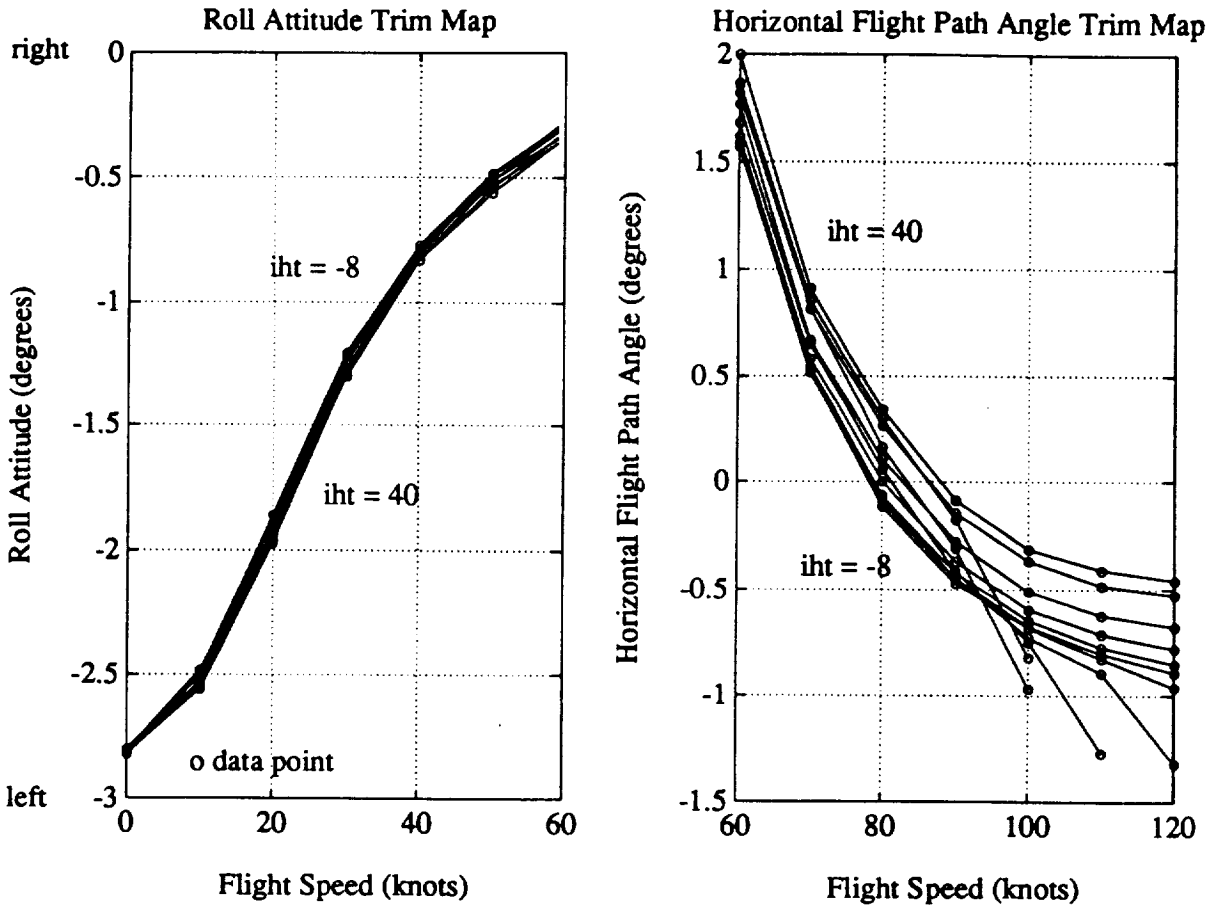

Figure 4.6 Roll Attitude and Horizontal Flight Path Angle Trim Maps Parameterized by Stabilator Incidence

degree of horizontal flight path angle corresponding to the range of stabilator settings.

From these results, it can be concluded that the stabilator is primarily a longitudinal force and moment producing device. The trim stabilator incidence has been shown have very little effect on the trim values of the variables used primarily to trim the lateral-directional forces and moments. The only significant effect of stabilator incidence is on the pedals as a result of the variation in collective demand.

4.1.3 Effect of Center of Gravity Location on Trim Envelope

Since the location of the center of gravity controls the size of the moment arm between the stabilator and the center of gravity, the location of the center of gravity is an important factor to consider in the analysis of the stabilator's power as a trim control. To determine the effect of the location of the center of gravity on the longitudinal trim variables, the center of gravity location was moved longitudinally from its nominal station of 355 inches forward to 345 inches and also aft to 365 inches (see Appendix A). These are the prescribed center of gravity limits for an aircraft weight of 16,700 pounds [9]. Trim conditions corresponding to stabilator settings of eight degrees trailing edge up and forty degrees trailing edge down were computed in a similar manner as above and used to determine the boundaries of the trim envelopes corresponding to the three different center of gravity locations. This issue is significant because it illustrates the amount of control margin that is available in the primary controls for different locations of the center of gravity and different stabilator incidence angles.

The trim pitch attitude envelopes, presented in Figure 4.7, show two important results. The first result is that moving the longitudinal center of gravity affects the size of the pitch attitude trim envelope. When the center of gravity is moved forward, the stabilator's moment arm is increased and so the stabilator becomes a more effective pitching moment generator. When the center of gravity is moved aft, the stabilator's moment arm is reduced and so the stabilator becomes less effective. The second result is that moving the center of gravity causes a vertical translation of the pitch attitude trim envelope. A ten inch deviation in the center of gravity location results in a vertical translation of approximately 2.5 degrees of trim pitch attitude. This is a consequence of changing the moment arm between the main rotor and the center of gravity. Since the main rotor is located forward of the center of gravity, it produces a nose up pitching moment. If the center of gravity is

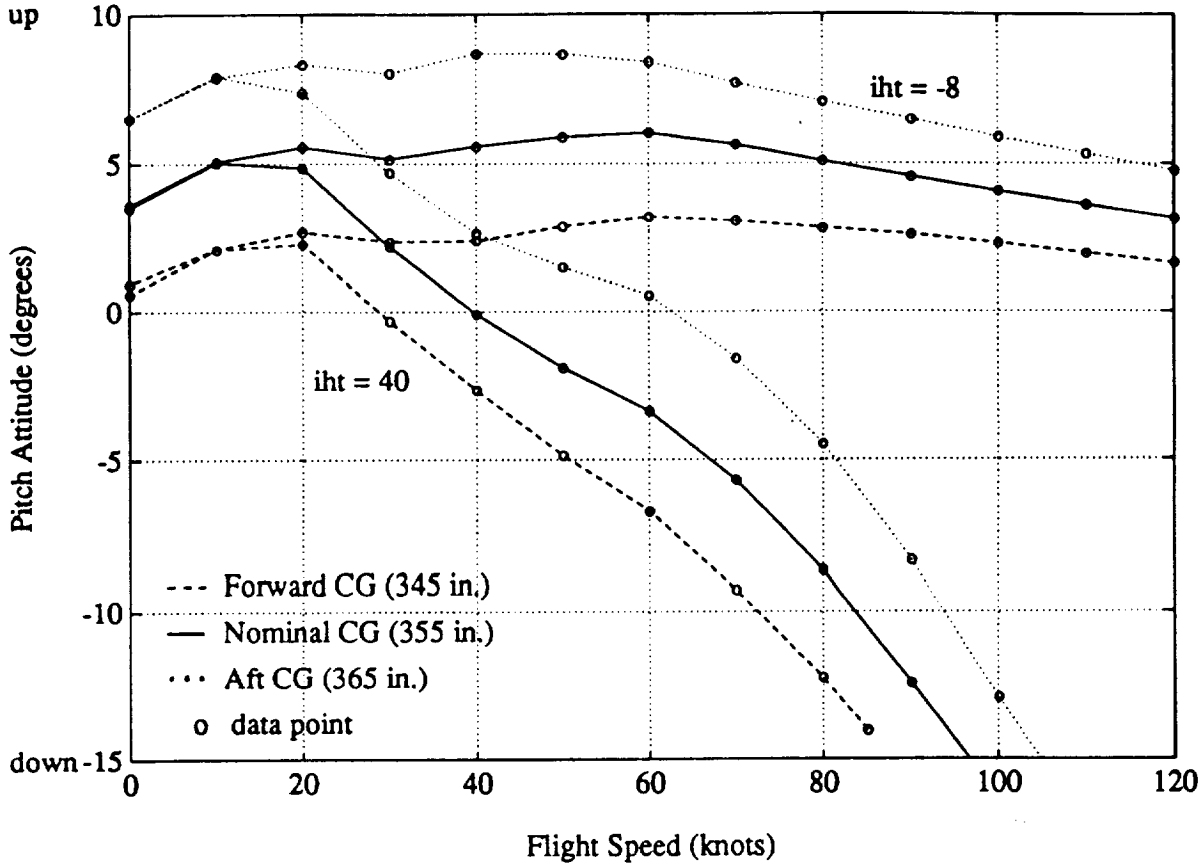

Figure 4.7 Pitch Attitude Trim Envelopes for Three Longitudinal C.G. Locations

moved forward, the moment arm between the main rotor and the center of gravity is decreased, and so is the pitching moment produced by the main rotor. This causes the trim pitch attitude to become more nose down. On the other hand, if the center of gravity is moved aft, the main rotor's moment arm is increased resulting in more nose up trim pitch attitudes.

The longitudinal cyclic trim envelopes, presented in Figure 4.8, show the same type of behavior as the pitch attitude trim envelopes. When the center of gravity is moved forward, the main rotor's moment arm is decreased while the stabilator's moment arm is increased and the resulting longitudinal cyclic trim envelope is larger. This indicates that a greater variation in longitudinal cyclic is required due to the greater variation in pitch attitude. As the center of gravity is moved aft, the opposite occurs and the longitudinal cyclic trim envelope becomes smaller. An important point to note is that, as the center of gravity is moved forward, a greater amount of aft longitudinal cyclic is required to compensate for the nose down pitching moment generated by the stabilator at an incidence of forty degrees. This result indicates that at high speeds, when the center of gravity is in the forward position and the stabilator is trailing edge down, there will be very little longitudinal cyclic left to generate nose up moment for control purposes. At higher flight speeds, when the stabilator is at an extreme trailing edge down incidence, the longitudinal cyclic cannot be pushed to its aft stop due to deflection limits in the actual control linkage between the pilot's stick and the swashplate. At these flight conditions, the aft limit of the longitudinal cyclic is approximately eight inches.

The plot of the collective control trim envelopes, presented in Figure 4.9, indicates that the longitudinal location of the center of gravity has little effect on the collective trim envelope. The results indicate that a greater amount of collective blade pitch is required when the center of gravity is moved forward.

These results show that the longitudinal location of the center of gravity has an important effect on the trim envelopes of the pitch attitude and longitudinal cyclic. From these results, it can be seen that the pitch attitude and longitudinal cyclic trim envelopes are more sensitive to the longitudinal location of the center of gravity than the collective trim envelope. This is due to the fact that the location of center of gravity affects the pitching moment balance which is achieved using primarily pitch attitude and longitudinal cyclic. This analysis points to the conclusion that the location of the center of gravity has a significant effect on the trim pitch attitude range and the longitudinal cyclic control margin.

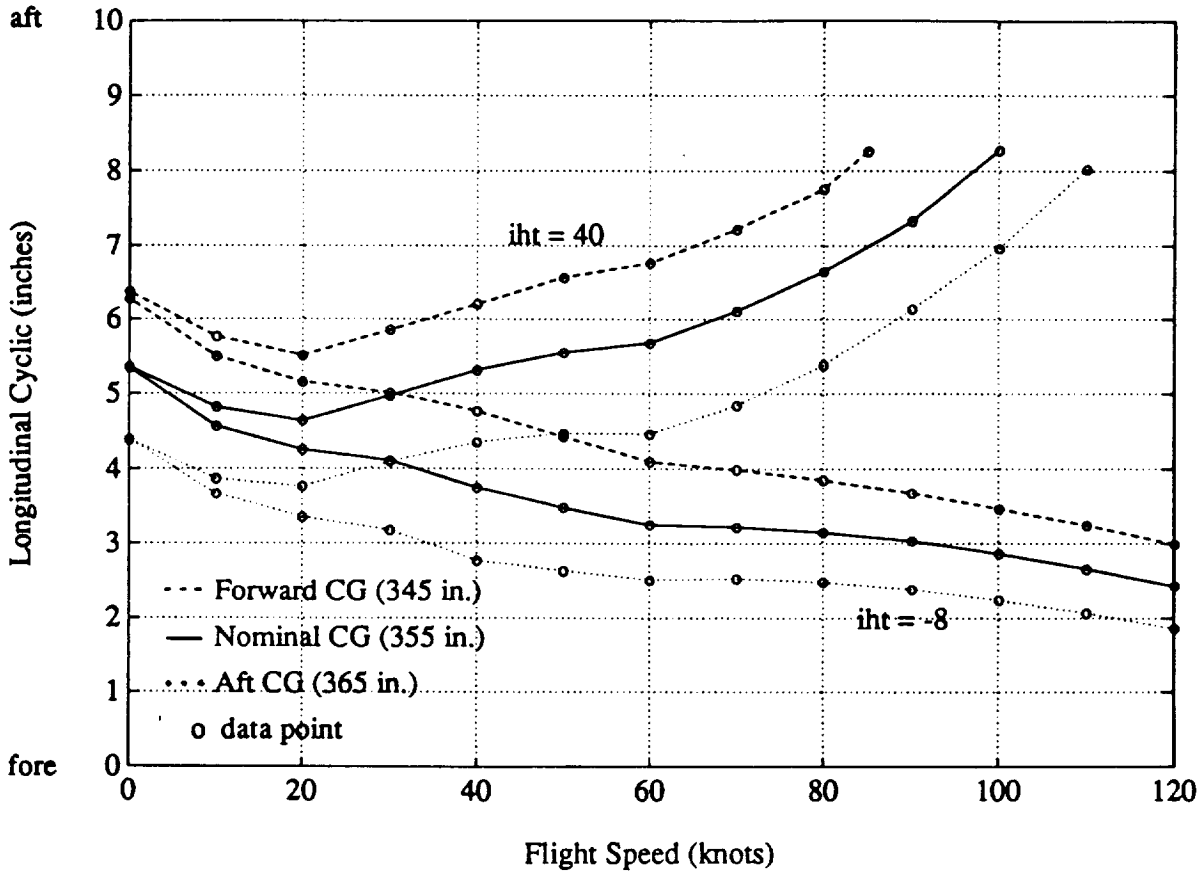

Figure 4.8 Longitudinal Cyclic Control Trim Envelopes for Three Longitudinal C.G. Locations

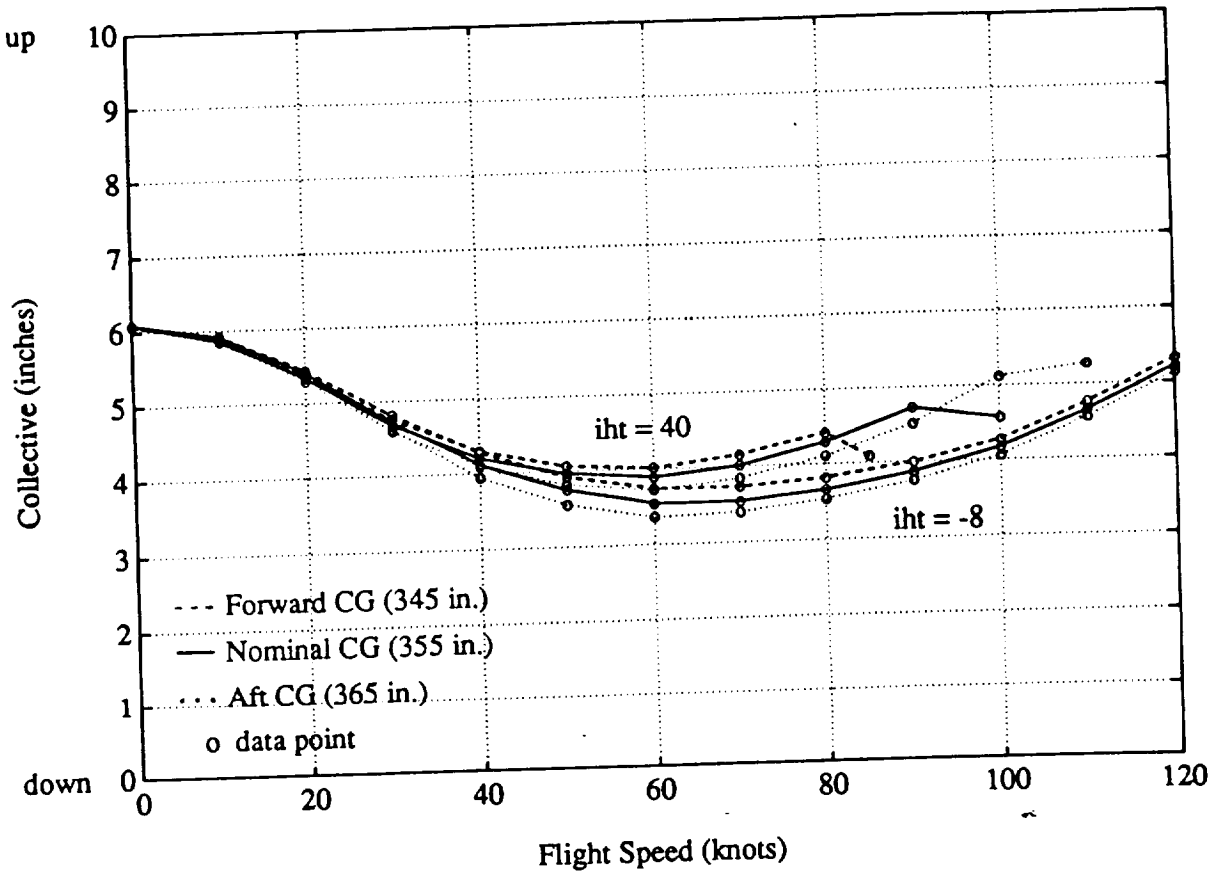

Figure 4.9 Collective Control Trim Envelopes for Three Longitudinal C.G. Locations

The center of gravity must be placed such that there is sufficient aft longitudinal cyclic to provide the control power required to maneuver within the operational flight envelope.

4.2 Control Effectiveness Comparison

The trim analysis illustrates the relationship between the primary controls and the stabilator and it can be seen that, at higher airspeeds, the stabilator incidence has a more pronounced effect on the deflections of the longitudinal pilot controls, particularly the longitudinal cyclic. As an active control, the stabilator must interact with the other controls to produce the desired aircraft response. To determine how the stabilator might be exploited as a fifth control, its force and moment generating capabilities were compared to those of the other controls with which it would have to interact. This analysis is intended to expose the stabilator's strengths and weaknesses relative to the other longitudinal controls and provide an indication as to how the stabilator could be utilized in a flight control system.

To compare the force and moment generating capabilities of the different controls, control derivatives were extracted from GENHEL over the flight speed range of 0 to 120 knots in increments of ten knots. To appreciate the effect of the trim incidence of the stabilator on the control derivatives, control derivatives were extracted over the flight speed range for stabilator settings of five degrees trailing edge up and ten and twenty five degrees trailing edge down. The reference frame used in this analysis is the same body fixed right coordinate system described in Section 3.1. It should be kept in mind that the reference frame is fixed in the aircraft and that the orientation of the reference frame with respect to the flight path depends on the pitch attitude. Since the stabilator primarily generates forces and moments in the longitudinal plane, only derivatives of the longitudinal forces (X, Z) and moments (M) were determined. Since the longitudinal cyclic and collective controls are the primary force and moment producers in the longitudinal plane of the aircraft, only the force and moment derivatives corresponding to these two controls were compared with those of the stabilator.

4.2.1 X-Force Effectiveness

The derivatives of X-force with respect to the longitudinal cyclic control are

presented in Figure 4.10. The results indicate that at flight speeds below forty knots, the longitudinal cyclic deflection of one inch will produce a force of roughly 600-700 pounds of force along the X-axis regardless of the stabilator trim incidence. Since the derivative is negative, it indicates that a positive deflection (aft) will result in a force acting in the negative X direction (aft) and a negative deflection will have the opposite effect. At higher flight speeds, the results indicate that the X-force produced by the longitudinal cyclic becomes dependent on the stabilator trim incidence. As the stabilator trim incidence becomes increasingly positive, causing the trim pitch attitude to become increasingly nose down, the results indicate that the X-force produced by the longitudinal cyclic increases.

The X-force derivatives with respect to the collective control, presented in Figure 4.11 show similar trends. At flight speeds below forty knots, an inch of collective will produce roughly 300-400 pounds of force in the positive X direction regardless of the stabilator trim incidence. Since the derivatives are positive, this indicates that increasing the collective deflection (increased collective pitch) will result in an increase in the force in the positive X direction and a decrease in collective deflection will have the opposite effect. However, at higher flight speeds, the X-force produced by the collective becomes dependent on the stabilator trim incidence. As the stabilator trim incidence increases, the derivatives decrease and eventually change sign as the flight speed is increased.

The X-force derivatives with respect to the stabilator, presented in Figure 4.12, also show the same trends. At a flight speed of zero knots, the results indicate that the stabilator produces no X-force. Since there is no airspeed and since the stabilator is not in the rotor's downwash, there is negligible dynamic pressure resulting in no aerodynamic lift. At low airspeeds, the results show that an increase in the stabilator incidence (trailing edge down) will result in an increase in X-force in the positive direction and a decrease in the stabilator incidence (trailing edge up) will result in the opposite. This indicates that at low speeds, increasing the incidence will reduce the drag causing an increase in forward X-force. At higher flight speeds, the derivatives change signs and the stabilator produces larger amounts of X-force as the flight speed is increased. This indicates that, at these flight speeds, increasing the incidence now increases the drag resulting in an increase in the X-force in the negative direction. The results also show that, as the stabilator trim incidence is increased, resulting in more nose down trim pitch attitude, the derivatives increase in magnitude.

The results presented in Figures 4.10-12 show that the longitudinal cyclic produces

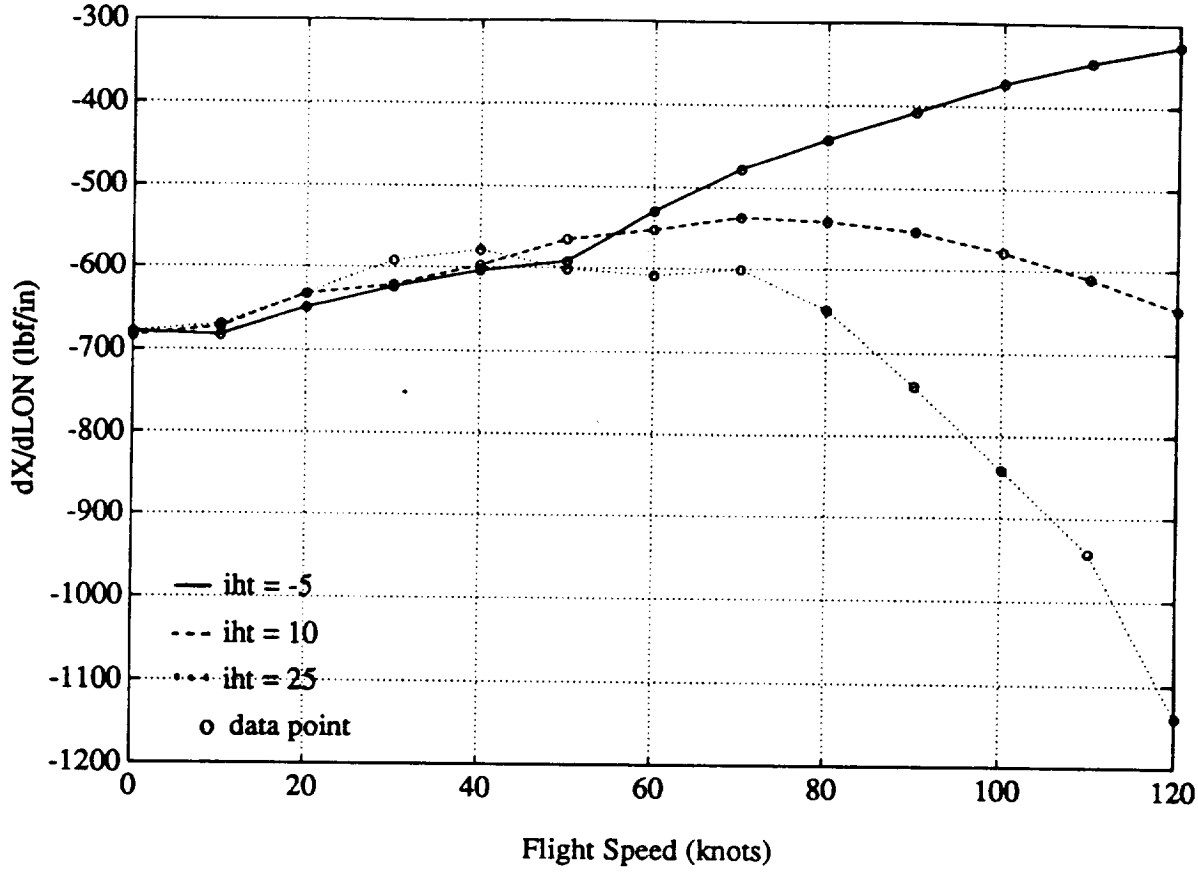

Figure 4.10 Control Derivatives of X-Force With Respect To Longitudinal Cyclic Control

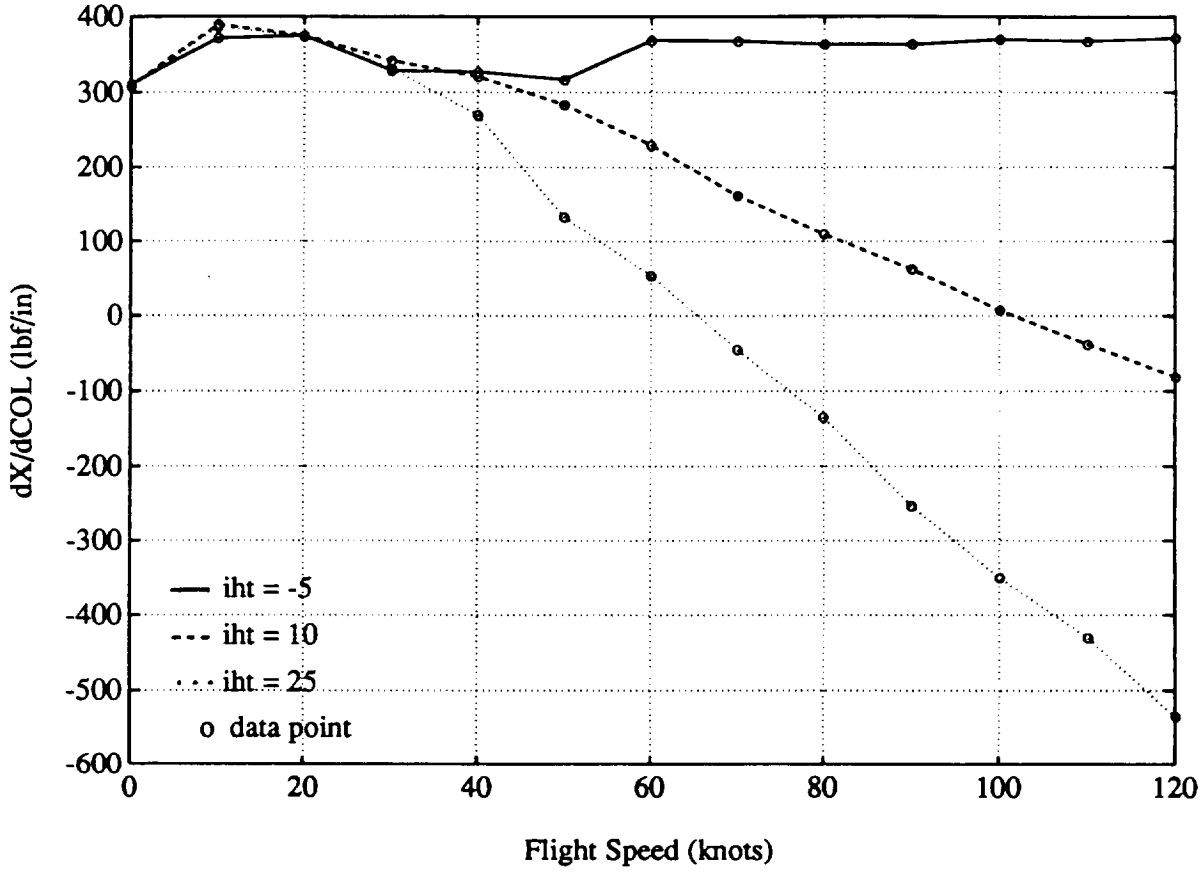

Figure 4.11 Control Derivatives of X-Force With Respect To Collective Control

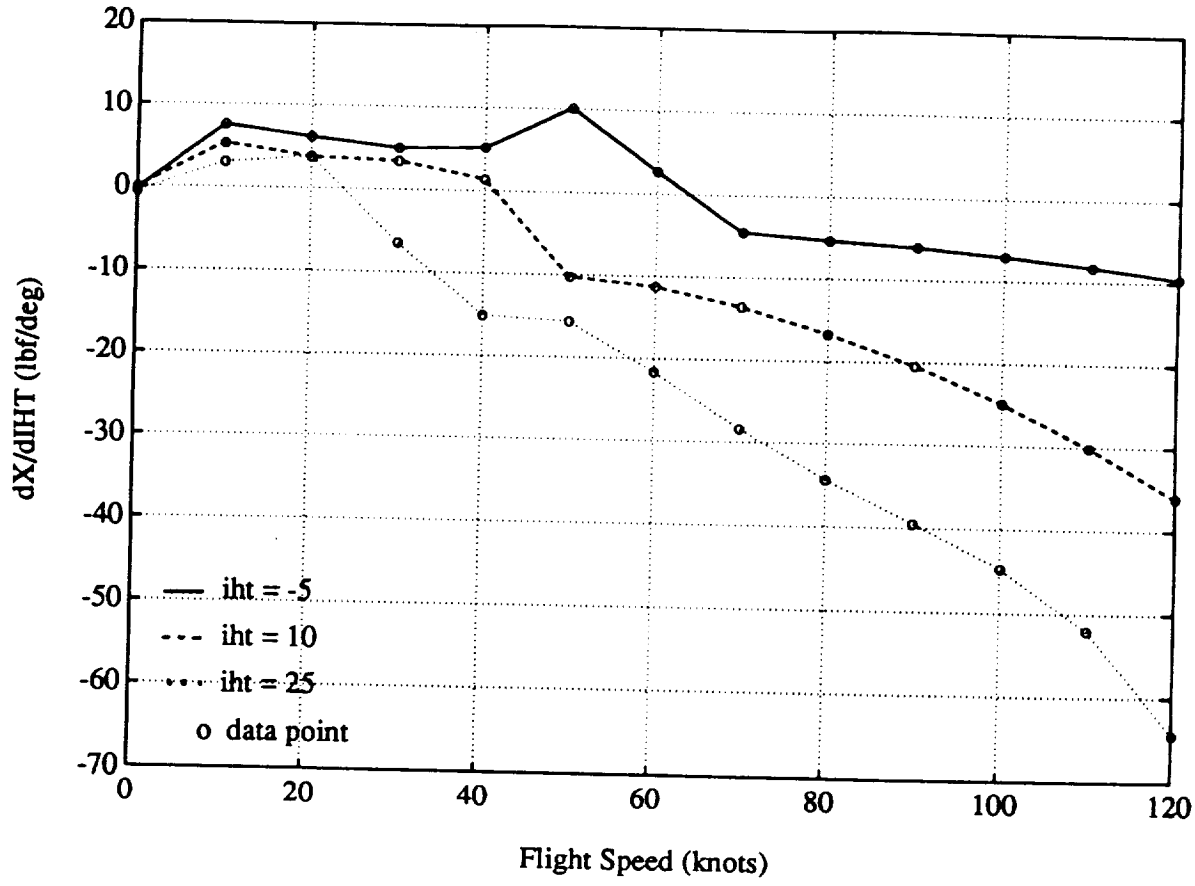

Figure 4.12 Control Derivatives of X-Force With Respect To Stabilator

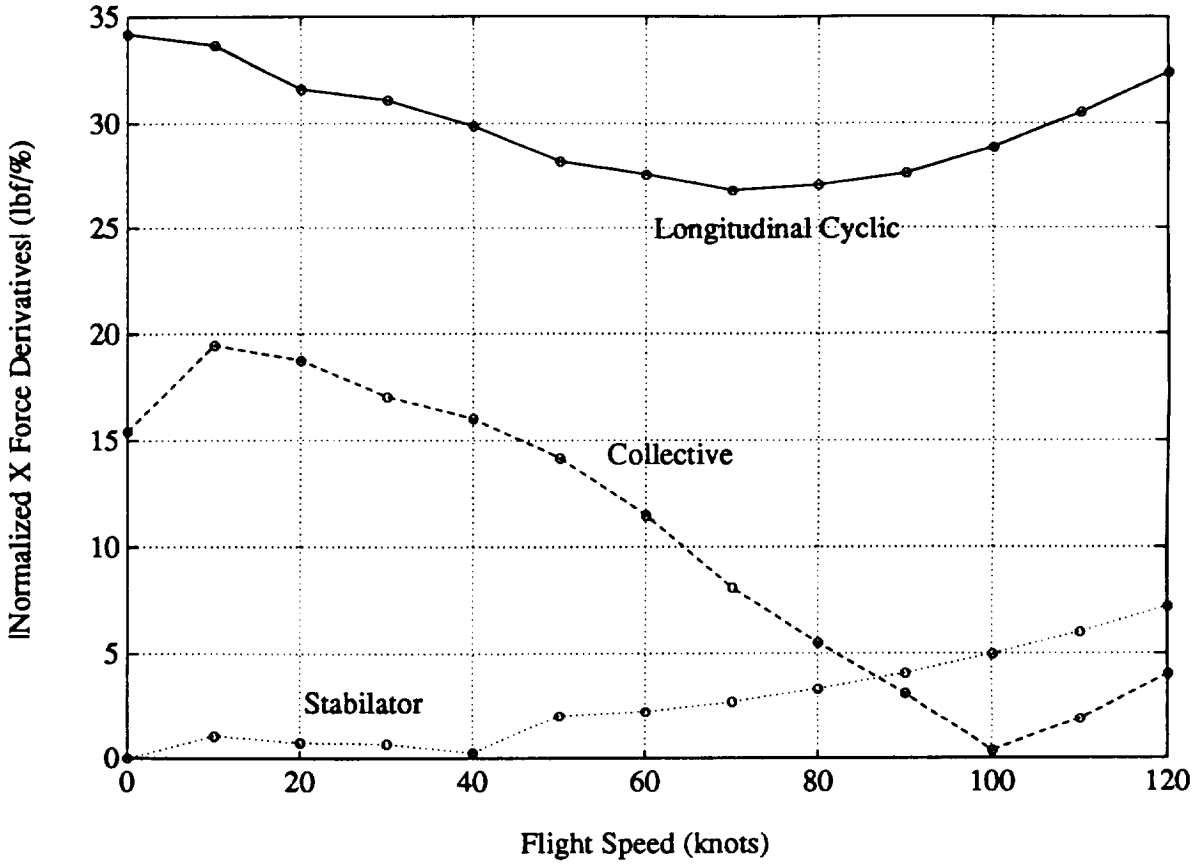

Figure 4.13 X-Force Effectiveness of the Longitudinal Controls with the Stabilator Trimmed at Ten Degrees

the largest X-force derivatives of the three controls. To compare the X-force generating capabilities of the controls, the control derivatives were normalized by multiplying their magnitudes by the maximum control deflections available divided by one hundred percent. This scales all the derivatives to units of force or moment per percent of available control travel. When the stabilator is trimmed at ten degrees trailing edge down, the longitudinal cyclic and the collective have approximately five inches of travel either way and the stabilator has approximately twenty degrees of travel. The results are presented in Figure 4.13 and show that, when the stabilator is trimmed at ten degrees, the longitudinal cyclic is capable of producing the greatest amount of X-force, followed by the collective and then the stabilator. However, at flight speeds exceeding ninety knots, the stabilator is able to produce more total X-force than the collective.

4.2.2 Z-Force Effectiveness

The derivatives of Z-force with respect to the longitudinal cyclic are presented in Figure 4.14. These results indicate that the derivatives of Z-force with respect to longitudinal cyclic increase in magnitude as the flight speed increases but show very little variation with the stabilator trim incidence. The results also show that the derivatives are negative indicating that positive longitudinal cyclic (aft) will produce an increase in Z-force in the negative Z-direction (up) and negative longitudinal cyclic will produce the opposite effect.

The derivatives of Z-force with respect to the collective are presented in Figure 4.15. The results show that the Z-force derivatives with respect to the collective also depend on the flight speed but show little dependence on the stabilator trim incidence when compared to the X-force derivatives. The results show the derivative to be negative, indicating that an increase in collective will cause an increase in Z-force in the negative direction (up).

The derivatives of Z-force with respect to the stabilator are presented in Figure 4.16. The results show that the Z-force derivatives with respect to the stabilator depend on flight speed and, between flight speeds of twenty and sixty knots, on the stabilator incidence. At very low flight speeds, Z-force due to the stabilator is primarily due to aerodynamic lift generated by the stabilator. In the twenty to sixty knot flight speed range, the local angle of attack of the stabilator is affected by the main rotor downwash as well as

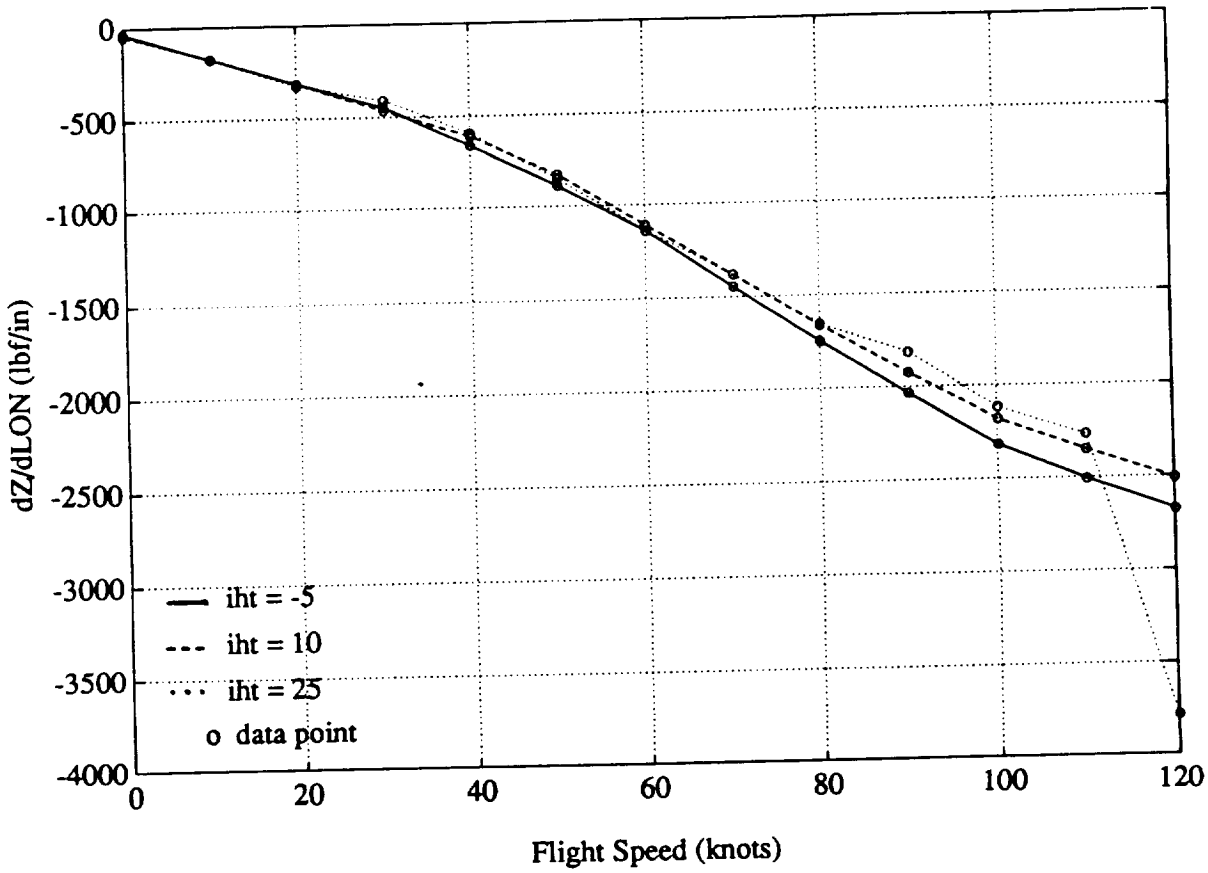

Figure 4.14 Control Derivatives of Z-Force With Respect To Longitudinal Cyclic Control

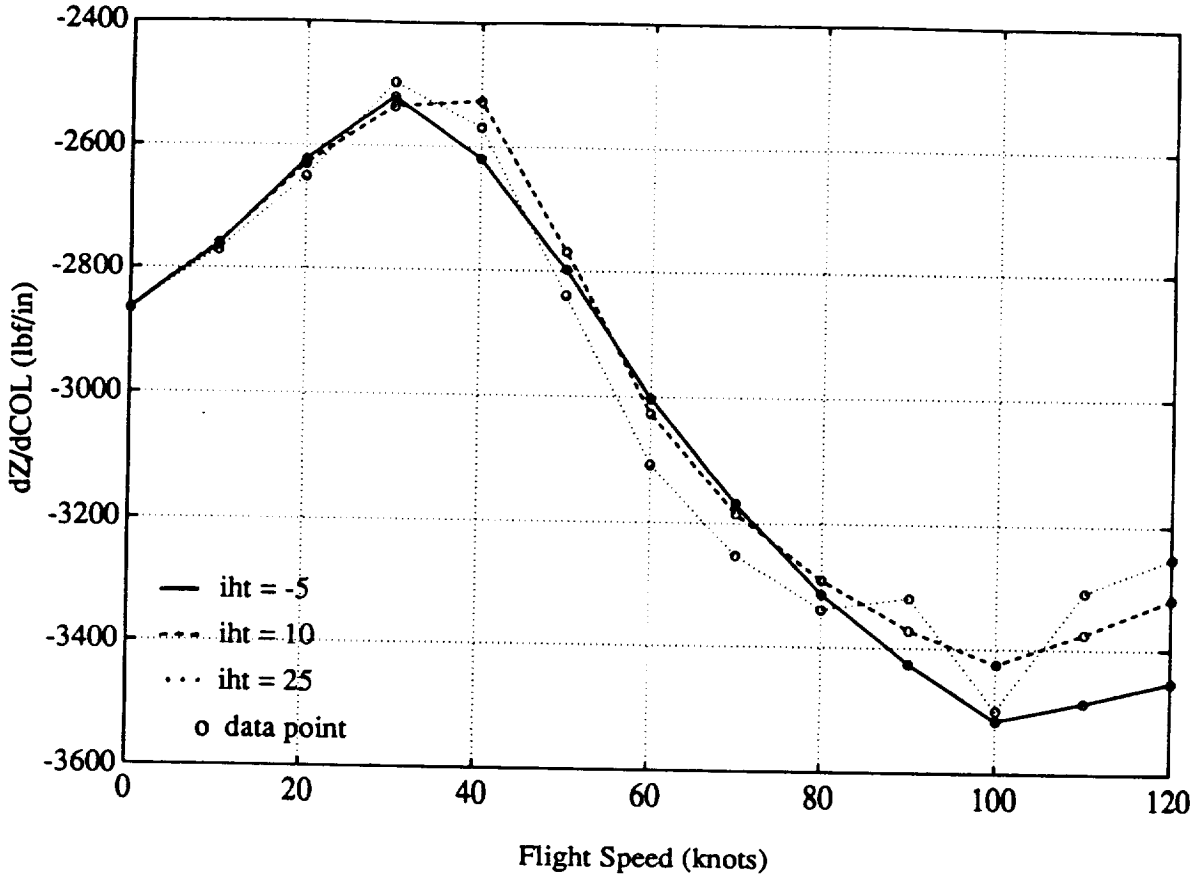

Figure 4.15 Control Derivatives of Z-Force With Respect To Collective Control

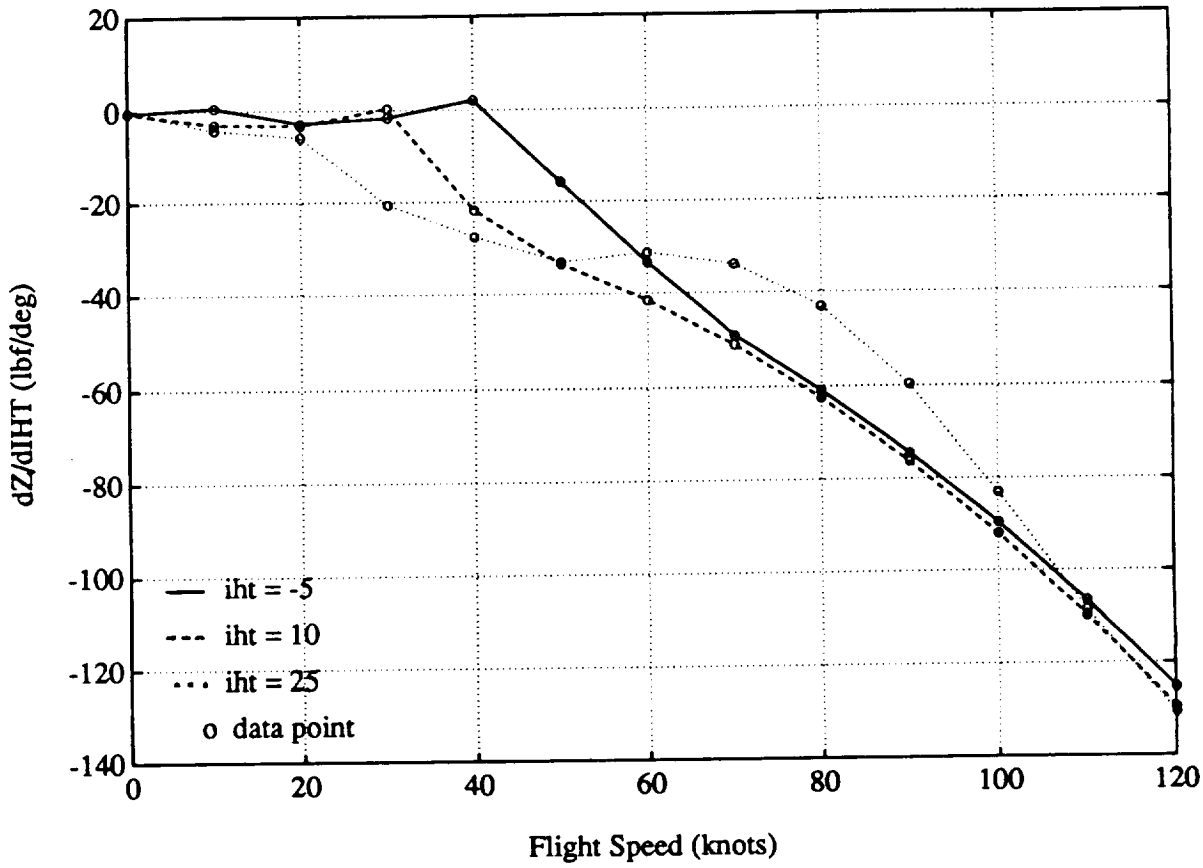

Figure 4.16 Control Derivatives of Z-Force With Respect To Stabilator

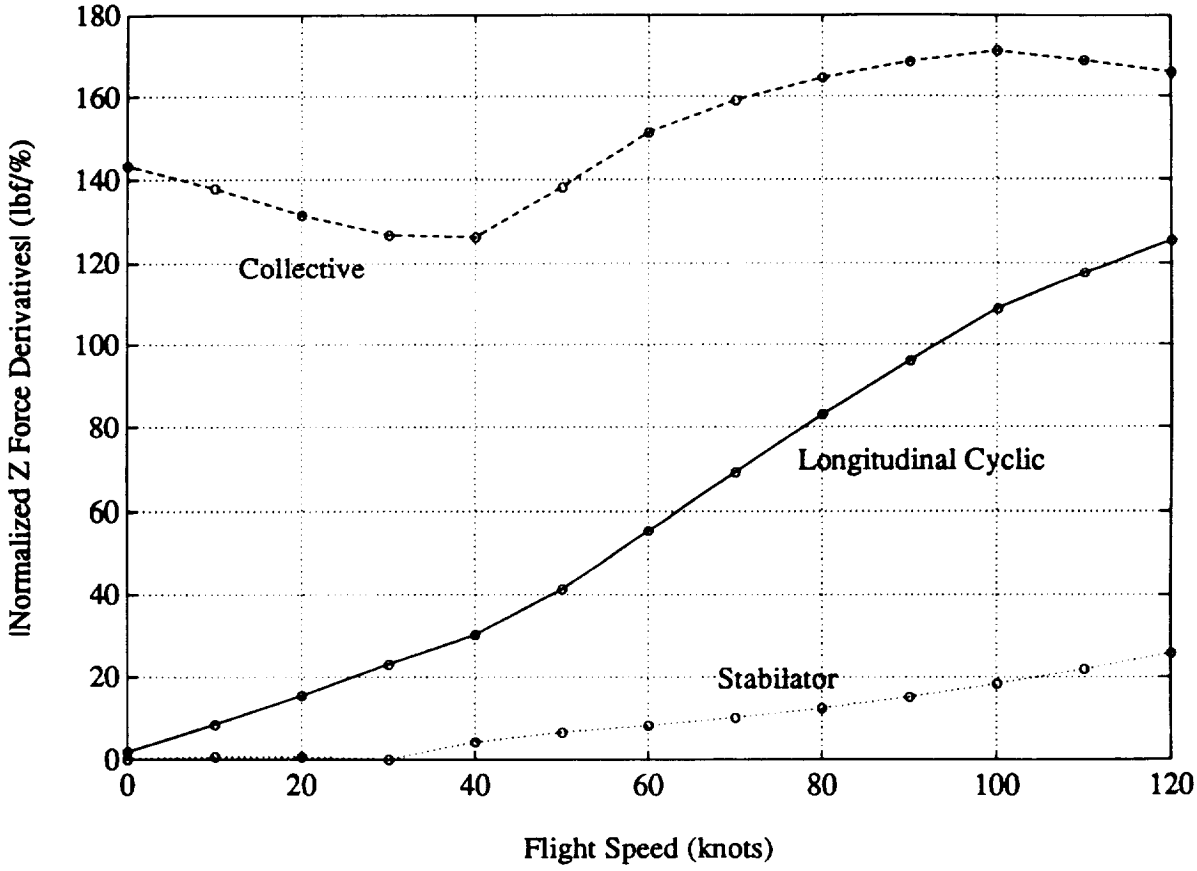

Figure 4.17 Z-Force Effectiveness of the Longitudinal Controls with the Stabilator Trimmed at Ten Degrees

the flight speed resulting in some difference in the force derivative. At higher flight speeds, the derivative continues to increase with the increasing dynamic pressure acting on the stabilator. The derivative of Z-force is negative over the flight speed range indicating that an increase in stabilator incidence (trailing edge down) will cause an increase in Z-force in the negative direction (up) and a decrease in stabilator incidence will have the opposite effect.

The results presented in Figures 4.14-16 show that the collective produces the largest Z-force derivatives of the three controls. To compare the total Z-force generating capabilities of the controls, the control deflection limits were again taken into account by multiplying the magnitudes of the derivatives by the maximum control deflections available divided by one hundred percent. The results are presented in Figure 4.17 and show that, when the stabilator is trimmed at ten degrees, the collective is capable of producing the greatest amount of Z-force, followed by the longitudinal cyclic and then the stabilator.

4.2.3 Pitching Moment Effectiveness

The derivatives of pitching moment with respect to longitudinal cyclic are presented in Figure 4.18. The results are slightly scattered but do show that the derivatives increase with flight speed. The results also show that the derivatives are positive indicating that positive longitudinal cyclic deflection (aft) will result in an increase in a positive pitching moment (nose up) and a negative deflection will have the opposite effect.

The derivatives of pitching moment with respect to the collective are presented in Figure 4.19. The results show that at flight speeds below twenty knots, the derivatives are negative with a positive trend. This indicates that, below twenty knots, an increase in collective will produce a negative pitching moment (nose down) and a decrease in collective will do the opposite. At higher flight speeds, the pitching moment generating capability of the collective reverses and an increase in collective will produce a positive pitching moment (nose up).

The derivatives of pitching moment with respect to stabilator are presented in Figure 4.20. Comparing these results to the Z-force derivatives in Figure 4.16 indicates that the pitching moment derivatives are equal to the Z-force derivative multiplied by the moment arm between the stabilator and the center of gravity. That distance is 360.0 inches, or 30.0

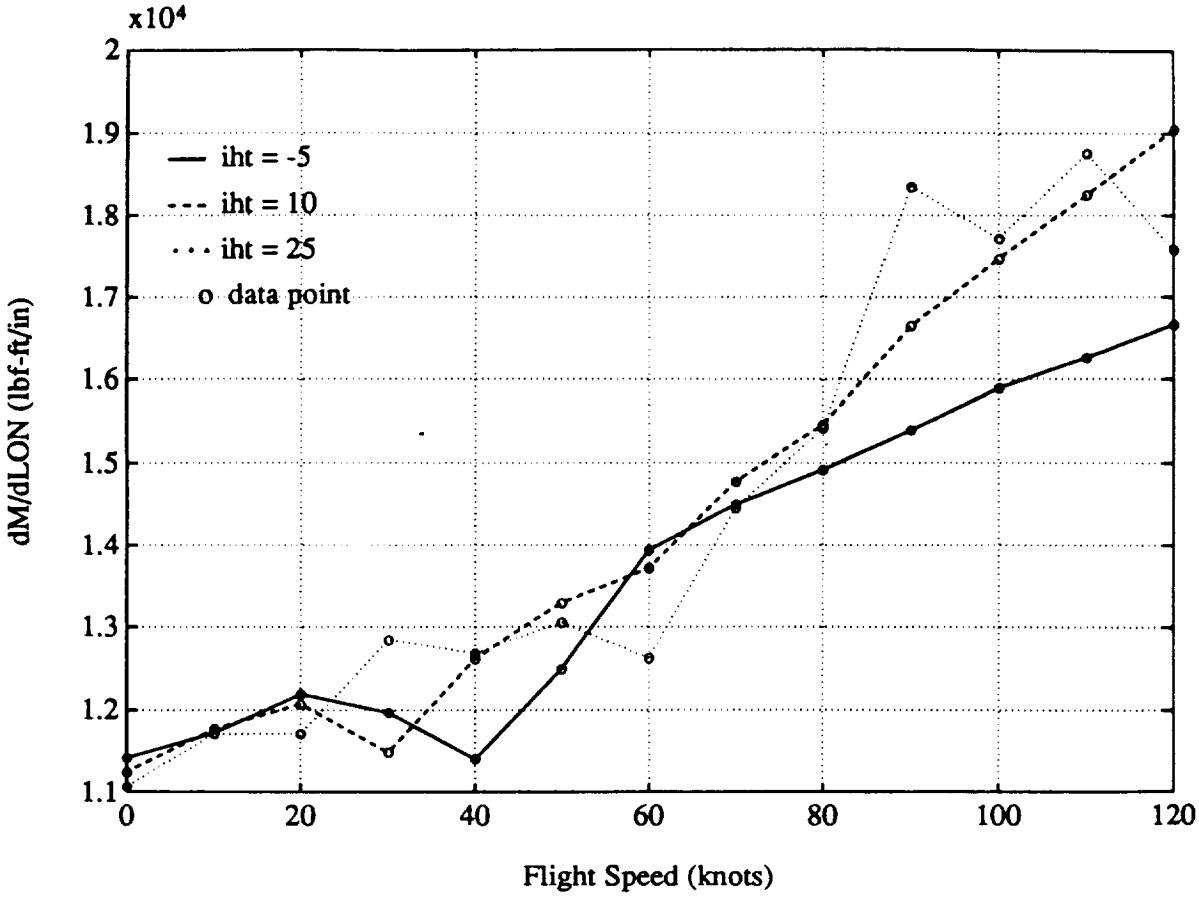

Figure 4.18 Control Derivatives of Pitching Moment With Respect To Longitudinal Cyclic Control

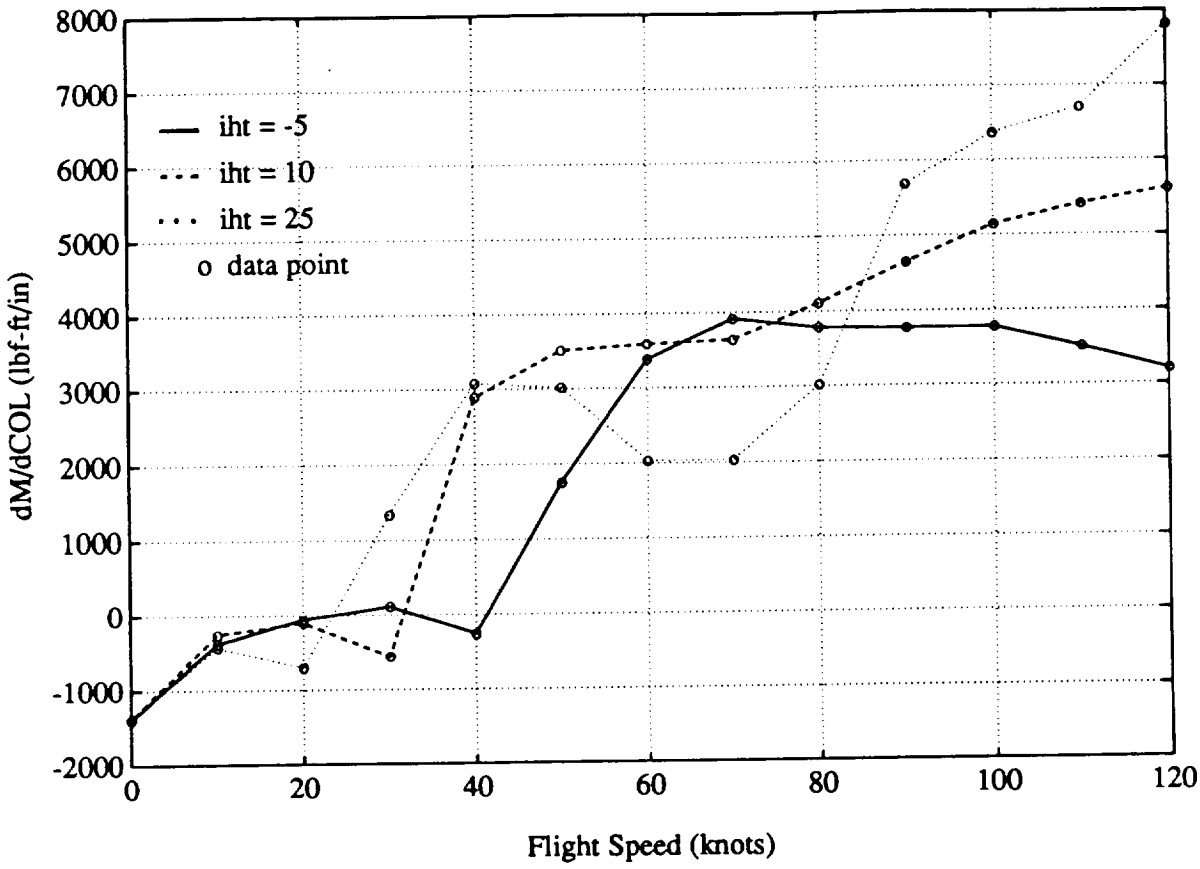

Figure 4.19 Control Derivatives of Pitching Moment With Respect To Collective Control

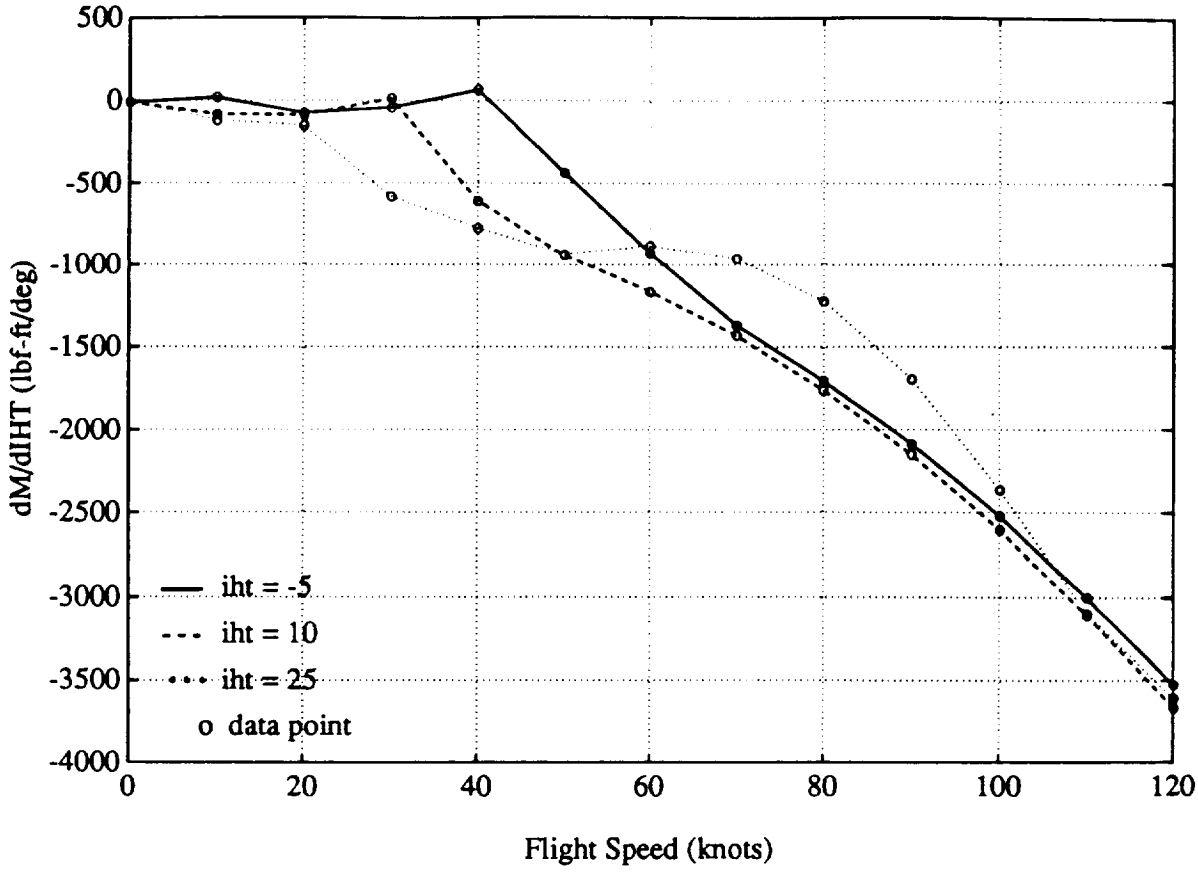

Figure 4.20 Control Derivatives of Pitching Moment With Respect To Stabilator

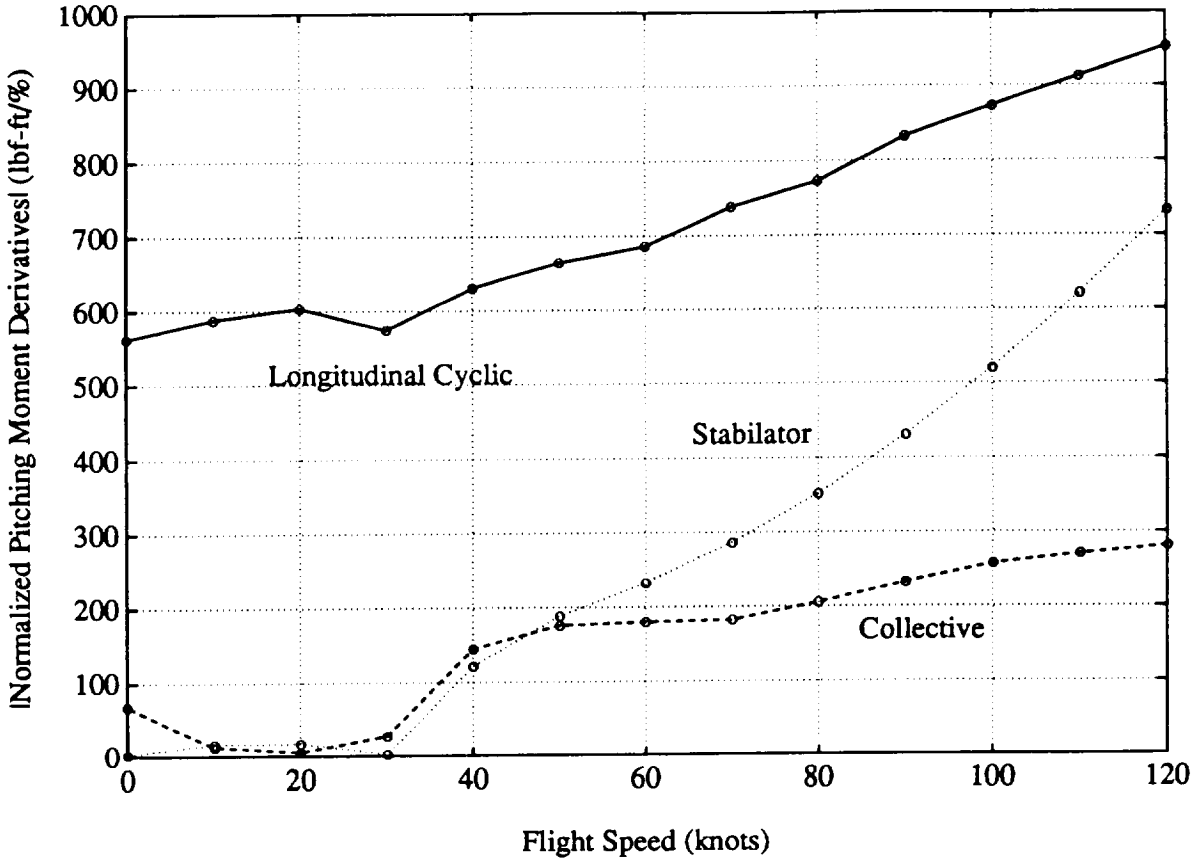

Figure 4.21 Pitching Moment Effectiveness of the Longitudinal Controls with the Stabilator Trimmed at Ten Degrees

feet on the nominal aircraft (Appendix A). The pitching moment derivatives are negative indicating that an increase in stabilator incidence (trailing edge down) will produce a negative pitching moment (nose down) resulting from the increase in Z-force, and that a decrease in stabilator incidence will produce the opposite effect.

The results presented in Figures 4.18-20 show that the longitudinal cyclic produces the largest pitching moment derivatives of the three controls. To compare the total pitching moment generating capabilities of the controls, the control deflection limits were once more taken into account by multiplying the derivatives by the maximum control deflections available divided by one hundred percent. The results are presented in Figure 4.21 and show that, when the stabilator is trimmed at ten degrees, the longitudinal cyclic is capable of producing the greatest amount of pitching moment. At higher flight speeds, the stabilator's pitching moment generating capabilities are significant. From this comparison, it can be concluded that, at the higher airspeeds, if the longitudinal cyclic is limited to about half its travel, the stabilator is capable of producing pitching moments in the same range as the two pilot controls.

From these results, it can be concluded that the stabilator's primary contribution to a flight control system is in the form of additional pitching moment control at the higher flight speeds. The X-force and Z-force comparisons indicate that the stabilator is not capable of producing forces comparable with the other two controls over the flight speed range. However, the stabilator was able to produce pitching moments comparable to the other two controls at high flight speeds. From this analysis, it would seem that the collective should be used to control Z-force, that the longitudinal cyclic could be used to effectively control either X-force or pitching moments and that, at high forward speeds, the stabilator could be used together with the longitudinal cyclic to control both X-force and pitching moment.

4.3 Model Following Performance

To evaluate the addition of the stabilator to the in-flight simulator's control system, the stabilator was included in an explicit model following control system which is described in Section 3.4. By examining the performance of the augmented aircraft and the resultant demand on the controls, the role of the stabilator in this type of control system was assessed. The control system was synthesized using the nine state linear model of the helicopter in steady, level flight at eighty knots as described in Section 3.4. The control

laws were applied to the higher order, thirty one state linear model to evaluate the role of the stabilator as an active control. To evaluate the improvement in system performance offered by the stabilator, the performance of the system with the stabilator was compared to the performance of the system without the stabilator. In addition, the influence of the stabilator actuator dynamics was investigated by adding a simple actuator model to the linear model and examining the resulting performance. In this investigation, the translational rates (u, v) are expressed in feet per second, the rotational rates (p, q, r) are expressed in degrees per second and the rotational angles (γ, θ, ϕ) are expressed in degrees. The pilot control deflections (δ_{lon}, δ_{col}, δ_{lat}, δ_{ped}) are expressed in inches and the stabilator deflection (i_{ht}) is expressed in degrees.

4.3.1 Model Following Performance With Stabilator

The performance of the model following system was evaluated by comparing frequency responses and step response time histories of the system with those of the model of the desired dynamics. Frequency responses of the transfer functions between the command inputs (u_c, γ_c, θ_c) and the system outputs (u, γ, θ) were used to evaluate the accuracy of the system in the frequency domain and expose the errors due to the additional high frequency dynamics. Time histories of the responses of the system to steps in the command inputs were used to evaluate the role that the stabilator plays as an active control in cooperation with the other controls. Time histories of step responses were also used to evaluate the degree of decoupling achieved by the control law. The results were generated using the Matlab Control System Toolbox [18,19].

The behavior of the system over the frequency ranges of interest is presented in Figures 4.22-24. Figure 4.22 shows that the frequency response of the transfer function between forward speed and commanded forward speed matches the frequency response of the desired transfer function at frequencies up to four radians per second where the phase angles begin to diverge due to the high frequency dynamics of the main rotor. This transfer function matches well beyond the desired bandwidth for the system which is 0.05 hertz, or 0.3 radians per second. The frequency response comparison of the transfer functions between flight path angle and commanded flight path angle is presented in Figure 4.23. This comparison shows that the frequency response of the actual system matches that of the desired system up to a frequency of ten radians per second where both the magnitudes and the phases diverge. The frequency response indicates that the magnitude of the actual

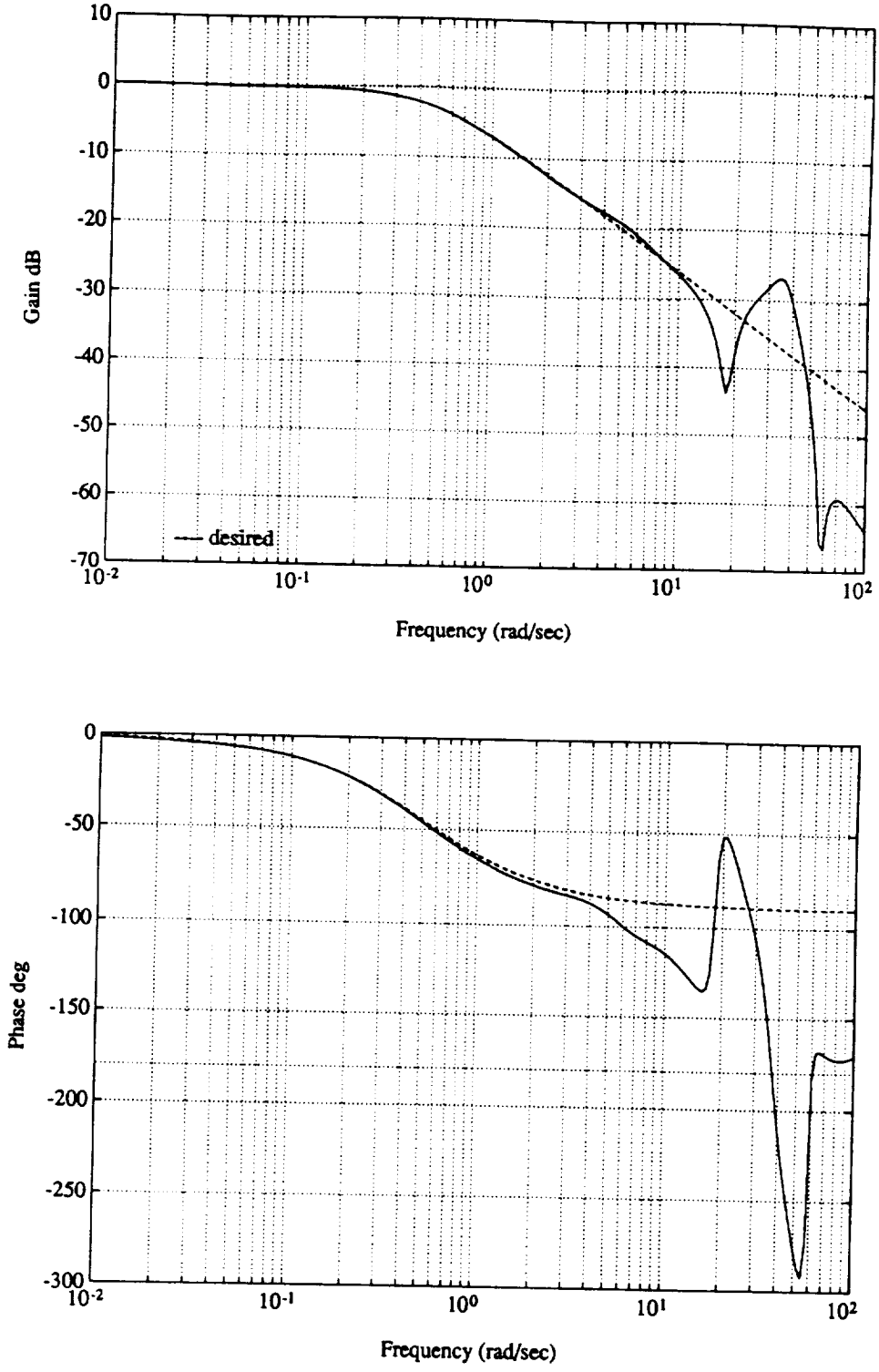

Figure 4.22 Frequency Response of the Transfer Function Between Forward Velocity and Commanded Forward Velocity

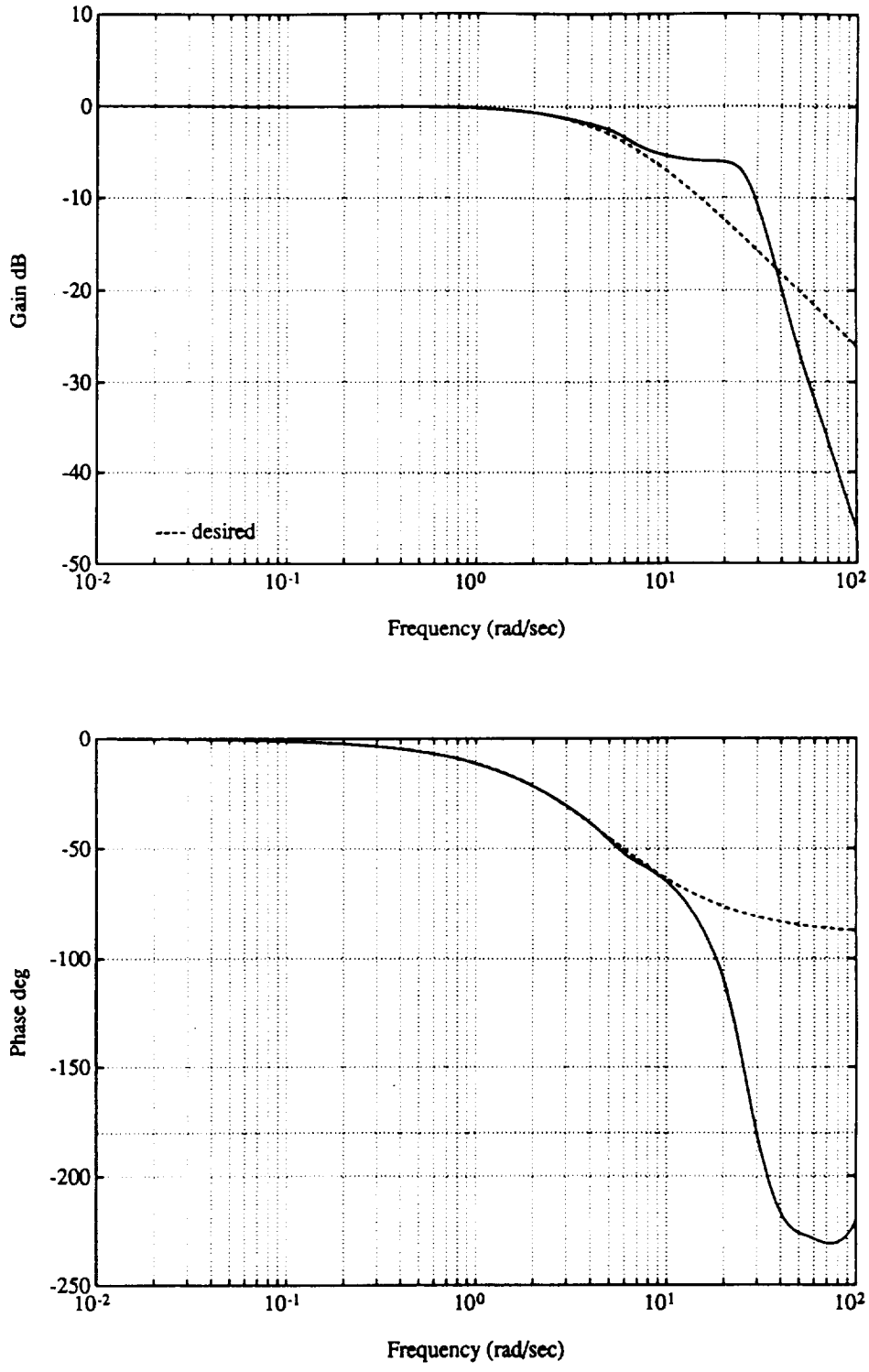

Figure 4.23 Frequency Response of the Transfer Function Between Flight Path Angle and Commanded Flight Path Angle

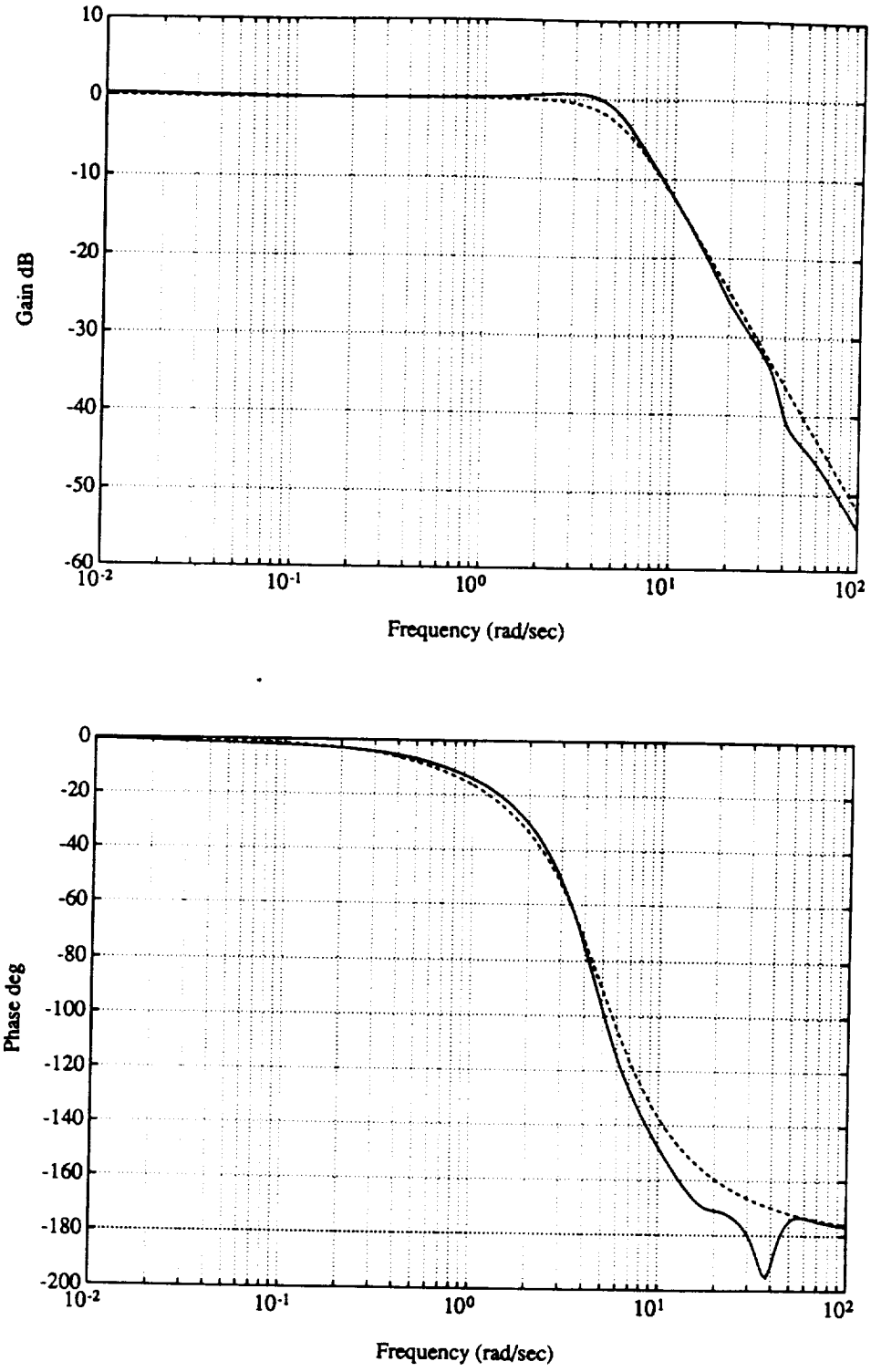

Figure 4.24 Frequency Response of the Transfer Function Between Pitch Attitude and Commanded Pitch Attitude

system possesses a peak at about twenty radians per second which the model does not. However, the frequency responses match in the frequency range below the desired bandwidth of 0.5 hertz, or three radians per second. Finally, Figure 4.24 presents the comparison of the frequency responses of the transfer functions between the pitch attitude and commanded pitch attitude. The frequency responses match well at frequencies below ten radians per second though the actual system exhibits a slightly larger resonance peak indicating that it is not as well damped as desired.

The response of the system to a one foot per second step input in the commanded forward speed is presented in Figure 4.25. The results show that the forward speed tracks the desired forward speed accurately with very little time lag. The other longitudinal responses are regulated well with the pitch rate exhibiting some high frequency response attributed to the main rotor dynamics. The lateral directional responses are also regulated well with the exception of the roll rate, which also exhibits high frequency response to the step input, and the lateral velocity which was left unconstrained and approaches a steady state value of approximately 0.1 feet per second. The plot of the control responses shows that the stabilator is being deflected trailing edge up while the main rotor is being tipped forward with forward longitudinal cyclic stick and the thrust of the main rotor is being increased with positive collective. This indicates that to increase the forward speed the rotor tip path plane must be tipped forward. However, to maintain the trim flight path angle the collective must be used to increase the main rotor thrust. Also, to maintain the trim pitch attitude the stabilator is deflected trailing edge up to provide the nose up pitching moment necessary to balance the increased nose down pitching moment resulting from tipping the main rotor forward.

The response of the system to a one degree step input in the commanded flight path angle is presented in Figure 4.26. The time history of the longitudinal states shows that the flight path angle tracks the desired flight path angle with some high frequency error but with little steady state error, which was predicted by the frequency response in Figure 4.23. The results show that the pitch rate again exhibits some high frequency response to the step input. The pitch attitude and the forward speed show very little deviation from the trim values. The lateral directional responses indicate some high frequency response in the roll rate and also some response in the yaw rate though the roll attitude and integral of the yaw rate show little deviation from the trim values. The lateral velocity also exhibits a slow increase in response to the flight path angle step input. The control responses indicate that

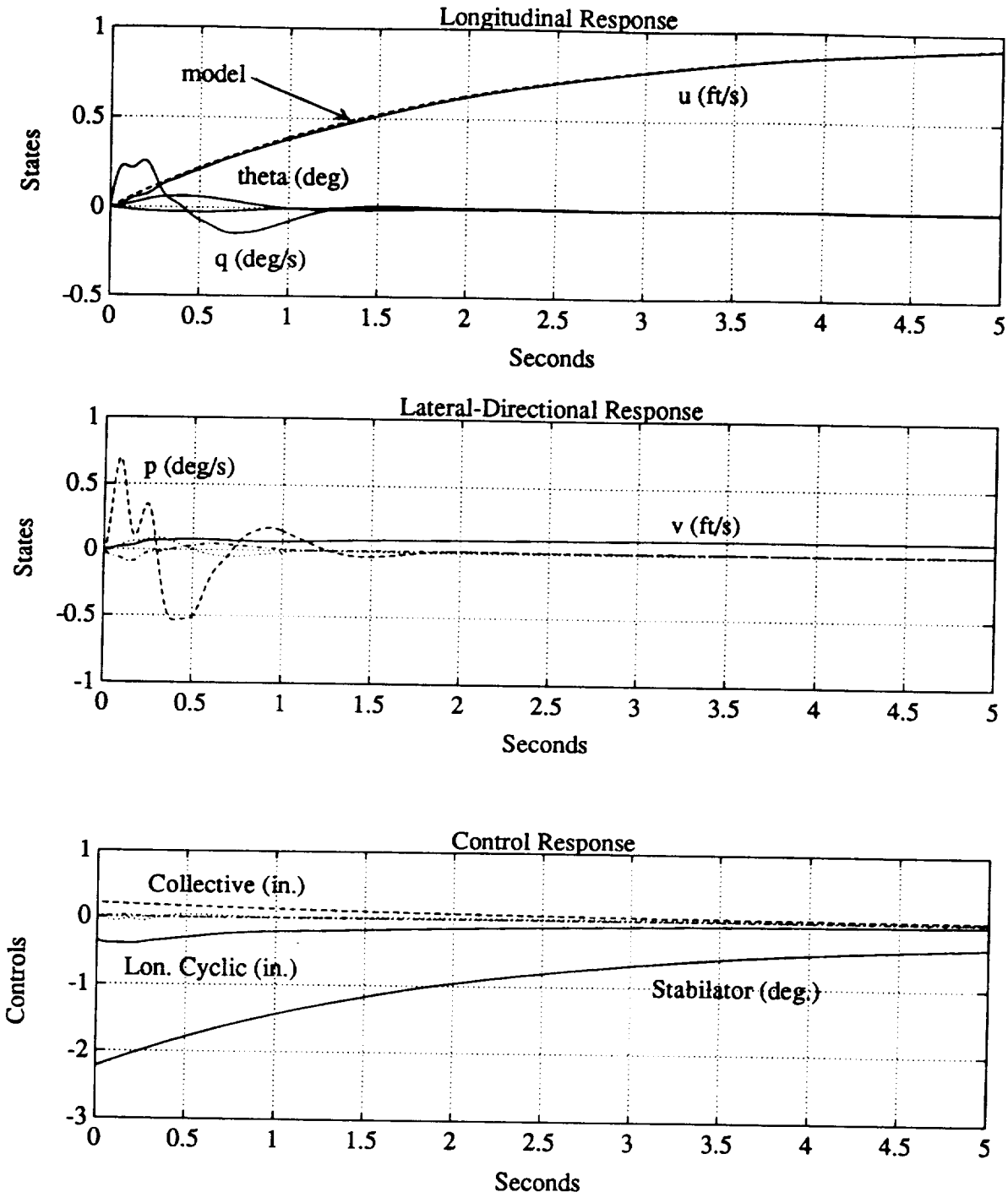

Figure 4.25 Response of the Model Following System to a One Foot Per Second Step Input in Commanded Forward Velocity

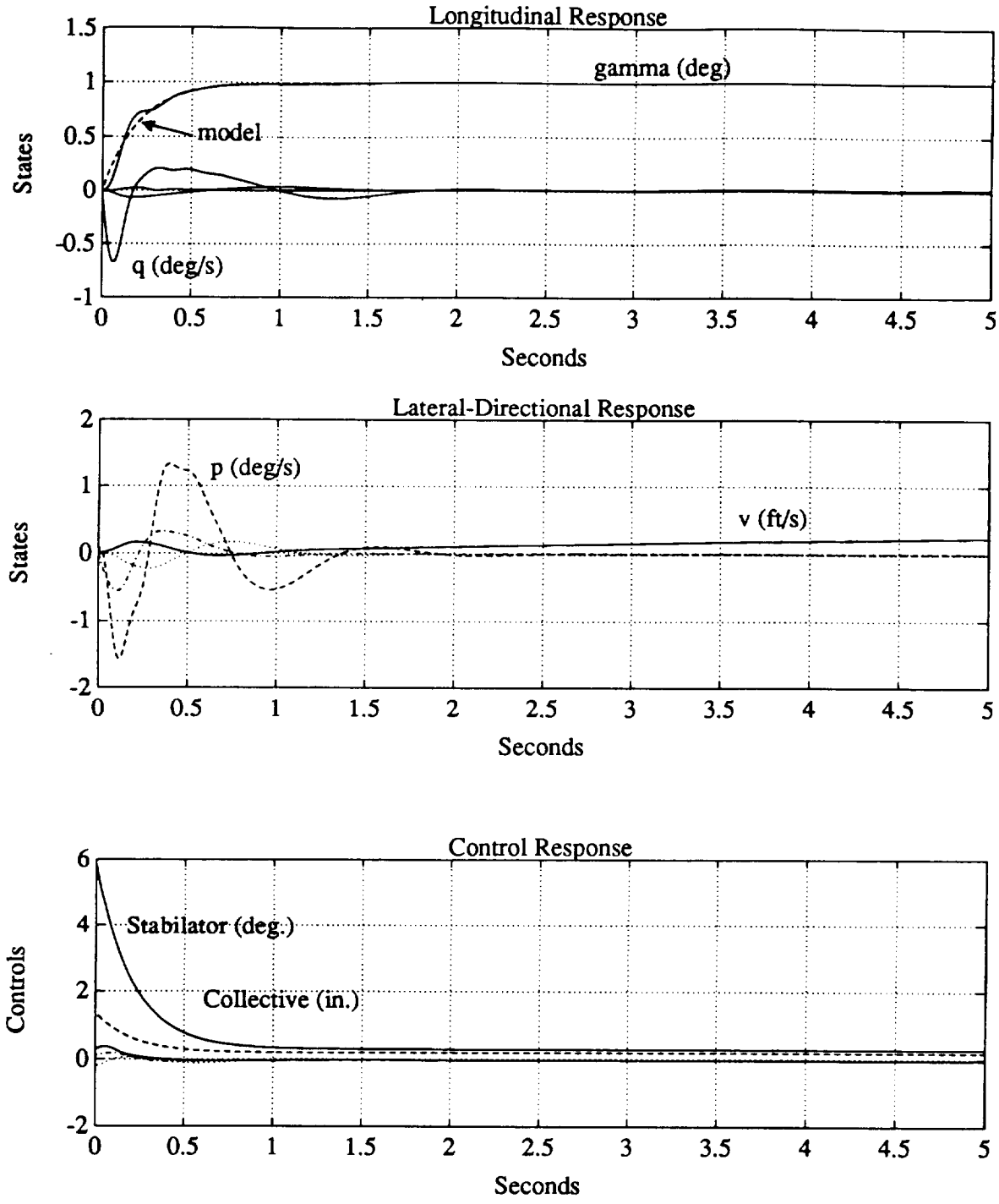

Figure 4.26 Response of the Model Following System to a One Degree Step Input in Commanded Flight Path Angle

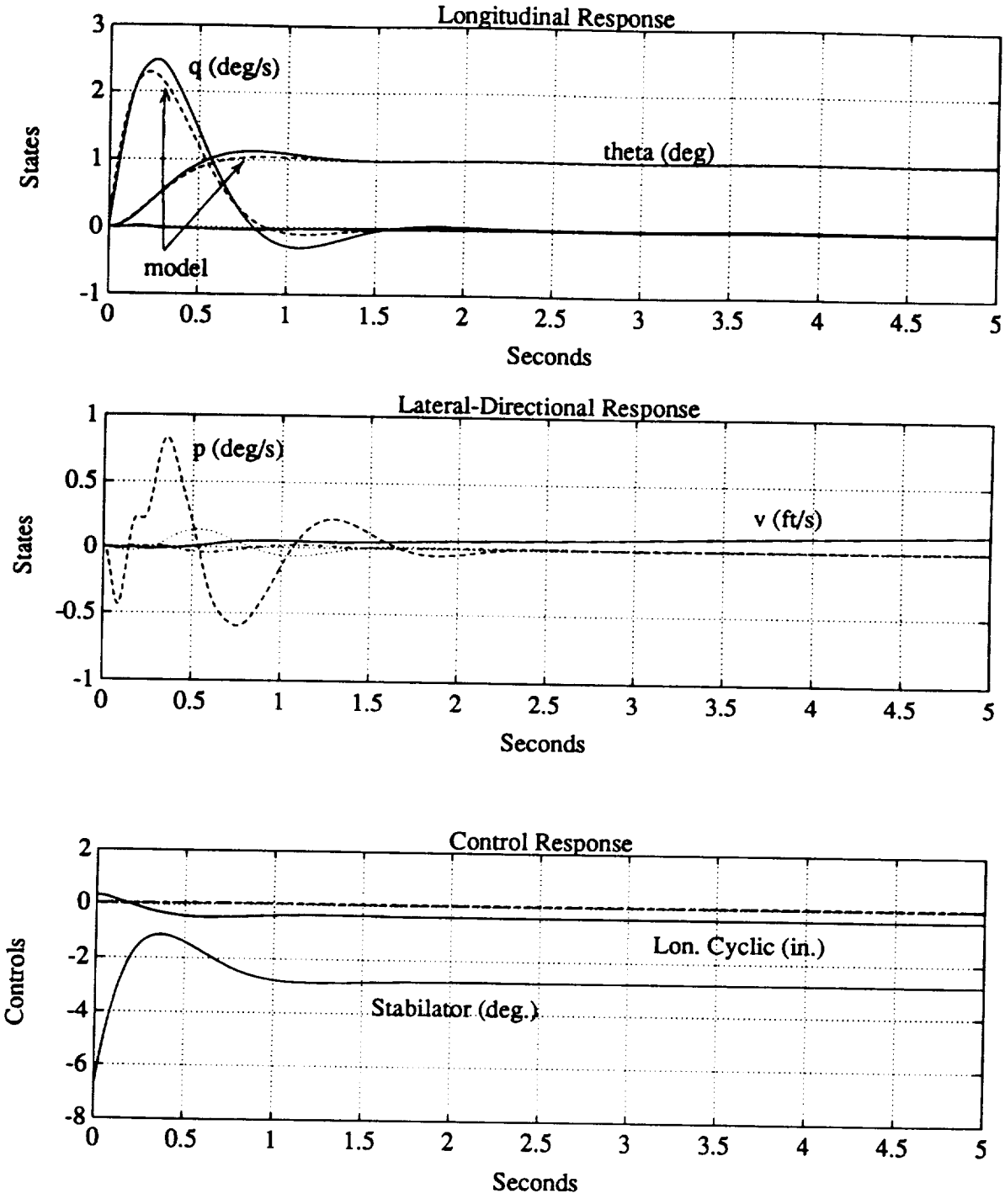

Figure 4.27 Response of Model Following System to a One Degree Step Input in Commanded Pitch Attitude

to increase the flight path angle the collective control is used to increase the collective pitch of the main rotor blades, increasing the magnitude of the main rotor thrust. The longitudinal cyclic stick is deflected aft by a small amount to tip the main rotor back and prevent an increase in the forward speed and the stabilator is deflected trailing edge down to produce the nose down moment required to maintain the trim pitch attitude.

The response of the system to a one degree step input in the commanded pitch attitude is presented in Figure 4.27. The results show that the desired pitch response is tracked with a small amount of overshoot in both pitch rate and pitch attitude. The overshoot is a result of the unmodelled dynamics and was predicted by the frequency response of the transfer function between pitch attitude and commanded pitch attitude presented in Figure 4.24. The forward velocity and flight path angle both show negligible deviation from their trim values. The lateral-directional responses show that the roll rate exhibits a high frequency response to the step input and the lateral velocity slowly approaches a steady state value of approximately 0.2 feet per second. The plot of the control responses indicates that initially the longitudinal cyclic is deflected aft, tilting the rotor tip path plane aft causing nose up moment and the stabilator is deflected trailing edge up, also providing nose up moment. As the pitch rate approaches a maximum, the longitudinal cyclic is deflected forward of its trim value causing the rotor tip path plane to be tipped forward to maintain forward speed. Meanwhile, the stabilator is still deflected trailing edge up to balance the change in the pitching moment due to the change in attitude and longitudinal cyclic.

From these results, it can be concluded that the stabilator plays a significant role as an active control. Due to its pitching moment generating capability, documented in Section 4.2, the stabilator is employed primarily to help control pitch attitude. These results also indicate that the demands on the stabilator are the greatest of the three controls, the flight path angle and pitch attitude responses requiring the greatest amount of stabilator deflection. The demand on the stabilator is the largest since its force and moment derivatives are the smallest of the three controls.

4.3.2 Model Following Performance Without Stabilator

To evaluate the improvement in performance that the stabilator offers, the stabilator was excluded and another set of feedforward gains was computed to provide model

following using only the four pilot controls. Since, without the stabilator, there are only four controls, it is no longer possible to independently control five degrees of freedom. In this design, the forward velocity degree of freedom was ignored the same way the lateral velocity was ignored in the design which included the stabilator. Ignoring both the forward and lateral velocities in the computation of the feedforward gains allowed independent control of the remaining four degrees of freedom. Time histories of the step responses of the new system to step commands in flight path angle and pitch attitude were used to evaluate the performance of the system without the stabilator. Frequency responses were used to compare the performance of the system without the stabilator to that of the system with the stabilator.

The response of the system without the stabilator to a one degree step input in the commanded flight path angle is presented in Figure 4.28. The plot of the longitudinal responses shows that, while the flight path angle tracks the desired flight path angle in a similar manner as the system including the stabilator (Figure 4.26), the forward velocity is now no longer maintained at its trim value. The results show that as the flight path angle is increased, the forward speed is increased by a ratio of about 1:2. The plot of the control response indicates the reason for the forward speed increase. The collective is used to increase the thrust of the main rotor by increasing the collective blade pitch. At the same time, the longitudinal cyclic is deflected forward, tipping the rotor tip path plane forward in an effort to maintain the trim pitch attitude. However, tipping the tip path plane forward and increasing the main rotor thrust will cause the forward speed to increase. Comparing these results to those illustrated in Figure 4.26 indicates that when the stabilator is included it is primarily responsible for regulating the pitch attitude while the longitudinal cyclic is used to tip the rotor tip path plane aft to maintain the trim forward velocity.

The response of the system without the stabilator to a one degree step input in the commanded pitch attitude is presented in Figure 4.29. The plot of the longitudinal response indicates that the pitch attitude and pitch rate responses are slightly degraded compared to those of the system which includes the stabilator. The results also show that the forward speed decreases as the pitch attitude is increased. The control response provides the reason for the forward speed decrease. The results indicate that the longitudinal cyclic is deflected aft initially and is deflected aft in steady state. Tipping the rotor tip path plane aft causes nose up moment which will increase the pitch attitude. At the same time, the collective is decreased to maintain the flight path angle. By tipping the tip

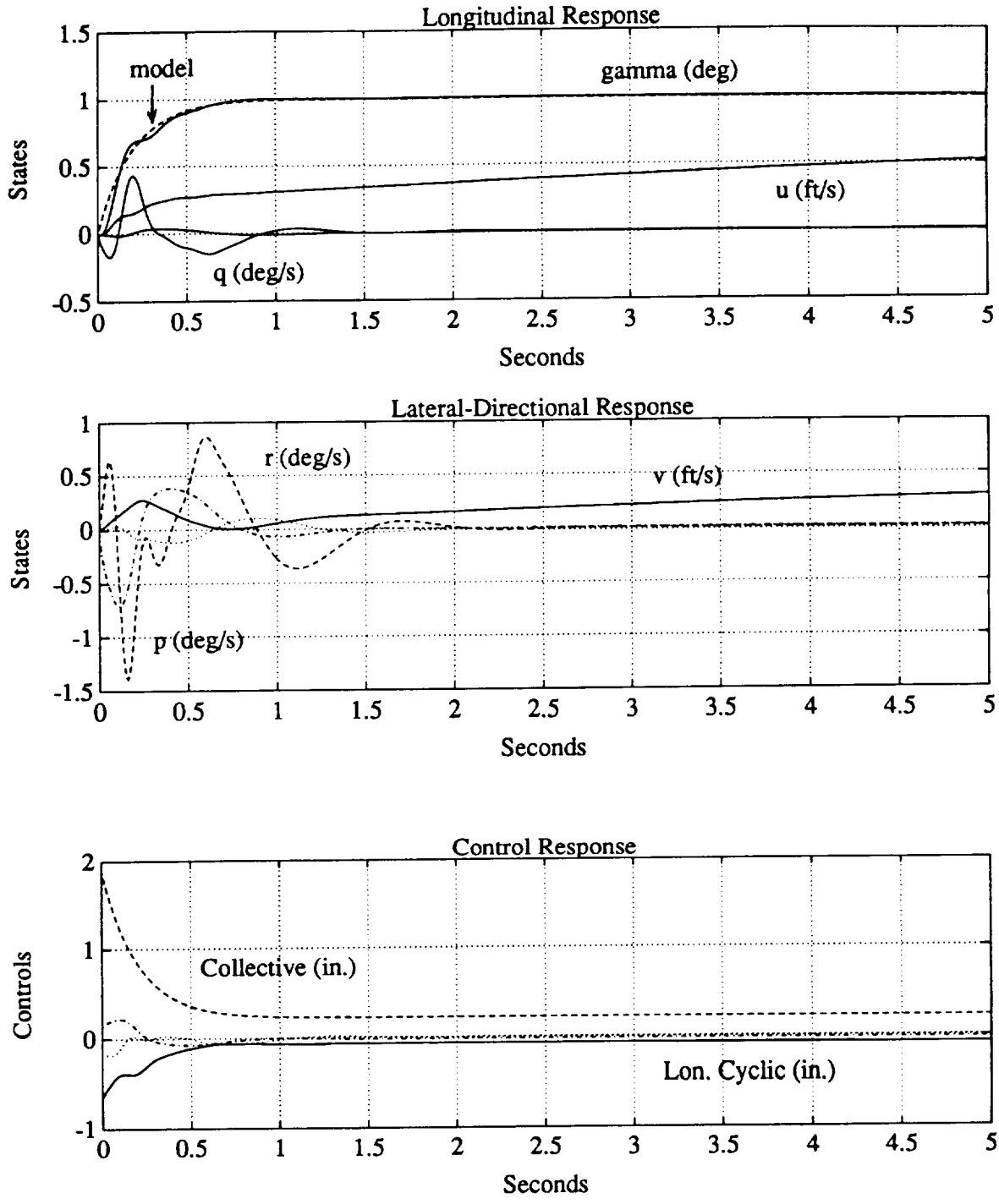

Figure 4.28 Response of the Model Following System Without the Stabilator to a One Degree Step Input in Commanded Flight Path Angle

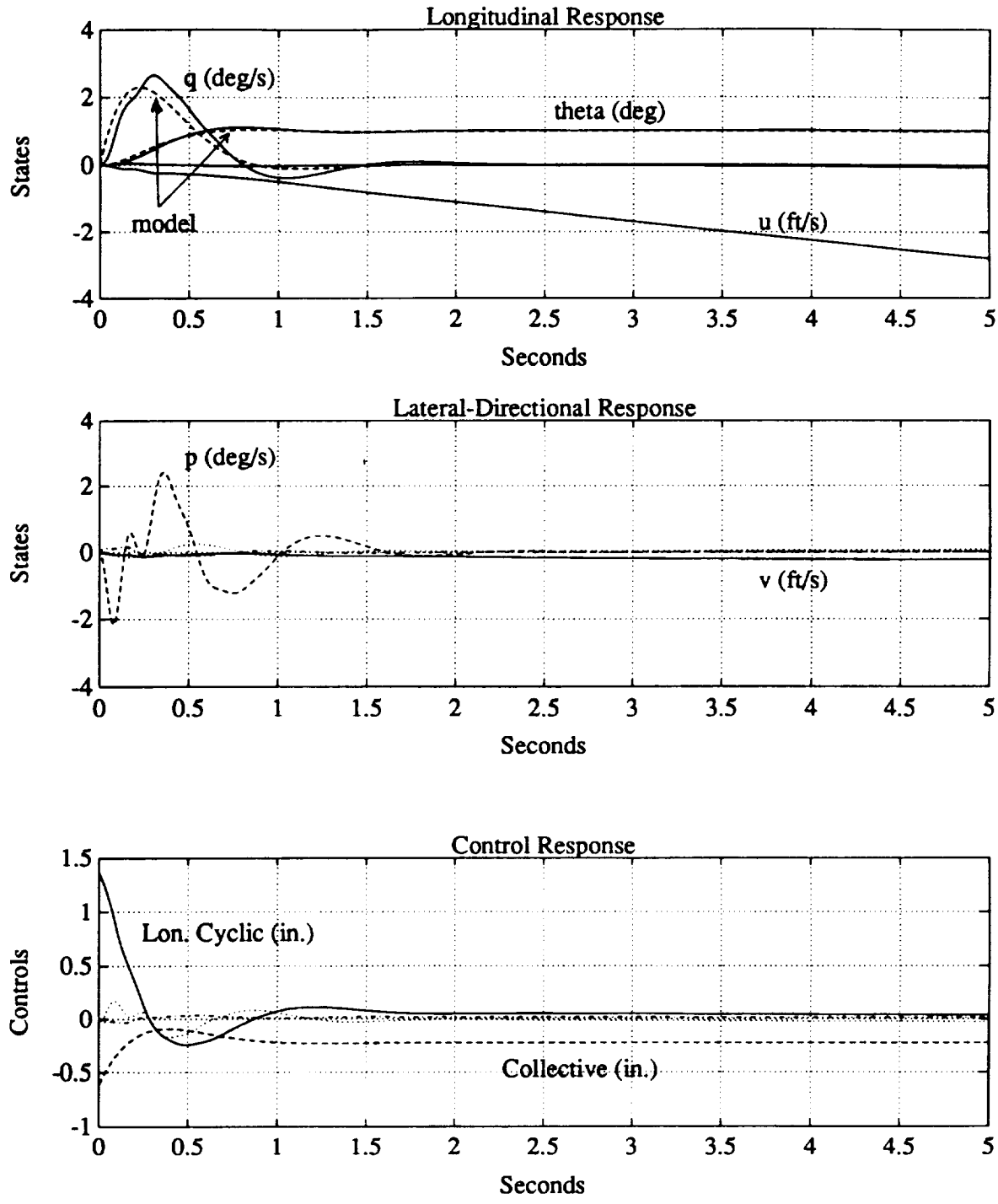

Figure 4.29 Response of the Model Following System Without the Stabilator to a One Degree Step Input in Commanded Pitch Attitude

path plane aft and decreasing the collective blade pitch, the component of main rotor thrust in the forward direction is decreased causing the forward velocity to decrease. The control response of the system which includes the stabilator shows that the longitudinal cyclic and the stabilator are the primary controls used to control the pitch attitude and that the collective control shows very little movement.

To evaluate the effect of the stabilator on the forward velocity response in the frequency domain, frequency responses of the transfer functions between the commanded inputs and the actual forward speed are presented in Figures 4.30 and 4.31. Figure 4.30 presents a comparison of the frequency responses of the transfer functions between the commanded flight path angle and the forward velocity for the system with and without the stabilator. This comparison shows that, at frequencies below ten radians per second, the stabilator provides at least an order of magnitude decrease in the magnitude of the response of the forward velocity to the commanded flight path angle. The results at low frequencies indicate that the steady state response will be decreased by an order of magnitude. Figure 4.31 presents a comparison of the frequency responses of the transfer functions between the commanded pitch attitude and the forward velocity for the system with and without the stabilator. This comparison shows that the addition of the stabilator also results in an attenuation of the forward velocity response to commanded pitch attitude. The results at low frequencies indicate that the steady state response should be attenuated by more than two orders of magnitude.

To evaluate the difference the stabilator makes to the response of the system to the commanded flight path angle and commanded pitch attitude, frequency responses of the transfer functions between the commanded flight path angle and actual flight path angle and also the transfer functions between the commanded pitch attitude and actual pitch attitude of the two systems were compared. Figure 4.32 presents a comparison of the frequency responses of the transfer functions between the commanded flight path angle and actual flight path angle of the two systems. The results show that the stabilator has very little effect on the flight path angle response of the system. Figure 4.33 presents a comparison of the frequency responses of the transfer functions between the commanded pitch attitude and the actual pitch attitude. This comparison indicates that the stabilator doesn't affect the response in the frequency range between 0.1 and 10.0 radians per second. However, the results indicate that without the stabilator, the system will be prone to steady state error in the pitch attitude response to commanded pitch attitude.

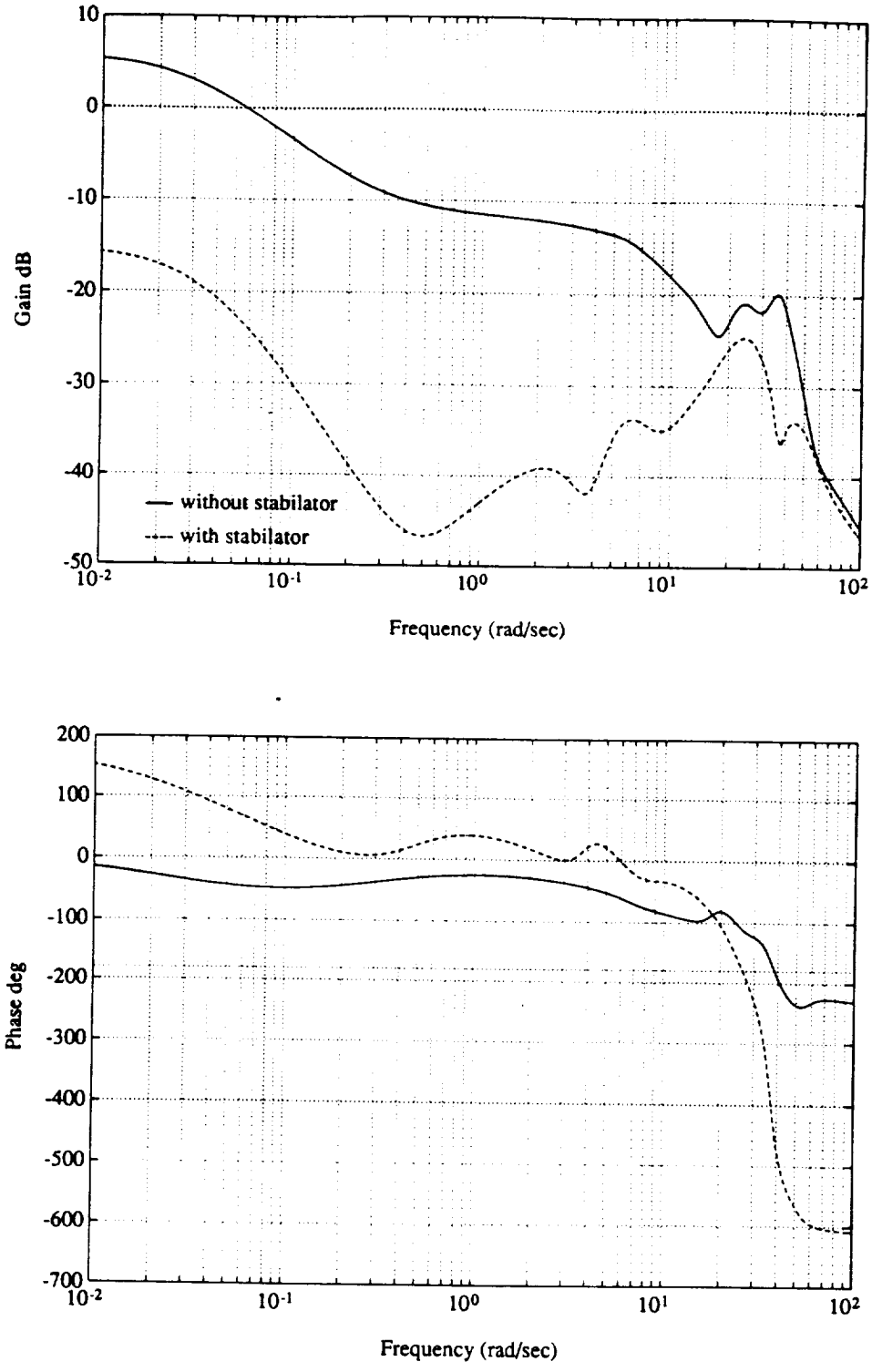

Figure 4.30 Comparison of the Frequency Responses of the Transfer Functions Between Commanded Flight Path Angle and Forward Speed

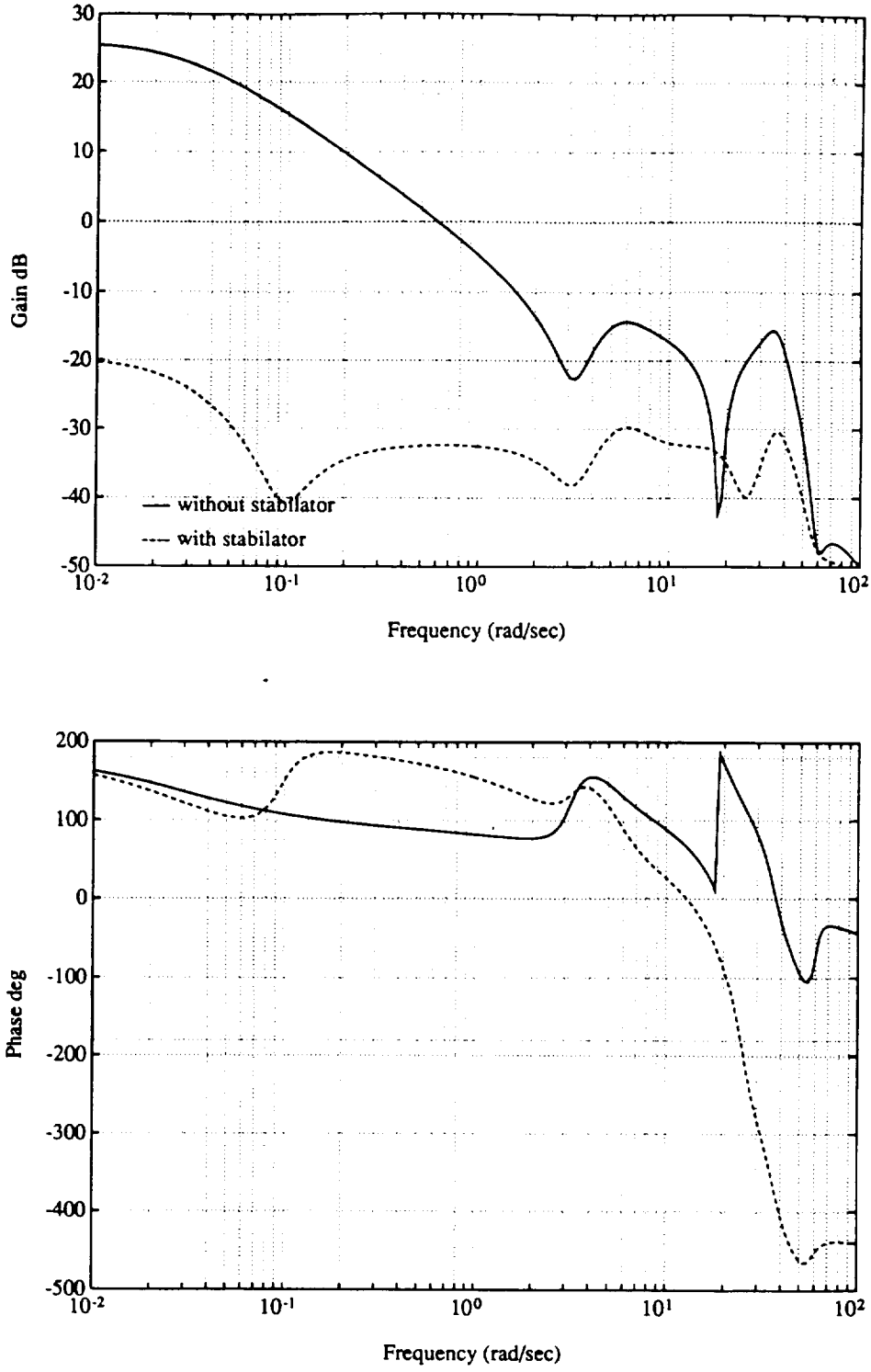

Figure 4.31 Comparison of the Frequency Responses of the Transfer Functions Between Commanded Pitch Attitude and Forward Speed

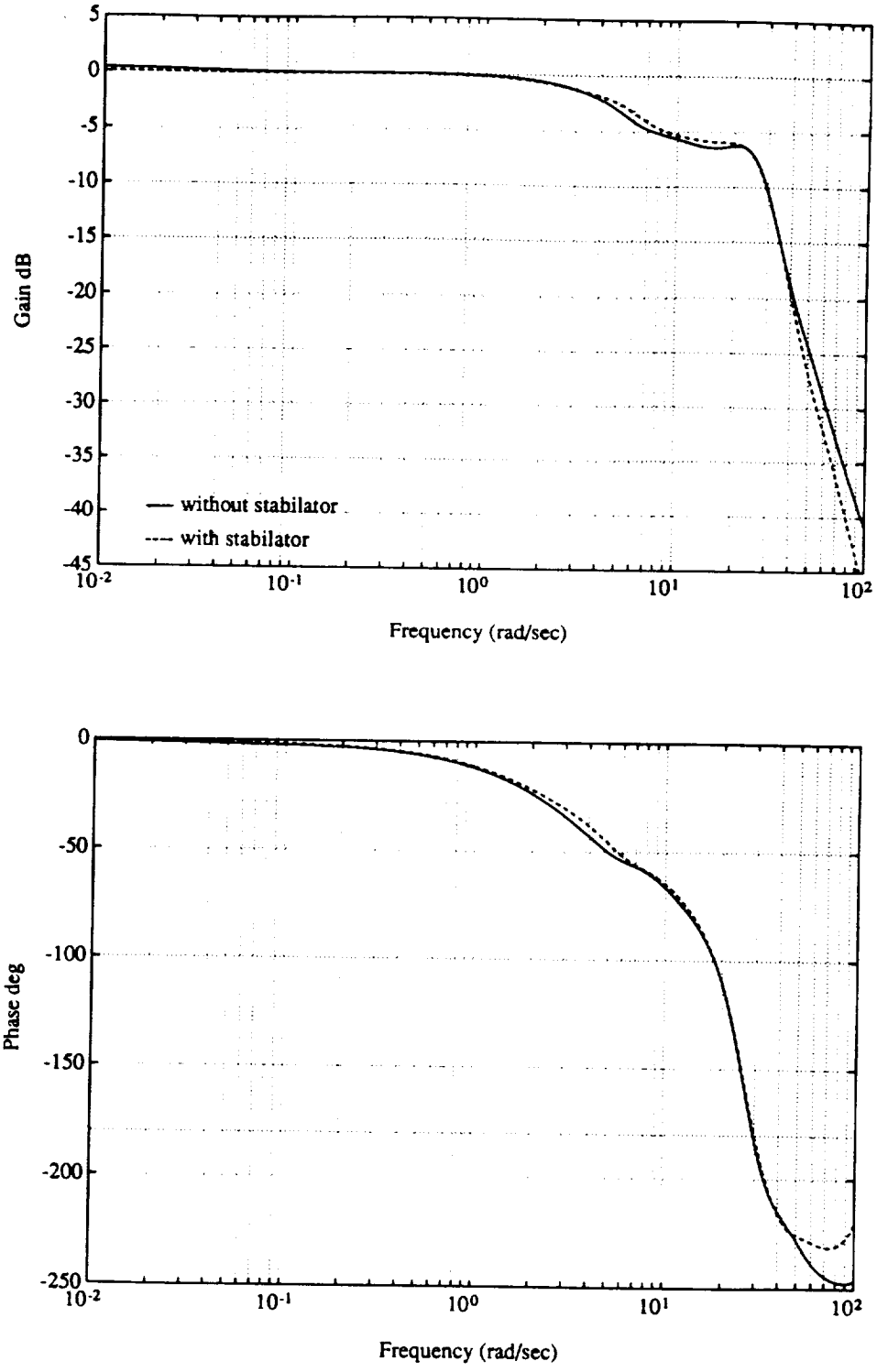

Figure 4.32 Comparison of the Frequency Responses of the Transfer Functions Between Commanded Flight Path Angle and Actual Flight Path Angle

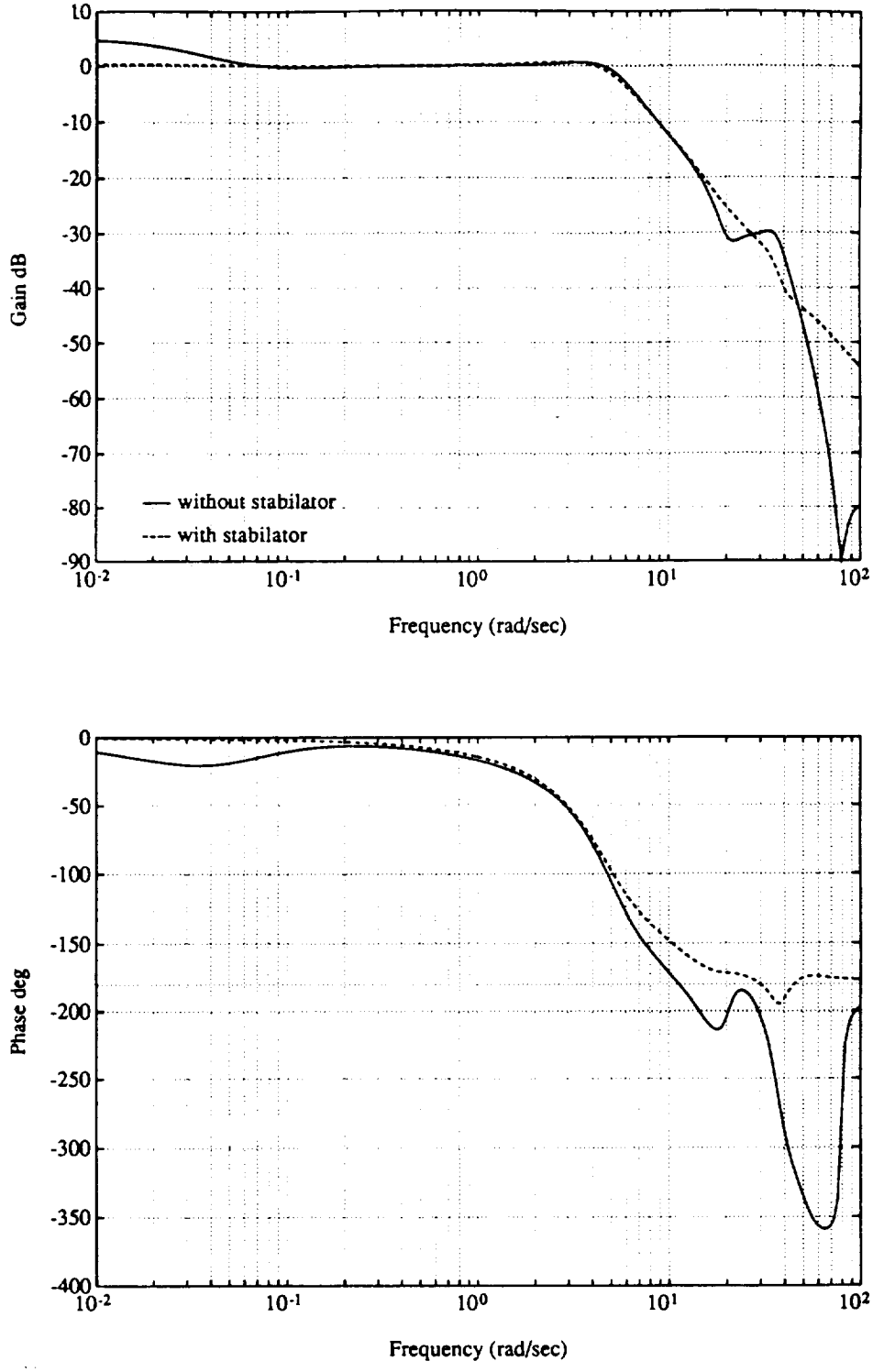

Figure 4.33 Comparison of the Frequency Responses of the Transfer Functions Between Commanded Pitch Attitude and Actual Pitch Attitude

From these results, it can be concluded that the stabilator does play a necessary role in model following. Its primary use is as a pitching moment generator and it can be used in conjunction with the longitudinal cyclic to modulate pitch attitude and forward speed. The collective is primarily used to control the flight path angle. Without the stabilator, these results indicate that the flight path angle and pitch attitude can be independently controlled but the steady state pitch attitude tracking will be degraded due to the influence of the unconstrained forward velocity.

4.3.3 Influence of Stabilator Actuator Dynamics

On the actual aircraft, the stabilator's position is controlled by an actuator system which contains its own dynamics. To evaluate the effect of the stabilator actuator dynamics, a first order actuator pole was added to the thirty one state linear model. The stabilator actuator acts as a low pass filter, attenuating the high frequency content of the control input to the stabilator. The effect of the stabilator actuator pole on the system performance was evaluated by adding different values of the actuator pole to the model following system without changing the feedforward gains. Time histories of the step responses of the resulting systems were used to compare the performance of the different systems. In this investigation, the response of the system without an actuator pole was used as a baseline. The performance of the system with actuator poles at 8.85 radians per second (used in GENHEL) and also twenty radians per second was compared to the baseline to determine how the actuator dynamics affect the model following response.

The response of the forward velocity to a one foot per second step input in the commanded forward velocity is presented in Figure 4.34. Also presented is the response of the longitudinal cyclic, collective and stabilator controls. The forward velocity responses show that the different values of actuator pole make very little difference in the response. When the actuator is added, the results show that the responses of the systems which include the actuator tend to lag the response of the system without the actuator. The responses of the controls show that when the actuator dynamics are added the stabilator deflection cannot respond instantly to the step input. Since the longitudinal cyclic is the primary X-force producer, it is responsible for modulating the forward speed. However, since the stabilator cannot respond immediately, the results indicate that the initial deflection of the longitudinal cyclic is slightly reduced to avoid generating more pitching moment than the stabilator can balance. The stabilator actuator dynamics have little effect on the forward

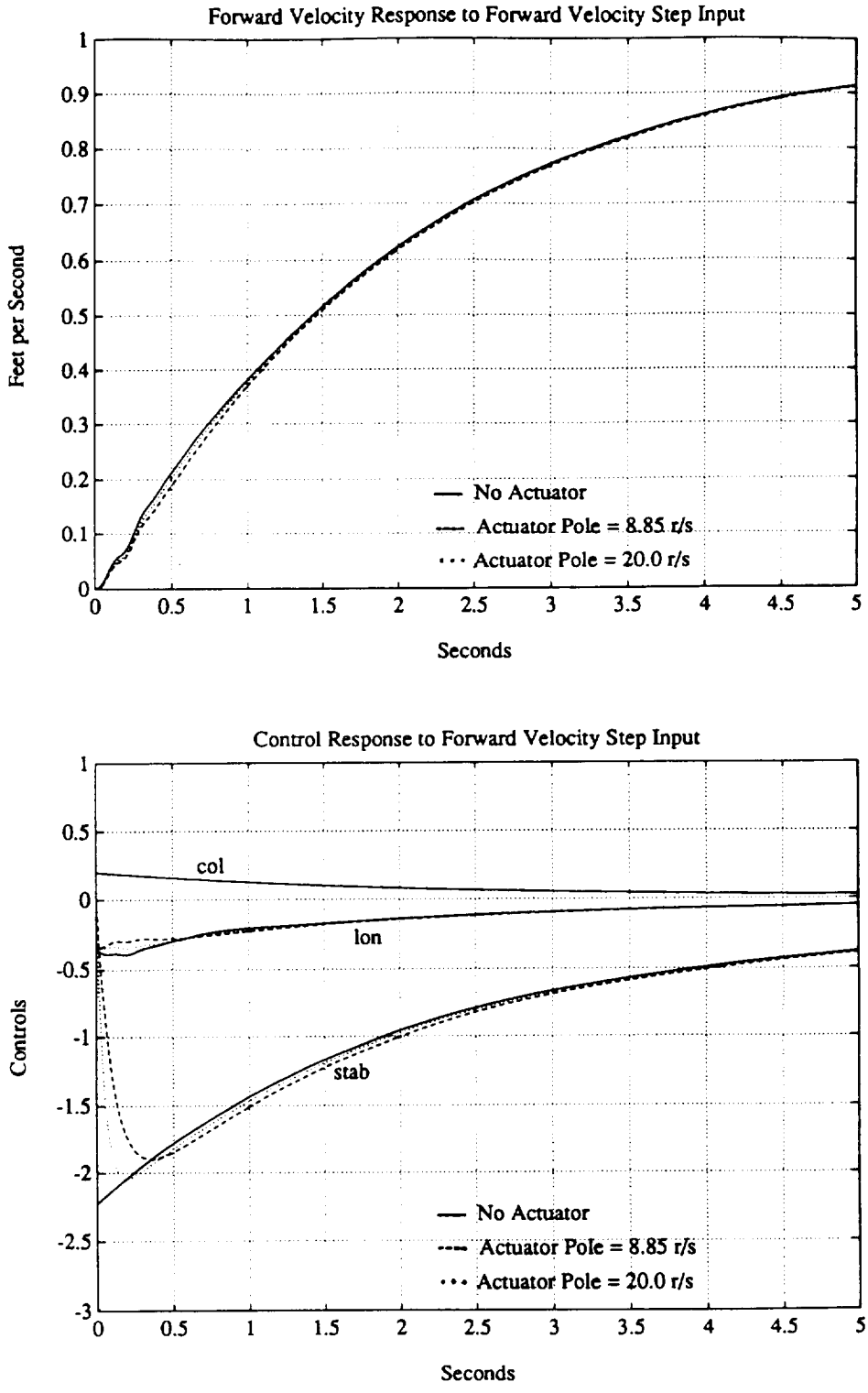

Figure 4.34 Response of the Model Following System to a Forward Velocity Step Input for Three Values of Stabilator Actuator Pole

velocity response because the time constant of the desired forward velocity response is 2.0 seconds (Appendix G) while the time constant of the slowest actuator pole considered is 0.133 seconds.

The response of the flight path angle to a one degree step input in the commanded flight path angle is presented in Figure 4.35. The results indicate that the stabilator actuator pole again has little effect on the response. The initial rise from zero shows no difference and the steady state values attained are the same. The control responses, also presented in Figure 4.35, indicate that the stabilator does not respond as quickly as the baseline system. The flight path angle response shows little dependence on the stabilator actuator dynamics since the collective control is the primary Z-force control. The stabilator and longitudinal cyclic are responsible for regulating the forward speed and pitch attitude. Since the dynamics of the collective haven't been changed, the flight path angle response doesn't change much either.

The responses of the pitch attitude and pitch rate to a one degree step input to the commanded pitch attitude are presented in Figure 4.36. The results indicate that adding the stabilator actuator dynamics adds a time lag to the pitch attitude and pitch rate responses. As the actuator dynamics become slower, the time lag increases. The results also indicate that there is an overshoot in the commanded pitch rate. The responses of the controls to the commanded step input show that, when the actuator dynamics are added, the response of the stabilator cannot keep up with the baseline response. Since the stabilator is used in cooperation with the longitudinal cyclic to control the pitching moment, the result is a degraded pitch response. Since the initial stabilator response is slower, less pitching moment is generated. This results in the time lag observed in the pitch response. To compensate for the time lag in the initial response, additional pitching moment is generated resulting in a larger peak in the pitch rate response. The results also show that the steady state responses match, indicating that the stabilator pole has no effect on the steady state pitch attitude response. Comparing the responses of the systems with the different actuator poles indicates that the system with the stabilator actuator pole at 20.0 radians per second performs better than the system with the actuator pole at 8.85 radians per second. When the actuator pole is at twenty radians per second, the stabilator response tracks the baseline response more closely resulting in better pitch attitude and pitch rate responses.

These results indicate that the actuator dynamics of the stabilator will primarily affect the pitch attitude response. The pitch rate and pitch attitude response to a step input

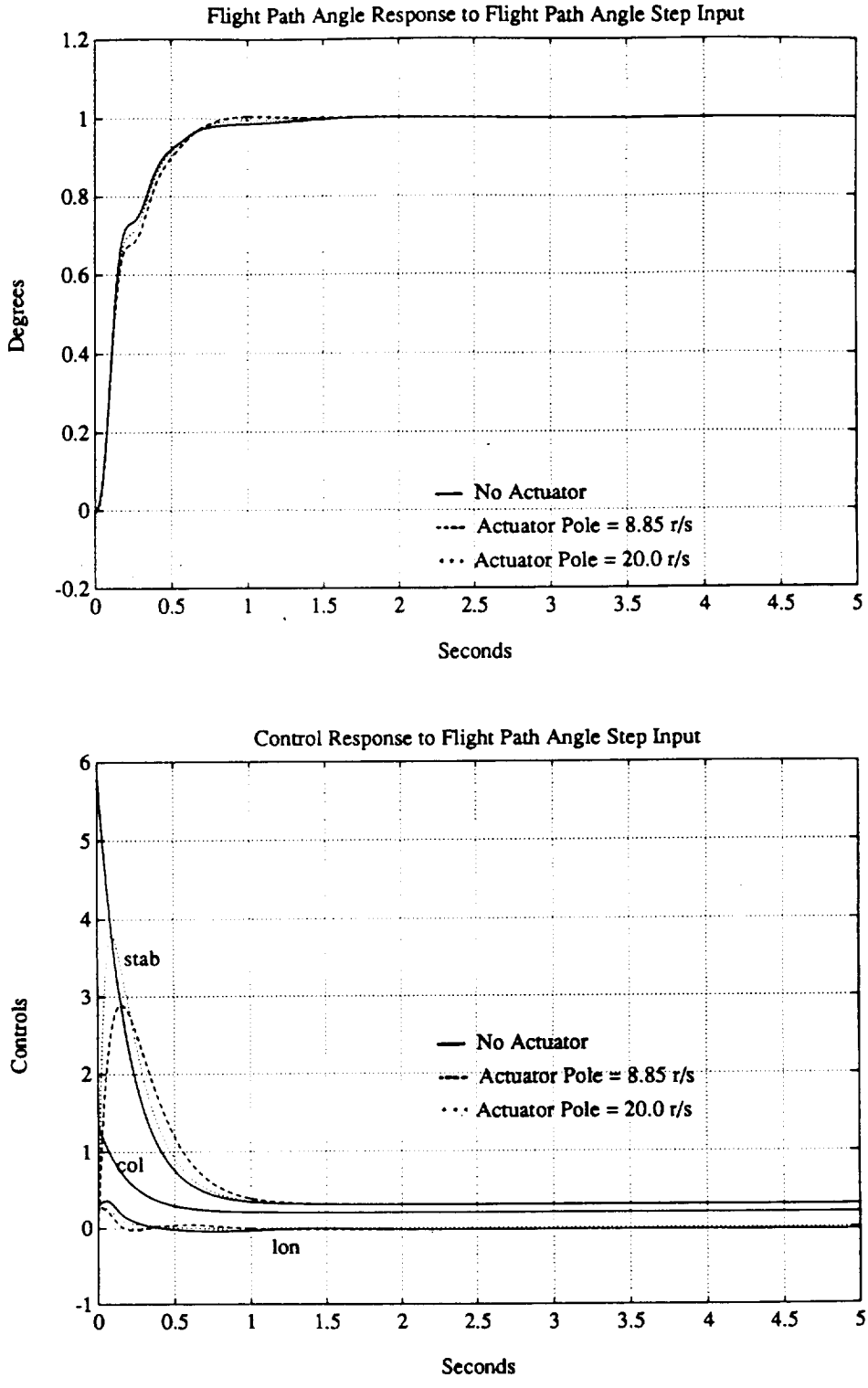

Figure 4.35 Response of the Model Following System to a Flight Path Angle Step Input for Three Values of Stabilator Actuator Pole

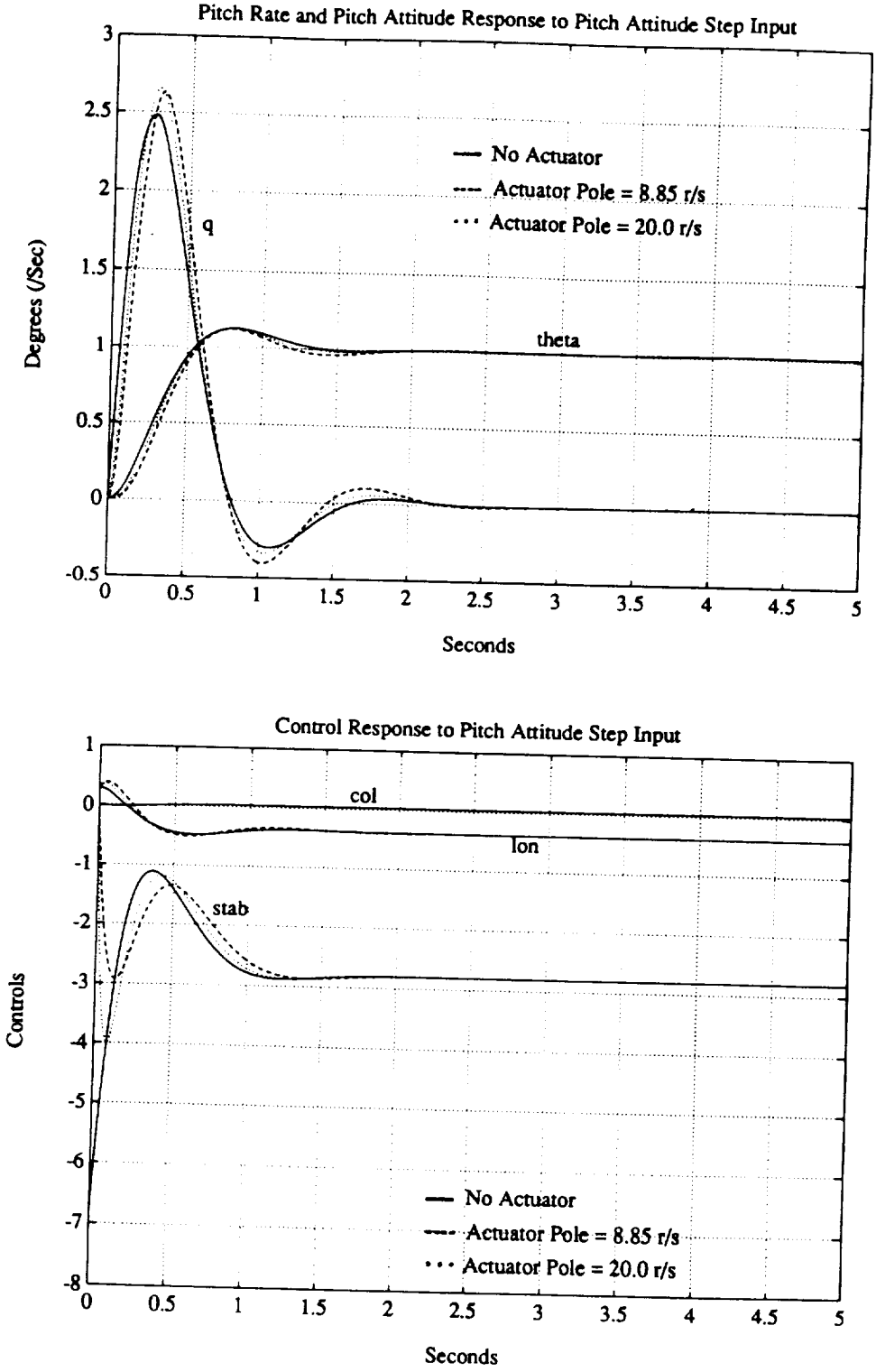

Figure 4.36 Response of Model Following System to Pitch Attitude Step Input for Three Values of Stabilator Actuator Pole

in the commanded pitch attitude showed the greatest dependence on the stabilator actuator pole. Since the stabilator is primarily a pitching moment generator in this design, the actuator pole affects the pitching moment generating capabilities the most. The forward speed response to a step input in the commanded forward speed showed little dependence on the stabilator pole due to the fact that the longitudinal cyclic is the primary X-force control and also because the speed of the desired forward speed response is much slower than the stabilator actuator speed. The flight path angle response to a step input in the commanded flight path angle showed little dependence on the stabilator actuator pole since the collective is the primary Z-force controller while the stabilator and the longitudinal cyclic are used to modulate the forward speed and pitch attitude through the use of X-force and pitching moment.

The results also showed that as the stabilator response was slowed down, the maximum deflection of the stabilator decreased. The initial response of the system without an actuator pole is the appropriate gain in the K_δ matrix multiplied by the amplitude of the step input. This produces the pitching moment required to generate the pitch rate necessary to cause the pitch attitude to follow the required pitch attitude. When the stabilator actuator pole is added, the stabilator takes a finite amount of time to respond to the input command. As the stabilator is responding, the commanded stabilator deflection decreases from the initial value. This causes the stabilator deflection to peak at a certain point and then reverse direction to move toward the steady state deflection. The reduction in the peak stabilator deflection, as a result of the actuator pole, indicates that the range of motion of the aircraft can be increased. When the stabilator pole is excluded, the maximum deflection of the stabilator is approximately seven degrees, indicating that a step input of no more than three degrees in the commanded pitch attitude could be followed without the stabilator reaching its travel limit of twenty degrees. However, when the stabilator pole is at 8.85 radians per second, the maximum stabilator response is only three degrees, indicating that the system could follow step inputs of up to six or seven degrees in commanded pitch attitude. The price paid is the time lag in the pitch response.

Since higher pitch attitude response bandwidths require larger amounts of pitching moment to provide the larger pitch rates, the effect of the pitch attitude response natural frequency on the control demand was explored. To investigate the effect of the pitch attitude natural frequency on the control demand, the pitch attitude natural frequency was doubled from five radians per second to ten radians per second and the pitch attitude and

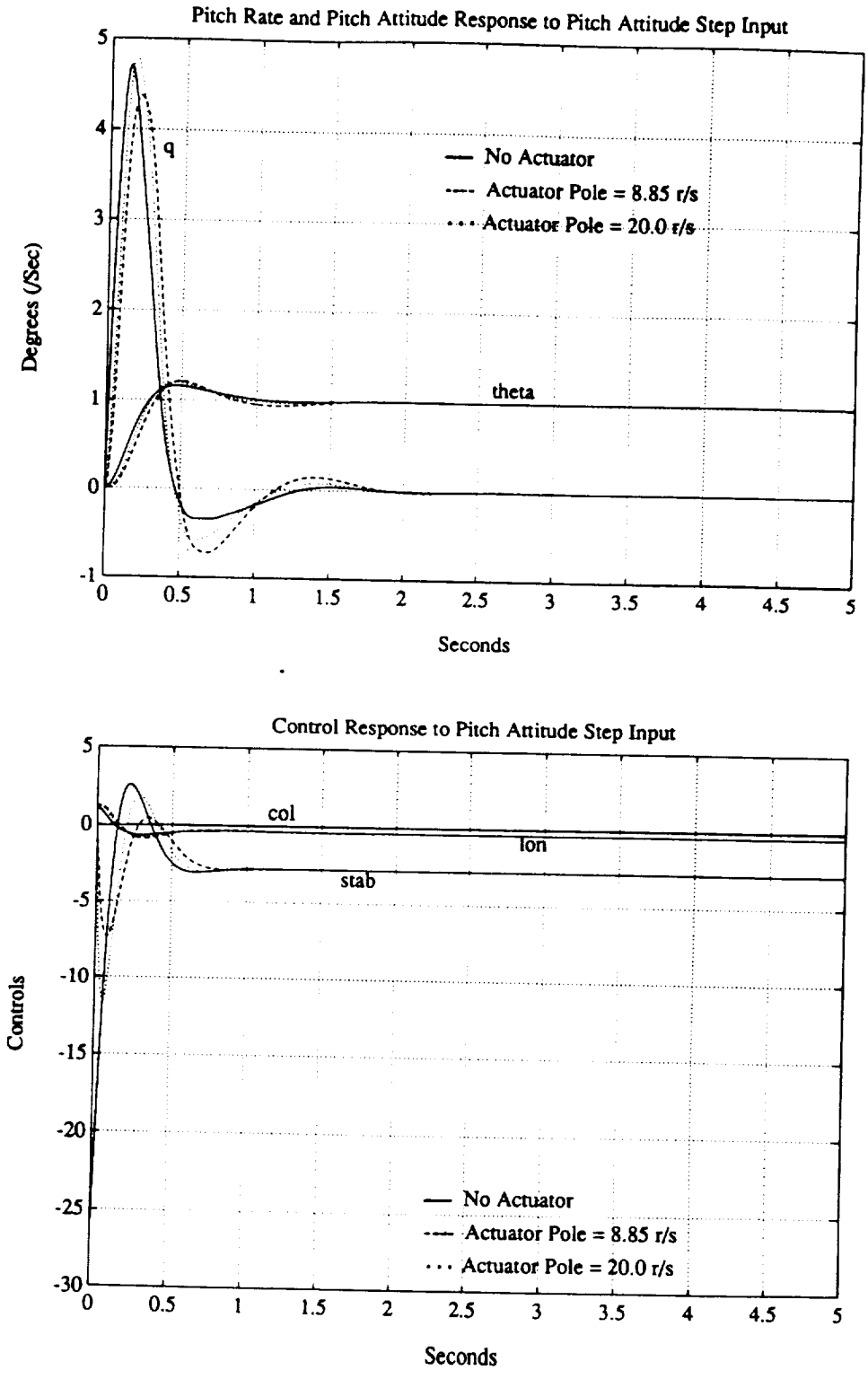

Figure 4.37 Response of the Model Following System With the Desired Pitch Response Bandwidth of Ten Radians Per Second to a Pitch Attitude Step Input

pitch rate responses of the systems with actuator poles at 8.85 radians per second and twenty radians per second were compared to the response of the baseline system which excludes the actuator dynamics. The resulting pitch rate, pitch attitude and control responses to a step input in the commanded pitch attitude are presented in Figure 4.37. The results show that the pitch attitude and pitch rate response lag the responses of the baseline system as they did in Figure 4.36. Since the pitch attitude response natural frequency has been doubled, the pitch attitude responds to inputs more quickly resulting in larger pitch rates. To generate the larger pitching moments required, the results indicate that much larger stabilator deflections are required. When the actuator is not included in the model, the initial stabilator incidence required is over twenty five degrees. This is beyond the stabilator deflection limit of twenty degrees. However, when the actuator pole is added, the maximum deflection demand on the stabilator decreases. When the stabilator actuator pole is at twenty radians per second, the maximum demand on the stabilator is twelve degrees and when the pole is at 8.85 radians per second, the maximum demand on the stabilator drops to seven degrees.

These results indicate that there is a compromise between the pitch attitude speed of response and range of motion due to the stabilator's physical limits. Increasing the speed of response of the pitch attitude means increasing the pitch attitude natural frequency. This results in an increased demand on the stabilator to produce the increased amount of pitching moment necessary a faster pitch response. This increase in demand on the stabilator deflection means that the stabilator will reach its physical limits more quickly than it would if the required pitch attitude speed of response was less. This compromise is affected by another compromise between the time lag in the response and the stabilator deflection due to the speed of the actuator. If the actuator is fast, there will be less time lag in the response than in the response of the slower actuator. However, the amount of control deflection required will be greater since the actuator can force the stabilator to approach the commanded deflection more quickly.

CHAPTER 5.

CONCLUSIONS AND RECOMMENDATIONS

This thesis is a preliminary feasibility study aimed at quantifying and demonstrating the stabilator's capabilities as an additional control available to an in-flight simulator. The stabilator was evaluated as a trim control, its force and moment generating capabilities were compared to the capabilities of the other controls and its potential as an active control was explored. The influence of an actuator pole on the stabilator's role as an active control was also evaluated.

The stabilator's effectiveness as a trim control was evaluated by determining its effect on the trim values of the pilot controls, the trim pitch attitude and the roll attitude or horizontal flight path angle. The results showed that the stabilator had the strongest effect on the trim pitch attitude and the trim deflection of the longitudinal cyclic control. The results also showed that the effect became more pronounced at higher forward flight speeds. It was concluded that, in forward flight, the stabilator can be used to effectively control the trim pitch attitude. However, the range of trim pitch attitude that the stabilator can control depends on the flight speed and the location of the longitudinal center of gravity.

The stabilator's potential as an active control was evaluated by comparing the force and moment generating capabilities of the stabilator with the those of the collective and longitudinal cyclic. The stabilator's force and moment generating capabilities were compared to those of the pilot controls through the use of derivatives of force and moment with respect to the control deflections. The comparison showed that the longitudinal cyclic is the primary X-force and pitching moment producer, while the collective is the primary Z-force producing control. The stabilator was relatively ineffective as a force producing device. However, due to the moment arm between the stabilator and the center of gravity, the stabilator can be an effective pitching moment generator at high speeds. It was

concluded that the stabilator could be used in cooperation with the longitudinal cyclic to modulate pitching moment and X-force while the collective can be used to modulate Z-force. Incorporating the stabilator into the flight control system should allow independent control of the motion in the longitudinal plane of the aircraft at flight speeds where the stabilator is effective.

To evaluate the stabilator's contribution in an in-flight simulation application, it was incorporated into a model following flight control system. The control system was designed using a linear model of the aircraft in steady, level flight at a flight speed of eighty knots. The model of the desired dynamics was a decoupled model of the longitudinal dynamics only. Evaluating the response of the system to step inputs, as well as frequency responses, indicated that the stabilator could be used to help provide independent control of the three longitudinal degrees of freedom (pitching and translation along the the X and Z axes). This application confirmed that the stabilator can be used in cooperation with the longitudinal cyclic to control the forward velocity and pitch response while the collective is primarily responsible for control of the flight path angle. It was also found that in steady, level flight at eighty knots, the demand on the stabilator was the greater than the demand on any of the other controls making the stabilator deflection the limiting factor in the performance of the simulator.

The impact of the stabilator actuator dynamics on the performance of a model following control system was investigated by adding a first order differential equation representing the actuator to the model that was used to evaluate the control design. The results showed that the stabilator actuator dynamics had the greatest effect on the pitch response of the aircraft. It was concluded that introducing an actuator pole resulted in a time lag in the pitch rate and pitch attitude response and also resulted in a decreased demand in the stabilator deflection required. It was found that the natural frequency of the pitch response and the range of pitch response available depend on the stabilator deflection limits and that there is a compromise between the two. Greater pitch natural frequency will result in a decreased range of motion and an increased range of motion will require a lower pitch response natural frequency.

This research was a preliminary investigation of the issues involved in using the stabilator to enhance the in-flight simulation capabilities of the RASCAL. There are still a number of possible avenues of investigation involving the addition of the stabilator to the flight control system of the RASCAL. A piloted simulation study involving the application

of the stabilator as an active control would be useful in evaluating the its contribution to the in-flight simulation capabilities of the RASCAL. Since the stabilator is an aerodynamic surface, whose force and moment generating capabilities depend on flight speed, an investigation into the gain scheduling requirements involved in adding the stabilator to the RASCAL's flight control system would also be useful. Due to its substantial pitching moment generating capabilities at high speeds, a more detailed study of the safety of flight issues involved in adding the stabilator as an active control would be advisable. It would be useful to define a flight envelope within which the stabilator could be safely used without encroaching too much on the control margins of the primary controls. Investigations into alternate uses for the stabilator including pitch attitude regulation in forward flight as well as incorporation into the other programs planned for the RASCAL would also be beneficial.

LIST OF REFERENCES

LIST OF REFERENCES

[1] Eshow, Michelle M., Aiken, Edwin W., Hindson, William S., Lebacqz, J. Victor, and Denery, Dallas G., "A Review of Recent Programs and Future Plans for Rotorcraft In-Flight Simulation at Ames Research Center", SAE Aerospace Technology Conference and Exposition, Long Beach, CA, Sept. 23-26, 1991.

[2] Hindson, W.S., "Past Applications and Future Potential of Variable Stability Research Helicopters," *Helicopter Handling Qualities*, NASA CP-2219, 1982.

[3] Sattler, D.E, "The National Aeronautical Establishment Airborne Simulation Facility", National Research Council of Canada, NAE Miscellaneous Report 58, May 1984.

[4] Baillie, Stewart W., and Morgan, J. Murray, "Control Sensitivity, Bandwidth and Disturbance Rejection Concerns for Advanced Rotorcraft", 45th Annual Forum of the American Helicopter Society, Boston, MA, May 1989.

[5] Gmelin, B., Bouwer, D., and Hummes, D., "DFVLR Helicopter In-Flight Simulator For Flying Quality Research," 10th European Rotorcraft Forum, The Hague, Netherlands, Aug. 28-31, 1984.

[6] Pausder, H. J., Bouwer, G., and Von Grunhagen, W., "A Highly Maneuverable Helicopter In-Flight Simulator - Aspects of Realization," 14th European Rotorcraft Forum, Milano, Italy, Sept. 20-23, 1988.

[7] Motyka, Paul R., Rynaski, Edmund G., and Reynolds, Philip A., "Theory and Flight Verification of the TIFS Model-Following System," *Journal of Guidance and Control*, Vol. 3, No. 2, March-April, 1980, pp. 347-353.

[8] Reynolds, Philip A., and Pruner, James R., "The Total In-Flight Simulator (TIFS) Design and Capabilities," AIAA 2nd Flight Test, Simulation, and Support Conference, Los Angeles, CA, March 25-27, 1968.

[9] "Operator's Manual UH-60A and EH-60A Helicopter", Headquarters, Department of the Army, TM 55-1520-237-10, January 1987.

[10] Howlett, J.J., "UH-60A Black Hawk Engineering Simulation Program: Volume I -- Mathematical Model", NASA CR-166309, 1981.

[11] Ballin, Mark G., "Validation of a Real-Time Engineering Simulation of the UH-60A Helicopter", NASA TM-88360, February 1987.

[12] Kim, F. D., Celi, R., and Tischler, M. B., "High Order State Space Simulation Models of Helicopter Flight Mechanics," Proceedings of the 16th European Rotorcraft Forum, Glasgow, Scotland, Sept. 1990.

[13] Kim, F. D., Celi, R., and Tischler, M. B., "Forward Flight Trim Calculation and Frequency Response Validation of a High-Order Helicopter Simulation Model," Proceedings of the 47th Annual Forum of the American Helicopter Society, Pheonix, Arizona, May 1991.

[14] Hall, W. E. Jr. and Bryson, A. E. Jr., "Inclusion of Rotor Dynamics in Controller Design," *Journal of Aircraft*, Vol. 10, No. 4, April 1973, pp. 200-206..

[15] Chen, Robert T. N. and Hindson, William S., "Influence of High-Order Dynamics on Helicopter Flight Control System Bandwidth," *Journal of Guidance and Control*, Vol. 9 No.2, March-April 1986, pp. 190-197.

[16] Prouty, Raymond W., Helicopter Performance, Stability and Control, PWS Engineering, Boston, 1986.

[17] Motyka, Paul R., "A Classical Approach to the Design of Model Following Control Systems," AIAA Mechanics and Control of Flight Conference, Anaheim, California, August 1974.

[18] Matlab User's Guide, The MathWorks, Inc., 1990.

[19] Grace, Andrew, Laub, Alan J., Little, John N. and Thompson, Clay, Control System Toolbox User's Guide, The MathWorks, Inc., 1990.

APPENDICES

Appendix A Stations, Waterlines and Butt Lines

This Appendix presents the reference frames used to measure the fuselage, waterline and buttline stations of components on the helicopter and points of interest such as the center of gravity. These figures are reprinted with permission from Sikorsky.

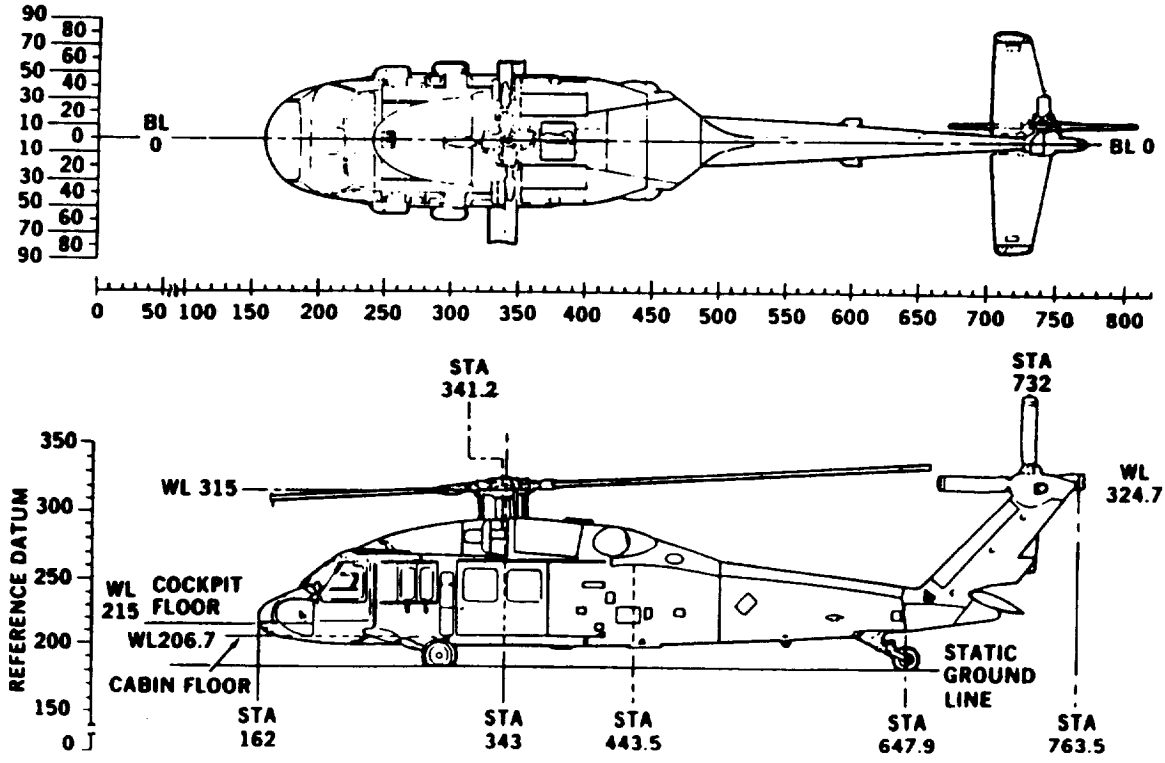

Figure A.1 Stations, Waterlines and Butt Lines (Sikorsky)

Appendix B GENHEL Stabilator Model

This Appendix presents the aerodynamic model of the stabilator used in the Generic Helicopter Simulation Program developed by Sikorsky Aircraft to simulate the the UH-60A Black Hawk helicopter. The aerodynamic behavior of the stabilator was modelled using wind tunnel data collected using the airfoil alone. The stabilator lift and drag coefficient data is reproduced from [10] in Figures B.1 and B.2. The plots indicate that the lift and drag coefficients of the stabilator are functions of the local angle of attack.

To compute the lift and drag acting on the stabilator (C_{Lht} and C_{Dht}), the local dynamic pressure (Q_{ht}), the stabilator area (S_{ht}) and the local angle of attack (α_{ht}) are required. The equations for the lift and drag acting on the stabilator are given by the following expressions:

$$L_{ht} = Q_{ht}\, S_{ht}\, C_{Lht}$$

$$D_{ht} = Q_{ht}\, S_{ht}\, C_{Dht}$$

The physical area of the stabilator is 45.0 square feet. The local angle of attack and the local dynamic pressure are determined by computing the local velocity components at the stabilator as follows:

$$V_x = V_{xb}*K_q - q*z_{ht} + r*y_{ht} + V_{xint}$$

$$V_y = V_{yb}*K_q + p*z_{ht} - r*x_{ht} + V_{yint}$$

$$V_z = V_{zb}*K_q + q*x_{ht} - p*y_{ht} + V_{zint}$$

where V_{xb}, V_{yb}, and V_{zb} are the translational rates of the center of gravity, p, q and r are th rotational rates of the aircraft, x_{ht}, y_{ht} and z_{ht} are the distances between the stabilator and the center of gravity, K_q is the dynamic pressure ratio and V_{xint}, V_{yint} and V_{zint} are the sums of the velocity interference due to the main rotor and fuselage. The local angle of attack (α_{ht}) and dynamic pressure (Q_{ht}) can then be computed as follows,

$$\alpha_{ht} = i_{ht} + \tan^{-1}(V_z/|V_x|)$$

$$Q_{ht} = 1/2*\rho*(V_x^2 + V_y^2 + V_z^2)$$

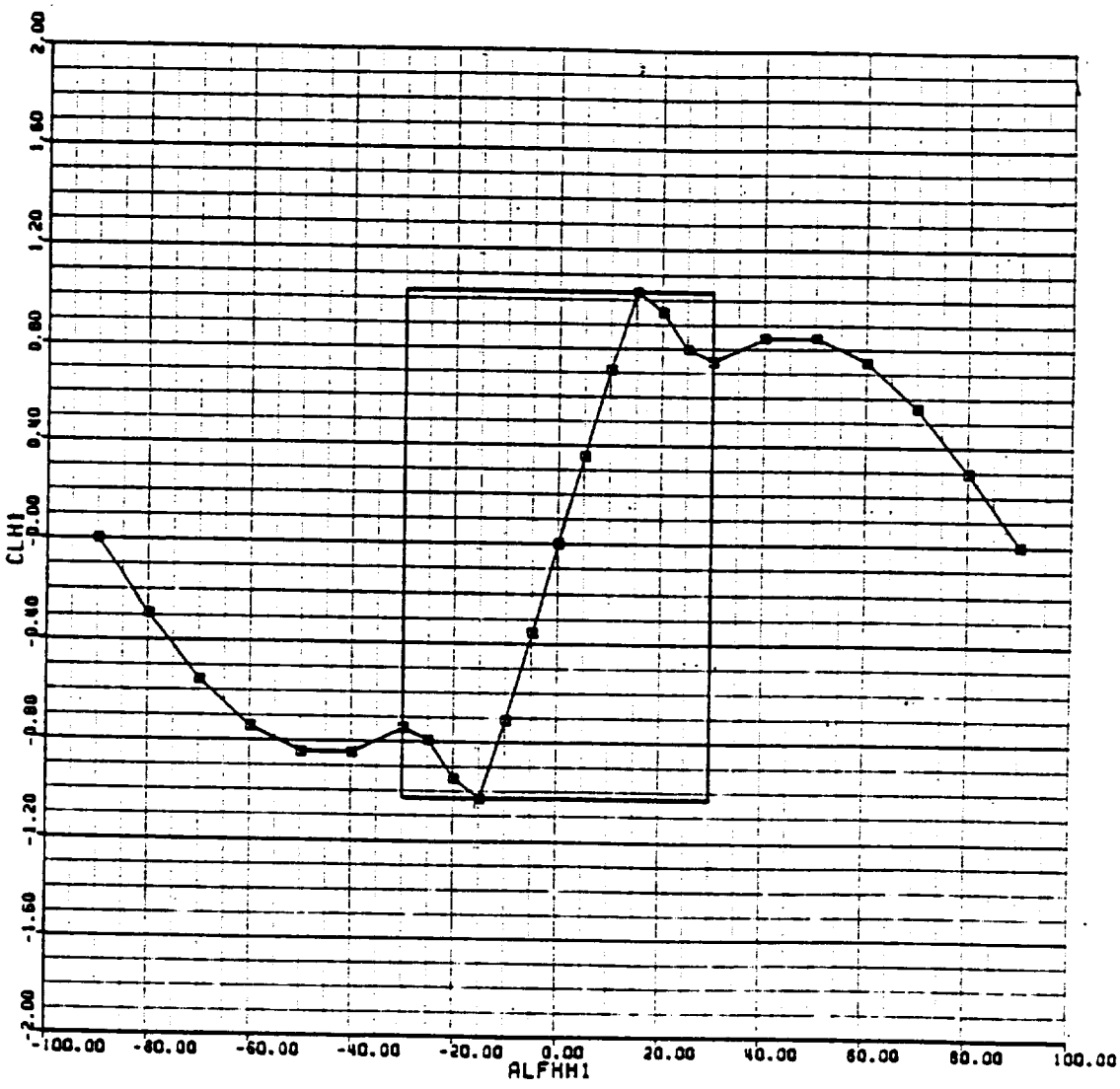

Figure B.1 Horizontal Tail Lift Coefficient Due To Angle of Attack

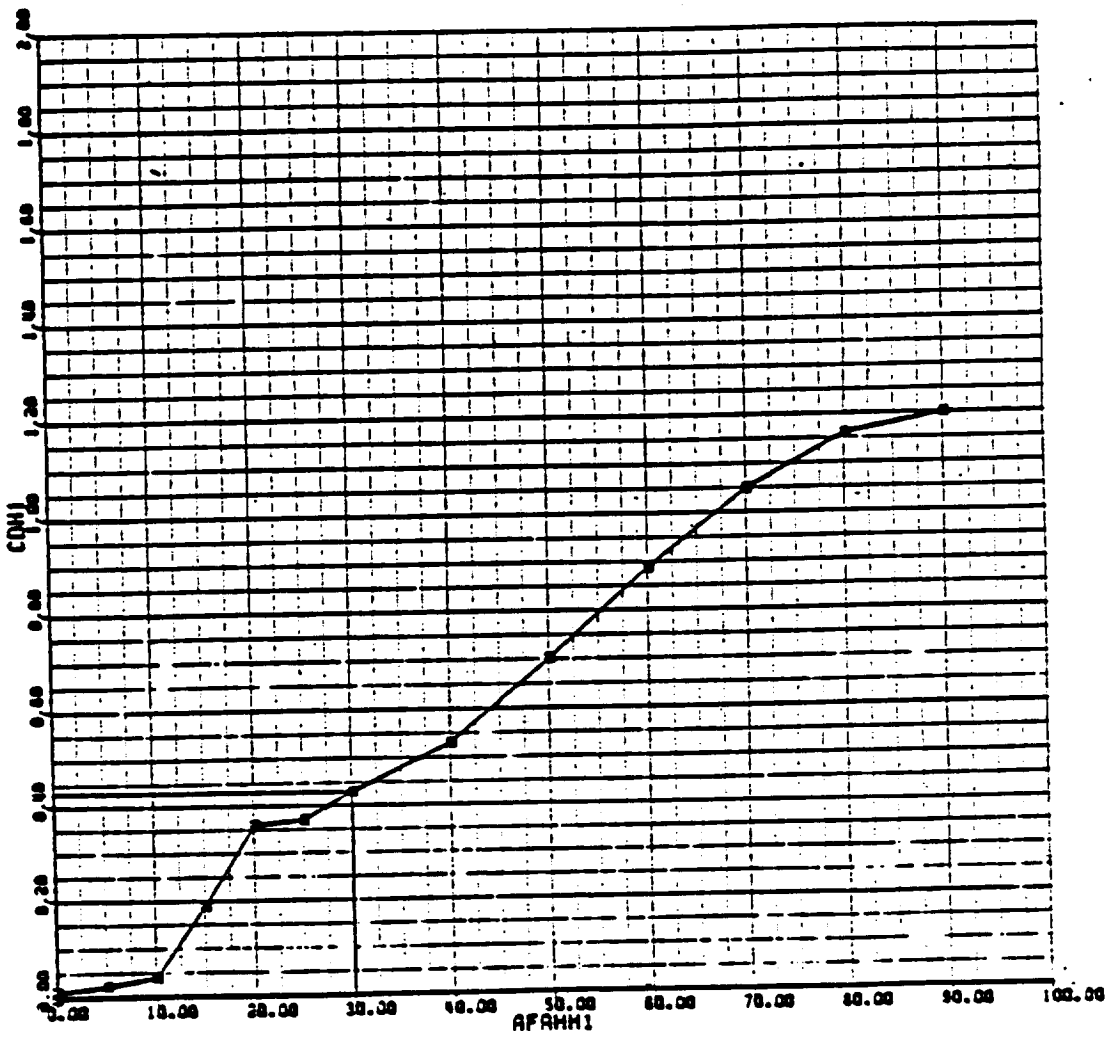

Figure B.2 Horizontal Tail Drag Coefficient Due to Angle of Attack

Appendix C Linear Model Trim State

```
ID: CASE80KT30_1_1:  7-APR-92 80kt case
FLIGHT CONDITIONS:
------------------
Velocity                80.00 Knots  => Mu = 0.1864
Altitude                 0.00 feet
Climb Angle              0.00 degrees
Beta [Beta is trim variable for Mu>0.1
Turn Rate                0.00 deg/sec


HELICOPTER CONFIGURATION:
-------------------------
Gross Weight          16790.00 lbs
Inertia wrt X-X        4659.00 slugs-ft2
Inertia wrt Y-Y       38512.00 slugs-ft2
Inertia wrt Z-Z       36796.00 slugs-ft2
Inertia wrt X-Z        1882.00 slugs-ft2
Buttline CG               0.00 inches
Fuselage Station CG     355.00 inches
Waterline CG            248.20 inches
Rotational Speed         27.00 rad/sec
Main Rotor radius        26.83 feet
Number of Blades          4.00


CONTROL VECTOR:
---------------
Lateral Cyclic             5.093328 inches
Longitudinal Cyclic        4.650049 inches
Collective Pitch           4.130504 inches
Tail Rotor Collective      3.027878 inches
Horizontal Stabilator     10.000000 degrees
```

STATE VECTOR:

Velocity - Forward	135.030794	ft/sec
Velocity - Sideward	1.488112	ft/sec
Velocity - Downward	0.521271	ft/sec
Roll Rate	-0.004995	deg/sec
Pitch Rate	-0.000003	deg/sec
Yaw Rate	-0.002703	deg/sec
Bank Angle	0.007321	degrees
Pitch Angle	0.208292	degrees
Heading	0.000000	degrees
Collective Flap Rate	-0.034198	deg/sec
Longitudinal Flap Rate	-0.786218	deg/sec
Lateral Flap Rate	-0.582595	deg/sec
Differential Flap Rate	-0.314566	deg/sec
Collective Flap	2.953387	degrees
Longitudinal Flap	0.601430	degrees
Lateral Flap	-0.602970	degrees
Differential Flap	0.161569	degrees
Collective Lag Rate	-0.003232	deg/sec
Longitudinal Lag Rate	-0.087195	deg/sec
Lateral Lag Rate	-0.012922	deg/sec
Differential Lag Rate	0.118083	deg/sec
Collective Lag	-3.511940	degrees
Longitudinal Lag	0.172414	degrees
Lateral Lag	0.017862	degrees
Differential Lag	0.004035	degrees
Dynamic Twist	-1.256921	degrees
Dynamic Twist Rate	-0.555913	deg/sec
Constant Inflow	0.015680	
1st Harmonic Cos Inflow	0.020084	
1st Harmonic Sin Inflow	-0.000737	
Tail Rotor Inflow	0.016117	
Delayed Downwash on Tail	0.495985	
Delayed Sidewash on Tail	0.103252	
Blade Azimuth Error	0.000000	degrees
Rotor Speed	27.000000	rad/sec
Gas Generator Speed	41090.000000	RPM
Fuel Flow	0.121300	lbm/sec
Fuel Flow Rate	0.000000	lbm/sec^2
p3, compressor discharge	173.400000	psi
p41, gas generator inlet	163.800000	psi
p45, power turbine inlet	35.300000	psi

Appendix D Linear Model of the UH-60A

This appendix presents the thirty state linear model of the UH-60A Black Hawk helicopter. Also presented is the eight state linear model which results from reducing the thirty state model as described in Chapter 3.0.

D.1 Thirty State Linear Model

The thirty state linear model is of the form:

$$\dot{x} = Fx + G\delta_a$$

where the order of the states (x) and controls (δ_a) and the corresponding units are presented in Tables D.1 and D.2. The F and G matrices are presented following the states and controls.

Table D.1 Order and Corresponding Units of the States of the Thirty State Linear Model

Symbol	State	Units
u	Forward Velocity	Feet per Second
v	Lateral Velocity	Feet per Second
w	Vertical Velocity	Feet per Second
p	Roll Rate	Radians per Second
q	Pitch Rate	Radians per Second
r	Yaw Rate	Radians per Second
ϕ	Roll Attitude	Radians
θ	Pitch Attitude	Radians
$\dot{\beta}_0$	Coning Rate	Radians per Second
$\dot{\beta}_{1c}$	Flap Rate Cosine Component	Radians per Second
$\dot{\beta}_{1s}$	Flap Rate Sine Component	Radians per Second
$\dot{\beta}_2$	Asymmetric Flap Rate	Radians per Second
β_0	Coning Angle	Radians
β_{1c}	Flap Angle Cosine Component	Radians
β_{1s}	Flap Angle Sine Component	Radians
β_2	Asymmetric Flap Angle	Radians
$\dot{\zeta}_0$	Average Lag Rate	Radians per Second
$\dot{\zeta}_{1c}$	Lag Rate Cosine Component	Radians per Second
$\dot{\zeta}_{1s}$	Lag Rate Sine Component	Radians per Second
$\dot{\zeta}_2$	Asymmetric Lag Rate	Radians per Second
ζ_0	Average Lag Angle	Radians
ζ_{1c}	Lag Angle Cosine Component	Radians
ζ_{1s}	Lag Angle Sine Component	Radians
ζ_2	Asymmetric Lag Angle	Radians
ϕ_{DYN}	Blade Dynamic Twist Angle	Radians
$\dot{\phi}_{DYN}$	Blade Dynamic Twist Rate	Radians per Second
λ_0	Average Dynamic Inflow	Dimensionless
λ_{1c}	Dynamic Inflow Cosine Component	Dimensionless
λ_{1s}	Dynamic Inflow Sine Component	Dimensionless
λ_2	Asymmetric Dynamic Inflow	Dimensionless

Table D.2 Order and Corresponding Units of the Controls of the Thirty State Linear Model

Symbol	Control	Units
δ_{lat}	Lateral Cyclic Stick	Inches
δ_{lon}	Longitudinal Cyclic Stick	Inches
δ_{col}	Collective Lever	Inches
δ_{ped}	Pedals	Inches
i_{ht}	Stabilator Incidence	Degrees
$\dot{\delta}_{lat}$	Lateral Cyclic Stick Rate	Inches per Second
$\dot{\delta}_{lon}$	Longitudinal Cyclic Stick Rate	Inches per Second
$\dot{\delta}_{col}$	Collective Lever Rate	Inches per Second
$\dot{\delta}_{ped}$	Pedal Rate	Inches per Second
$\dot{i}_{ht}$	Stabilator Rate	Degrees per Second

F30 =

Columns 1 through 5

-2.1555e-02	1.5260e-04	-9.5858e-04	-7.8979e-01	-9.9683e-01
-7.8761e-03	-1.0538e-01	9.3987e-03	2.5894e-01	-8.4934e-01
-2.2618e-02	5.5364e-03	-1.1070e-01	-1.4420e+00	1.3335e+02
-5.0073e-03	-2.0735e-02	2.2643e-03	-1.1253e-03	4.2457e-01
-4.8630e-03	1.6540e-02	-1.3384e-02	-2.2549e-02	-6.4062e-01
-2.1585e-03	1.5897e-02	-4.9613e-03	1.3749e-01	-1.4991e-01
0	0	0	1.0000e+00	4.6313e-07
0	0	0	0	1.0000e+00
-9.6912e-02	2.2233e-02	1.4736e+00	5.6697e+00	-1.2898e+00
7.3108e-02	2.4616e-01	2.9937e-01	5.9254e+01	-1.2248e+01
2.0100e-01	-1.2469e-01	4.1384e-01	-1.1146e+01	-5.8585e+01
-8.0016e-03	5.1742e-03	5.6225e-03	9.6161e-01	-3.2328e+00
0	0	0	0	0
0	0	0	0	0
0	0	0	0	0
0	0	0	0	0
-2.6442e-03	1.5226e-02	2.6860e-02	3.8459e-01	-7.8512e-01
-7.7641e-03	2.3323e-03	-2.4567e-02	2.7059e-03	2.9860e-01
-1.5696e-02	7.2279e-03	1.7273e-02	3.9840e-01	-5.3747e-01
1.0545e-03	1.5231e-03	5.5258e-03	-4.4122e-03	1.9323e-01
0	0	0	0	0
0	0	0	0	
0	0	0	0	0
0	0	0	0	0
0	0	0	0	0
7.6387e-01	-2.2742e-01	-1.5015e+01	-5.6477e+01	1.3738e+01
-1.6084e-03	5.3554e-05	6.8436e-03	2.1896e-02	1.1927e-03
-2.8505e-04	2.6305e-03	5.0488e-03	1.9443e-02	2.7551e-01
2.2342e-03	-1.1564e-03	5.3209e-03	2.8165e-01	-2.2946e-02
-2.9395e-03	-2.4033e-02	1.2234e-02	-1.8632e-01	3.7703e-01

Columns 6 through 10

1.2764e+00	-2.7836e-13	-3.2174e+01	1.5362e-01	2.5505e-02
-1.3324e+02	3.2174e+01	-1.4901e-05	-1.4267e-01	-3.2733e-02
1.8503e+00	-4.0986e-03	-1.1697e-01	-1.4517e+00	-8.4560e-02
6.0357e-01	-3.4169e-13	-3.5610e-13	-1.1292e-01	-8.1839e-02
-2.2187e-01	2.0325e-14	1.1156e-15	1.1177e-02	-8.4458e-03
-8.1409e-01	-2.5606e-14	-2.8010e-14	-6.0701e-03	-1.7802e-03
3.6355e-03	-3.3887e-09	4.7282e-07	0	0
-1.2739e-04	-4.7281e-07	0	0	0
-1.3573e+00	2.6170e-14	3.0465e-14	-2.8093e+01	-2.7972e+00
3.6675e+00	8.3898e-14	-2.1196e-14	-5.6447e+00	-2.7949e+01
2.6754e-01	-4.6299e-13	-4.1556e-13	-7.2711e+00	5.3948e+01
1.9916e-01	2.6295e-31	1.2358e-14	-1.3083e-01	2.7982e+00
0	0	0	1.0000e+00	-3.9606e-16
0	0	0	-7.9212e-16	1.0000e+00
0	0	0	-6.9389e-18	-3.8681e-20
0	0	0	-1.1565e-18	3.9613e-16
-8.1241e-01	-8.6395e-15	-8.6457e-15	2.3254e+00	2.6733e-01
-1.2128e-01	1.8869e-13	1.8624e-13	5.6590e-01	2.4277e+00
9.1184e-02	3.5692e-14	-2.4961e-14	-9.4552e-01	-2.7438e-02
2.3260e-02	-2.2954e-15	3.1173e-15	-8.2243e-02	-2.6265e-01
0	0	0	0	0
0	0	0	0	0
0	0	0	0	0
0	0	0	0	0
0	0	0	0	0
4.8435e+01	0	0	2.5818e+02	2.6454e+01
-1.8896e-02	0	0	-1.0114e-01	-1.0347e-02
-3.2028e-03	0	0	-3.1032e-04	-1.8791e-01
2.3927e-02	0	0	-9.7009e-02	-1.4870e-01
9.3273e-01	0	0	0	0

Columns 11 through 15

-1.2633e-01	-1.4585e-01	3.6760e+01	3.0987e+01	-2.0129e+01
-8.0547e-02	1.0376e-01	4.3231e+00	-1.4365e+01	-2.3577e+01
-1.1653e-01	-1.9429e-02	-5.3297e+02	5.5892e+00	-3.0740e+00
-1.2178e-01	6.4136e-02	2.7402e+00	-2.9097e+01	-4.1706e+01
1.8345e-02	1.2927e-02	5.5566e+00	-5.9231e+00	4.2673e+00
5.6542e-05	7.1335e-03	2.2807e-02	-2.0824e+00	-2.6058e+00
0	0	0	0	0
0	0	0	0	0
-3.5956e+00	-1.3232e-01	-8.1550e+02	2.8963e+01	-1.8905e+01
-5.4045e+01	5.6882e+00	-1.3098e+02	-1.0887e+02	-7.7016e+02
-2.8264e+01	-7.1426e+00	1.1245e+02	7.4573e+02	-7.3123e+01
-3.5805e+00	-2.8009e+01	2.2962e+01	1.6497e+02	1.3258e+02
-3.4694e-18	-1.1565e-18	0	7.6906e-17	-1.0665e-14
-4.7857e-20	7.9226e-16	0	1.1600e-18	-1.1546e-14
1.0000e+00	-2.8912e-18	0	1.1602e-14	-1.2112e-18
-1.4456e-18	1.0000e+00	0	5.2620e-17	1.0652e-14
-4.5097e-01	-7.8904e-02	1.7683e+00	1.4904e+00	6.9951e+00
5.3921e-02	-5.3378e-01	-2.0953e+01	1.2414e+01	8.1693e+01
2.2293e+00	-8.6980e-01	2.1703e+00	-7.3576e+01	-1.0014e+01
-4.5852e-01	2.3242e+00	-5.7804e+00	2.3065e+01	-6.9007e+00
0	0	0	0	0
0	0	0	0	0
0	0	0	0	0
0	0	0	0	0
0	0	0	0	0
3.4279e+01	1.0349e+00	7.8714e+01	-2.1565e+02	1.4507e+02
-1.3425e-02	-4.0977e-04	-3.9345e-02	6.7491e-03	1.1825e-02
1.4603e-01	5.9026e-02	-1.8861e+00	-4.6102e+00	-4.7647e+00
-1.9297e-01	-1.5023e-02	3.7911e-02	5.0311e+00	-3.9263e+00
0	0	-2.7776e-15	-1.3614e-01	1.1914e-01

Columns 16 through 20

3.4108e+00	-3.4150e-01	-1.0763e+01	1.3581e+01	1.0409e+00
4.9305e+00	-1.1938e+00	1.0514e+01	9.1817e+00	-9.1708e-02
-8.0798e-01	-2.1388e+00	-6.4194e-01	8.0809e-01	5.4103e-02
2.9748e+00	-6.7437e-01	6.6611e+00	5.8121e+00	-1.1662e-02
-2.4738e-01	5.4803e-02	8.1012e-01	-1.0280e+00	-8.3682e-02
1.5756e-01	-2.1298e+00	8.0956e-01	2.3566e-01	-4.8567e-01
0	0	0	0	0
0	0	0	0	0
2.2912e+01	1.5388e+00	-1.1443e-01	-9.3948e-02	-1.1760e-01
1.3770e+02	-7.5315e-01	7.8613e+00	1.5925e+00	-7.4254e-02
1.1715e+02	-7.9712e-01	3.9736e+00	7.7886e+00	-1.0198e-01
-7.8465e+02	-1.2082e-01	6.6374e-02	-1.6765e-01	1.6609e+00
0	0	0	0	0
0	0	0	0	0
0	0	0	0	0
0	0	0	0	0
-5.7610e+00	-1.4581e+01	2.1004e+00	-1.2763e+00	-3.2945e+00
1.9243e+01	3.6048e+00	-1.1167e+01	-5.7222e+01	-3.3872e+00
7.4102e-01	-2.6733e+00	5.7175e+01	-1.4856e+01	-2.4880e+00
1.9370e+00	-2.7712e+00	-1.6849e+00	-1.1825e+00	-1.2341e+01
0	1.0000e+00	3.1131e-17	-1.3300e-17	-7.3148e-17
0	6.2262e-17	1.0000e+00	-2.2460e-19	-6.0904e-17
0	-2.6599e-17	-2.1712e-19	1.0000e+00	-2.4864e-17
0	-7.3148e-17	-3.0452e-17	-1.2432e-17	1.0000e+00
0	0	0	0	0
-2.4424e+02	-4.7498e+01	-6.2226e-01	3.3484e+00	1.2366e+00
9.5949e-02	1.8495e-02	2.3739e-04	-1.3023e-03	-4.8448e-04
2.7267e-01	6.2265e-03	3.1846e-02	-2.3656e-02	5.5920e-03
1.1921e+00	-9.8716e-03	2.2954e-02	2.8452e-02	-5.2367e-03
-2.7774e-15	0	0	0	0

Columns 21 through 25

3.8246e-01	-2.2491e+02	-1.0544e+02	-3.1776e-01	-6.4930e+00
-1.1697e-01	-8.2883e+01	1.5748e+02	1.1463e+00	3.8488e-01
-7.6843e-02	-1.6435e+01	-6.2596e+00	1.1252e+00	4.8389e+01
1.7640e-02	-5.0931e+01	9.8657e+01	9.5670e-01	1.3680e+00
-6.8250e-02	1.6972e+01	7.7277e+00	1.0227e-02	-2.7167e-01
-9.1526e+00	1.7448e+00	1.5584e+01	2.4698e-02	9.3488e-02
0	0	0	0	0
0	0	0	0	0
8.7208e+00	2.4015e+01	-3.7837e+00	1.0744e+00	7.9746e+02
4.1881e+01	8.6991e+00	1.3138e+02	-4.1462e+01	2.5481e+02
-3.2575e+00	-1.0684e+02	7.4551e+01	-2.2536e+00	3.2246e+02
1.0120e+00	-1.6897e+01	2.9232e-01	8.7206e+00	8.4831e+00
0	0	0	0	0
0	0	0	0	0
0	0	0	0	0
0	0	0	0	0
-6.2498e+01	3.5982e+01	5.5368e+01	-7.0927e-03	-2.4077e+01
-9.9445e-01	7.1191e+02	-2.8642e+02	1.1010e+00	-1.0557e+01
2.8267e-01	4.1658e+02	7.1876e+02	1.0290e+00	1.2139e+01
2.7325e-02	3.2487e+01	-4.4551e+01	-5.2711e+01	4.3521e+00
0	3.3188e-16	8.3292e-16	0	0
0	6.2162e-18	-4.9960e-15	0	0
0	8.9188e-15	-5.9249e-18	0	0
0	3.3426e-16	-8.3241e-16	0	0
0	0	0	0	0
-8.8687e+01	-3.2567e+02	2.1800e+01	6.6046e+00	-2.9300e+04
3.4596e-02	1.2691e-01	-8.5069e-03	-2.5181e-03	2.8282e+00
3.8292e-01	4.8021e-01	5.3631e-01	-2.1319e-01	5.2155e-02
2.5130e-01	-4.2464e-01	4.5603e-01	-1.8478e-01	4.3629e+00
0	0	0	0	0

Columns 26 through 30

0	-3.0434e+00	1.9431e+00	-5.5859e-01	4.0406e-01
0	-1.2227e+01	-8.0724e-01	-8.5136e-01	-1.1802e+01
0	1.1827e+02	-2.4309e-01	-3.8162e+00	4.8169e+00
0	-4.4542e+00	-6.7420e-01	-3.2645e+00	-5.7453e+00
0	2.1043e+01	-4.4802e-01	1.2215e-01	1.8940e+00
0	5.9260e+00	-4.5989e-02	-1.7505e-01	5.3174e+00
0	0	0	0	0
0	0	0	0	0
0	-1.0630e+03	1.5870e-01	-1.4580e+02	1.7944e-01
0	-2.0619e+02	-5.6601e+02	-4.5095e+02	-1.8345e+00
0	-2.9786e+02	4.4210e+02	-5.8052e+02	-5.3698e+00
0	-3.7062e+00	8.9660e+01	-2.2071e+01	1.1073e-02
0	0	0	0	0
0	0	0	0	0
0	0	0	0	0
0	0	0	0	0
0	-1.8406e+01	8.0484e+00	-1.3837e-01	6.0303e+00
0	1.9937e+01	-7.7657e+00	-5.4181e+00	2.2014e+00
0	-1.2122e+01	9.3770e+00	-1.3955e+01	-8.8900e-01
0	-4.0989e+00	-2.0145e+00	-5.6454e+00	9.7318e-03
0	0	0	0	0
0	0	0	0	0
0	0	0	0	0
0	0	0	0	0
1.0000e+00	0	0	0	0
-8.9100e+01	1.0821e+04	-7.5597e+00	1.3984e+03	0
0	-9.3382e+00	-5.8078e+00	-4.8390e-01	0
0	4.1229e+01	-4.2076e+01	2.0711e-01	0
0	-4.2269e+00	2.6433e-01	-2.0711e+01	0
0	-1.9601e+01	0	0	-6.6492e+01

G30 =

Columns 1 through 5

2.2227e-02	1.9036e-02	-2.3610e-01	4.3555e-02	-3.5957e-02
8.2029e-03	-7.8725e-03	4.1004e-01	-1.5980e+00	-2.6178e-05
-4.6244e-03	1.3200e-01	7.9123e-01	5.7817e-01	-1.3361e-01
-6.8416e-03	1.1615e-01	1.8628e-01	-8.4664e-01	1.7087e-05
-9.6404e-03	-6.2399e-03	-7.0883e-02	2.5905e-01	-4.8697e-02
1.0668e-02	1.0224e-03	-2.2123e-01	7.2208e-01	2.1076e-05
0	0	0	0	0
0	0	0	0	0
-8.1844e-01	1.2030e+01	2.1799e+01	-6.8881e+00	-5.0315e-03
-1.7671e+01	2.0276e+01	7.1994e+00	-1.1902e+01	-3.7509e-02
1.0821e+01	3.2983e+01	2.7209e+00	-1.9681e+01	2.9230e-02
4.0834e+00	2.6484e+00	-8.3587e-01	-1.5207e+00	-7.0042e-05
0	0	0	0	0
0	0	0	0	0
0	0	0	0	0
0	0	0	0	0
3.1232e-01	6.7527e-02	-1.1027e+00	7.8071e-01	2.7564e-04
7.3582e-01	-7.6152e-01	-1.9994e-01	7.3608e-01	-9.2766e-03
-2.3071e-01	-9.6590e-01	5.0053e-01	4.3397e-01	-1.1997e-02
9.8926e-02	5.5124e-02	1.2276e-01	-3.0328e-02	2.0261e-04
0	0	0	0	0
0	0	0	0	0
0	0	0	0	0
0	0	0	0	0
0	0	0	0	0
8.1055e+00	-1.1818e+02	-2.0340e+02	6.7910e+01	0
-3.1466e-03	4.6256e-02	7.9334e-02	-2.6580e-02	0
-2.1542e-01	-4.0983e-02	4.2713e-02	2.3546e-02	0
-2.5345e-02	4.1009e-01	6.7982e-02	-2.3566e-01	0
0	0	3.7796e-01	-1.3084e+00	0

Columns 6 through 10

-4.5471e-04	-1.6872e-03	-3.6002e-03	9.6957e-04	0
1.0357e-03	1.0056e-03	1.3688e-03	-5.7788e-04	0
-2.8108e-05	-1.0768e-04	-2.1023e-04	6.1876e-05	0
6.5455e-04	5.3956e-04	8.6911e-04	-3.1006e-04	0
3.6570e-05	1.3195e-04	2.7544e-04	-7.5825e-05	0
4.4539e-04	1.9753e-03	2.5447e-04	-1.1351e-03	0
0	0	0	0	0
0	0	0	0	0
-8.4961e-06	-3.9069e-05	-5.4287e-05	2.2451e-05	0
5.2351e-04	6.2778e-04	7.9457e-04	-3.6075e-04	0
3.8824e-04	2.2458e-04	5.1439e-04	-1.2906e-04	0
-9.2658e-06	-2.5141e-05	-2.4685e-05	1.4447e-05	0
0	0	0	0	0
0	0	0	0	0
0	0	0	0	0
0	0	0	0	0
2.6835e-03	1.3077e-02	1.2786e-03	-7.5146e-03	0
-1.2544e-03	5.7378e-05	1.9497e-03	-3.2972e-05	0
3.3646e-03	7.1048e-03	1.1351e-02	-4.0827e-03	0
2.9174e-03	6.9860e-03	4.8901e-04	-4.0145e-03	0
0	0	0	0	0
0	0	0	0	0
0	0	0	0	0
0	0	0	0	0
0	0	0	0	0
0	0	0	0	0
0	0	0	0	0
0	0	0	0	0
0	0	0	0	0

D.2 Eight State Linear Model

The eight state linear model is of the form:

$$\dot{x}_8 = F_8 x_8 + G_8 \delta_a$$

where the order of the states (x_8) and controls (δ_a) of the eight state model as well as the corresponding units are presented in Tables D.3 and D.4. The F_8 and G_8 matrices are presented following the states and controls.

Table D.3 Order and Corresponding Units of the States of the Eight State Linear Model

Symbol	State	Units
u	Forward Velocity	Feet per Second
γ	Flight Path Angle	Degrees
q	Pitch Rate	Degrees per Second
θ	Pitch Attitude	Degrees
v	Lateral Velocity	Feet per Second
p	Roll Rate	Degrees per Second
ϕ	Roll Attitude	Degrees
r	Yaw Rate	Degrees per Second

Table D.4 Order and Corresponding Units of the Controls of the Eight State Linear Model

Symbol	Control	Units
δ_{lon}	Longitudinal Cyclic Stick	Inches
δ_{col}	Collective Lever	Inches
δ_{lat}	Lateral Cyclic Stick	Inches
δ_{ped}	Pedals	Inches
i_{ht}	Stabilator Incidence	Degrees

F8 =

Columns 1 through 5

-3.1815e-02	-5.6974e-02	1.4734e-02	-5.0452e-01	3.2261e-03
1.4061e-02	-6.3225e-01	8.8614e-03	6.3311e-01	5.1438e-03
-2.9342e-01	-2.2105e-01	-1.2779e+00	2.2105e-01	9.4964e-01
0	0	1.0000e+00	0	0
-7.2442e-03	6.2077e-04	-8.9640e-03	-6.2103e-04	-1.0358e-01
-4.0208e-01	-2.3819e+00	-8.4664e-02	2.3819e+00	-1.8469e+00
0	0	4.6313e-07	4.7282e-07	0
-1.6762e-01	9.1460e-01	-3.3803e-02	-9.1460e-01	6.2178e-01

Columns 6 through 8

-1.3050e-02	-3.8862e-15	2.1829e-02
-4.6750e-05	2.9887e-05	-1.2805e-02
1.8792e-01	1.3904e-14	-1.8932e-01
0	-4.7281e-07	-1.2739e-04
-2.1758e-03	5.6150e-01	-2.3291e+00
-2.9243e+00	-3.3573e-13	3.2823e-01
1.0000e+00	-3.3887e-09	3.6355e-03
-1.2658e-01	-2.3593e-14	-6.4776e-01

G8 =

-9.7218e-01	3.1948e-01	-7.5831e-02	6.5398e-01	-4.0908e-02
1.4435e+00	3.1958e+00	-2.1830e-01	-1.0527e+00	5.6659e-02
2.1747e+01	7.4702e+00	1.6490e-01	-4.0417e-01	-2.7731e+00
0	0	0	0	0
-1.5333e-01	2.2539e-01	3.1447e-01	-1.2208e+00	1.2206e-05
5.4859e+00	1.0167e+01	6.0052e+01	-4.0496e+01	1.2692e-01
0	0	0	0	0
-8.1107e-01	-1.9791e+00	3.3917e+00	3.0067e+01	6.9885e-03

Appendix E Frequency Response Comparison of Eight State and Thirty State Linear Models

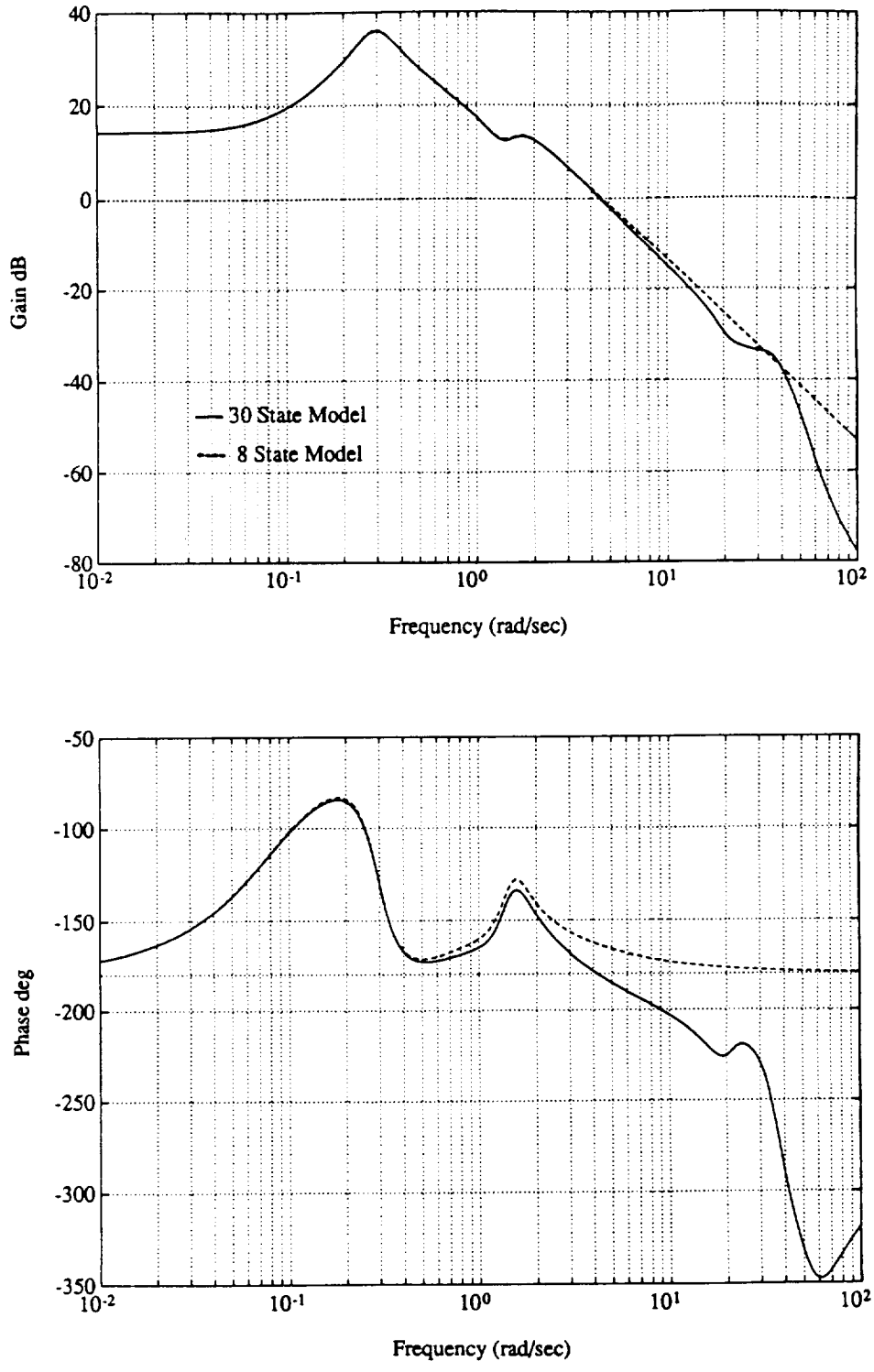

Figure E.1 Frequency Response Comparison of the Pitch Attitude To Longitudinal Cyclic Transfer Functions

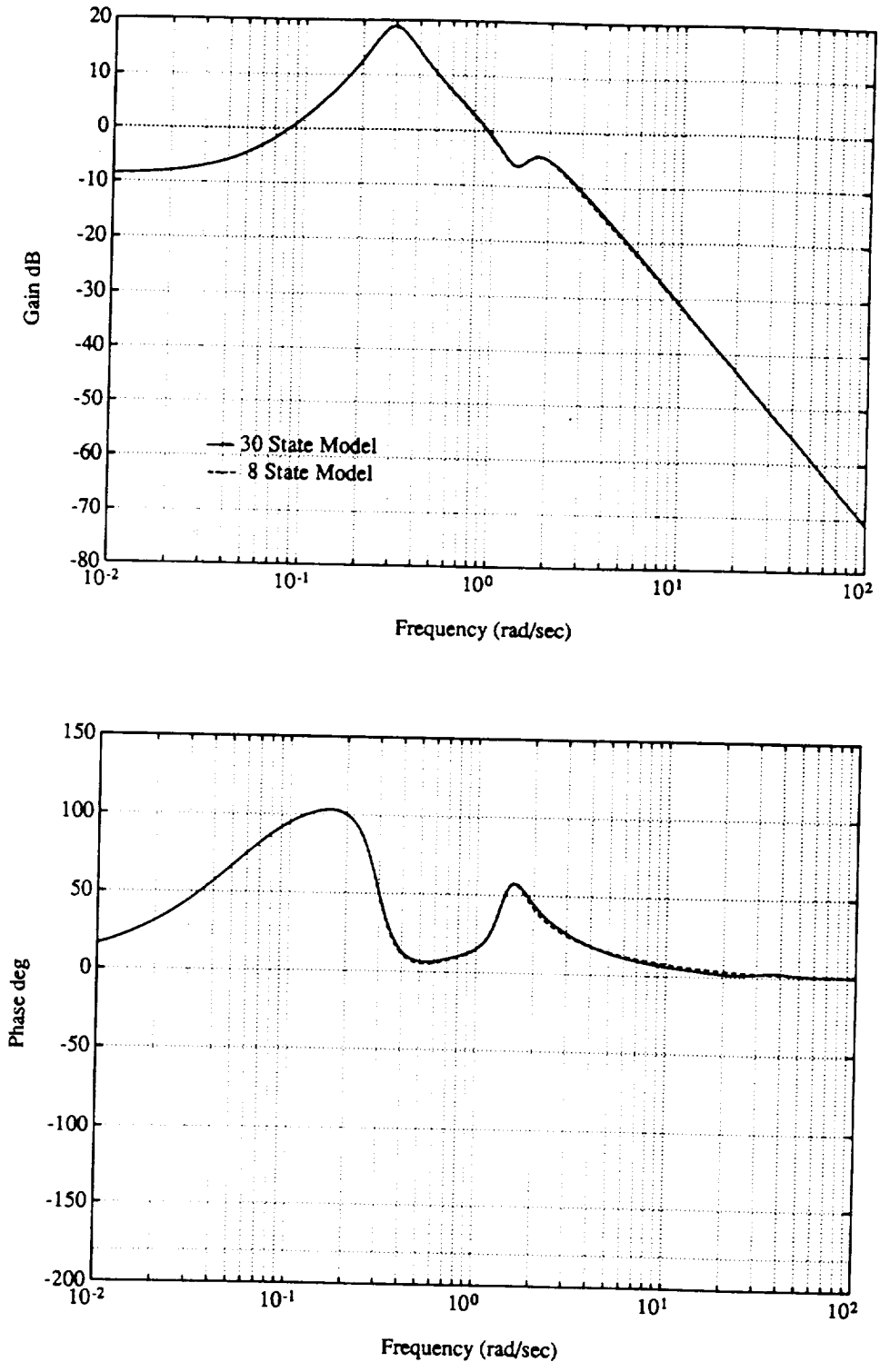

Figure E.2 Frequency Response Comparison of the Pitch Attitude To Stabilator Transfer Functions

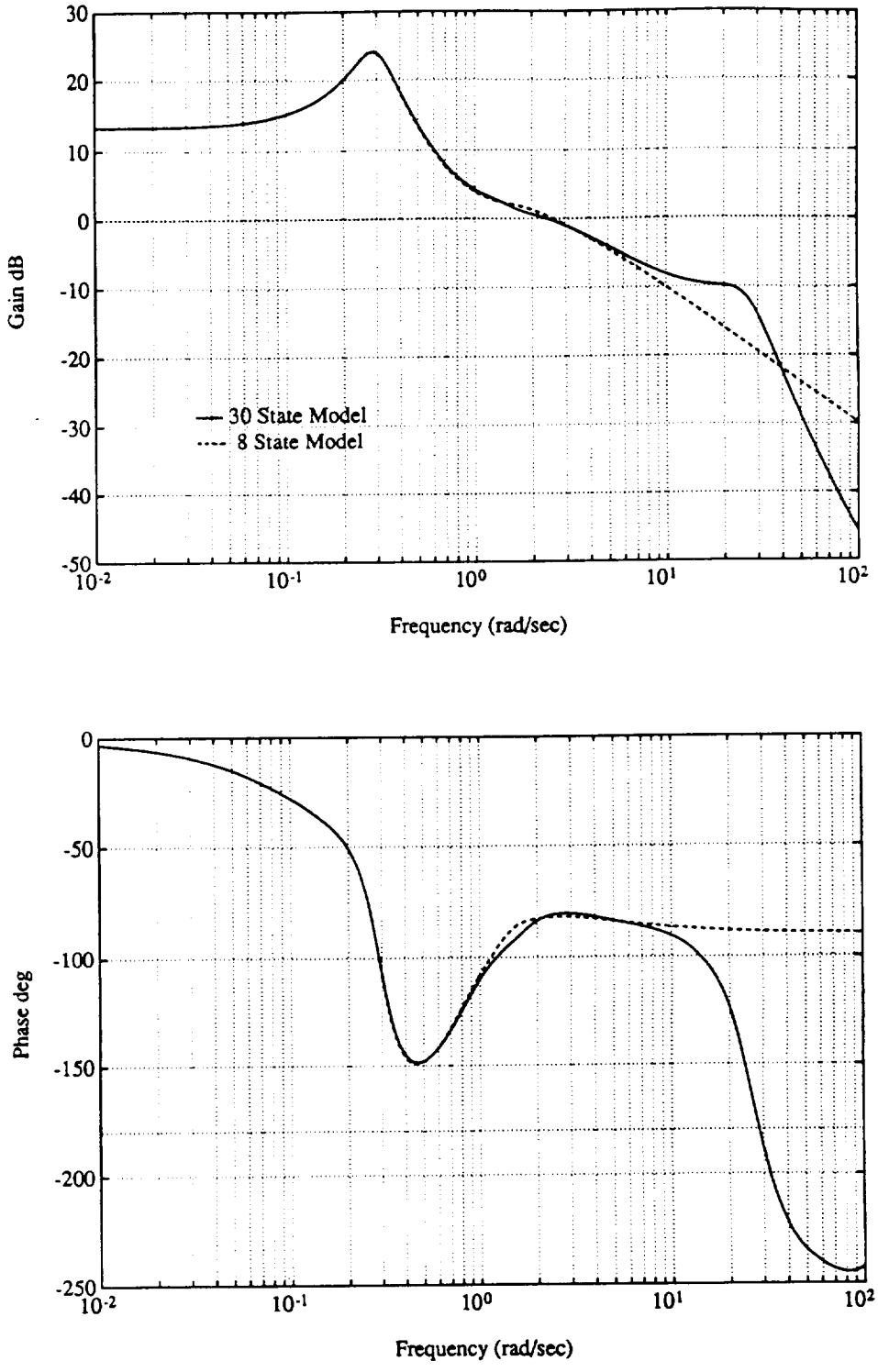

Figure E.3 Frequency Response Comparison of the Flight Path Angle To Collective Transfer Functions

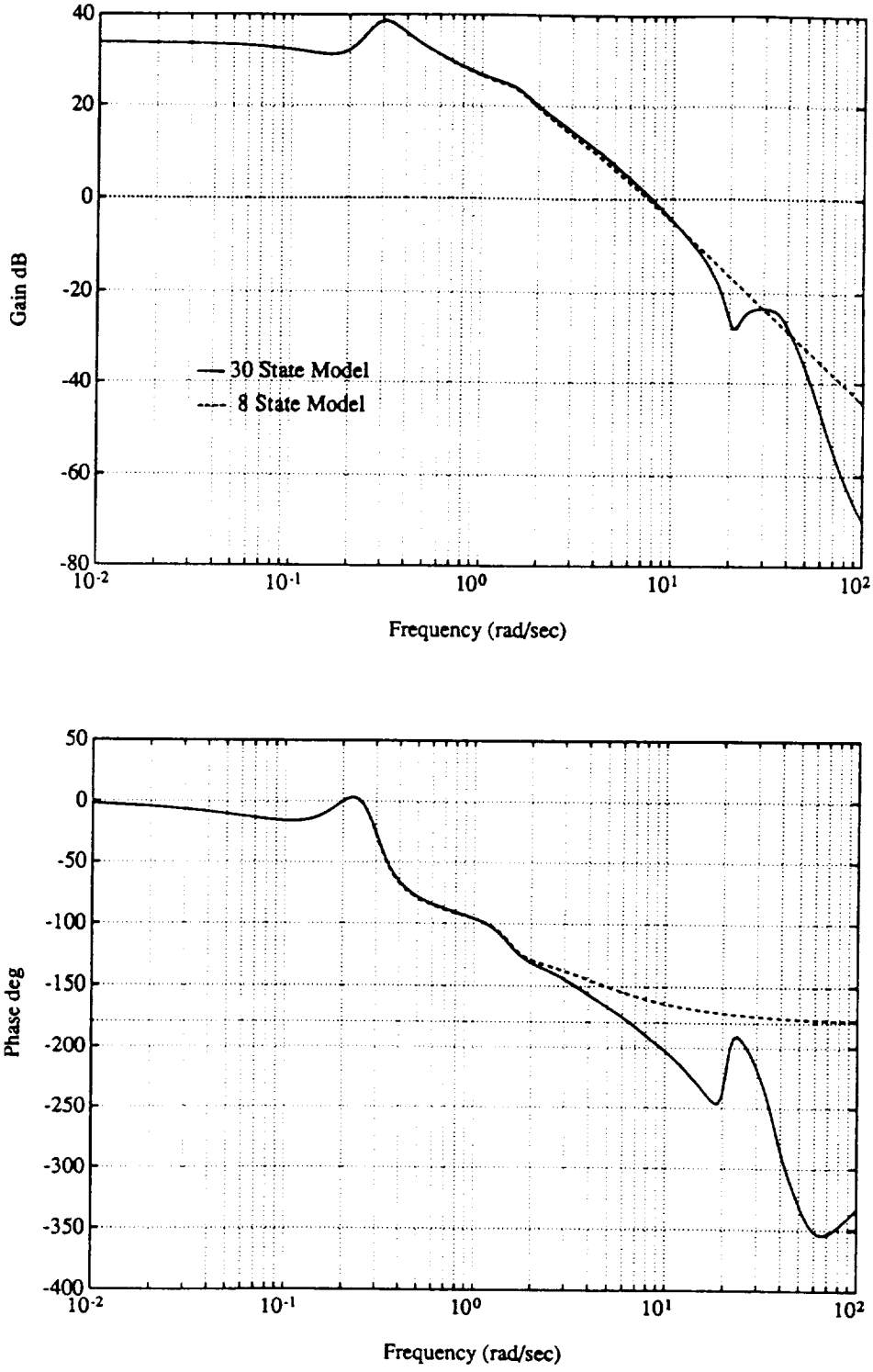

Figure E.4 Frequency Response Comparison of the Roll Attitude To Lateral Cyclic Transfer Functions

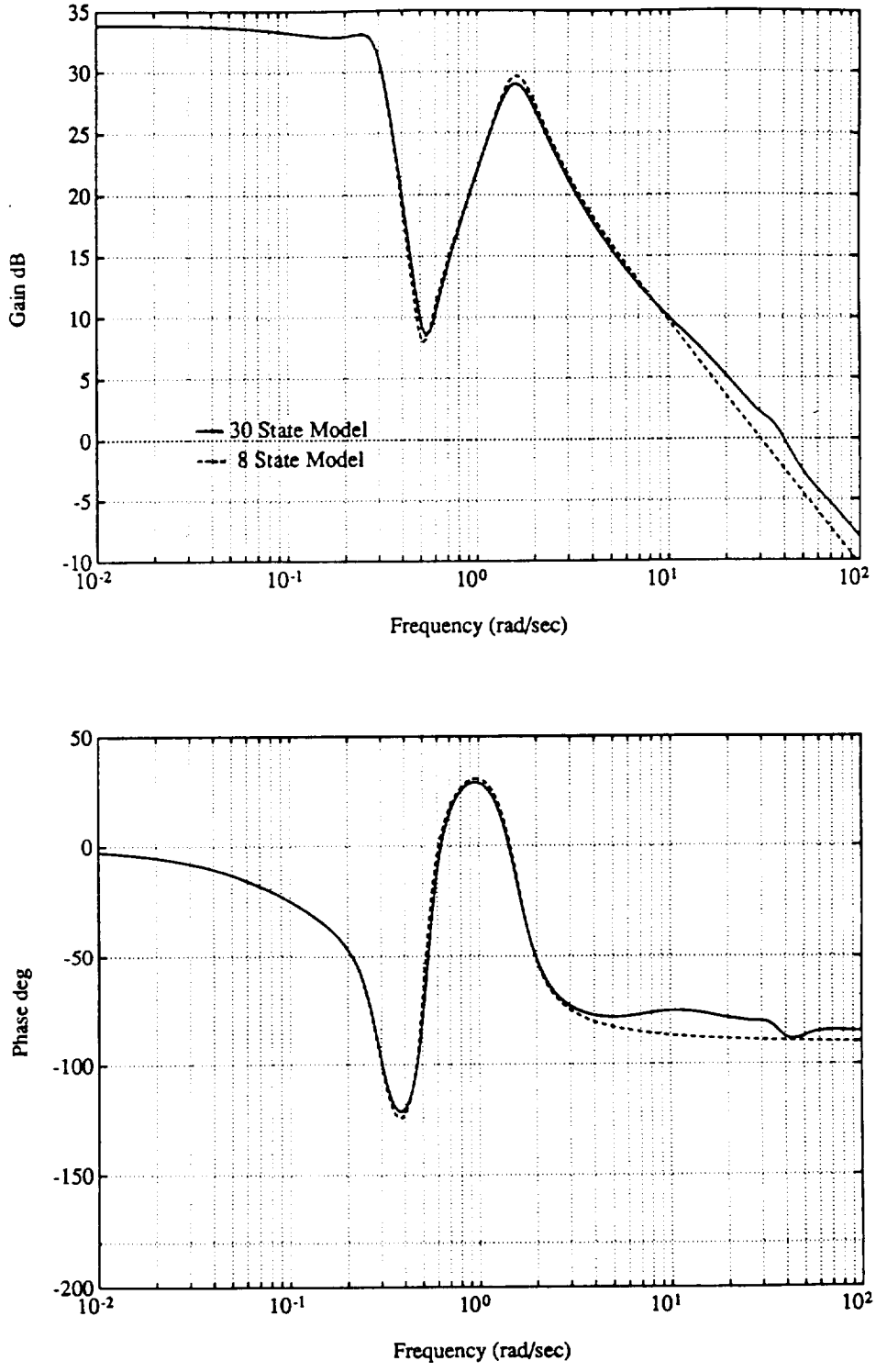

Figure E.5 Frequency Response Comparison of the Yaw Rate To Pedals Transfer Functions

Appendix F Feedback Control Design

The feedback design consisted of feeding back the rotational rates and attitudes of the aircraft to the pilot controls to improve the aircraft's stability and performance. The loops were closed sequentially beginning with the roll loop since the lateral cyclic is the fastest and the most decoupled. To regulate the aircraft's roll response, roll rate and roll attitude were fed back to the lateral cyclic since it is the primary rolling moment control. The yaw loop was closed next to regulate the yaw response. Yaw rate and the integral of yaw rate were fed back to the pedals since the pedals are the primary yawing moment control. Finally, to stabilize the divergent longitudinal mode, pitch rate and pitch attitude were fed back to the longitudinal cyclic since the longitudinal cyclic is the primary pitching moment control. The feedback design was conducted using the eight state, linear model of the aircraft since the thirty state model was too cumbersome for classical control design.

In the feedback design process, the closed loop bandwidths were kept near or below 5.0 radians per second. This was done since the frequency response comparisons in Appendix E show that the unmodelled rotor dynamics begin to add significant phase lag in the decade between one and ten radians per second. In closing the feedback loops, a phase margin of seventy five degrees was desired. This specification was chosen to allow approximately thirty degrees to account for the unmodelled dynamics and forty five degrees as a stability margin.

The roll rate and attitude were fed back to the lateral cyclic to reduce the sensitivity of the roll response. The roll loops were closed first since the roll axis is the fastest and most decoupled. Because of this the yaw and pitch loops shouldn't change the closed loop roll dynamics very much. To carry out the feedback design, the eight state model was converted to the roll attitude to lateral cyclic transfer function using Matlab's SS2TF function. Figure F.1 presents the frequency response of this transfer function. Since the open loop system is unstable, the frequency responses of the transfer functions don't have any physical meaning. However, as long as the closed loop system is stable, the frequency responses can be used to provide useful information about the system. It can be seen that at frequencies below 0.1 rad/sec, the roll attitude to lateral cyclic transfer function has a gain of approximately thirty four dB indicating a steady state roll attitude response of approximately fifty degrees per inch of lateral cyclic. At frequencies above one rad/sec, the magnitude rolls off at forty dB/decade indicating roll acceleration response to lateral cyclic stick. However, the higher order dynamics are not accounted for in this model. From

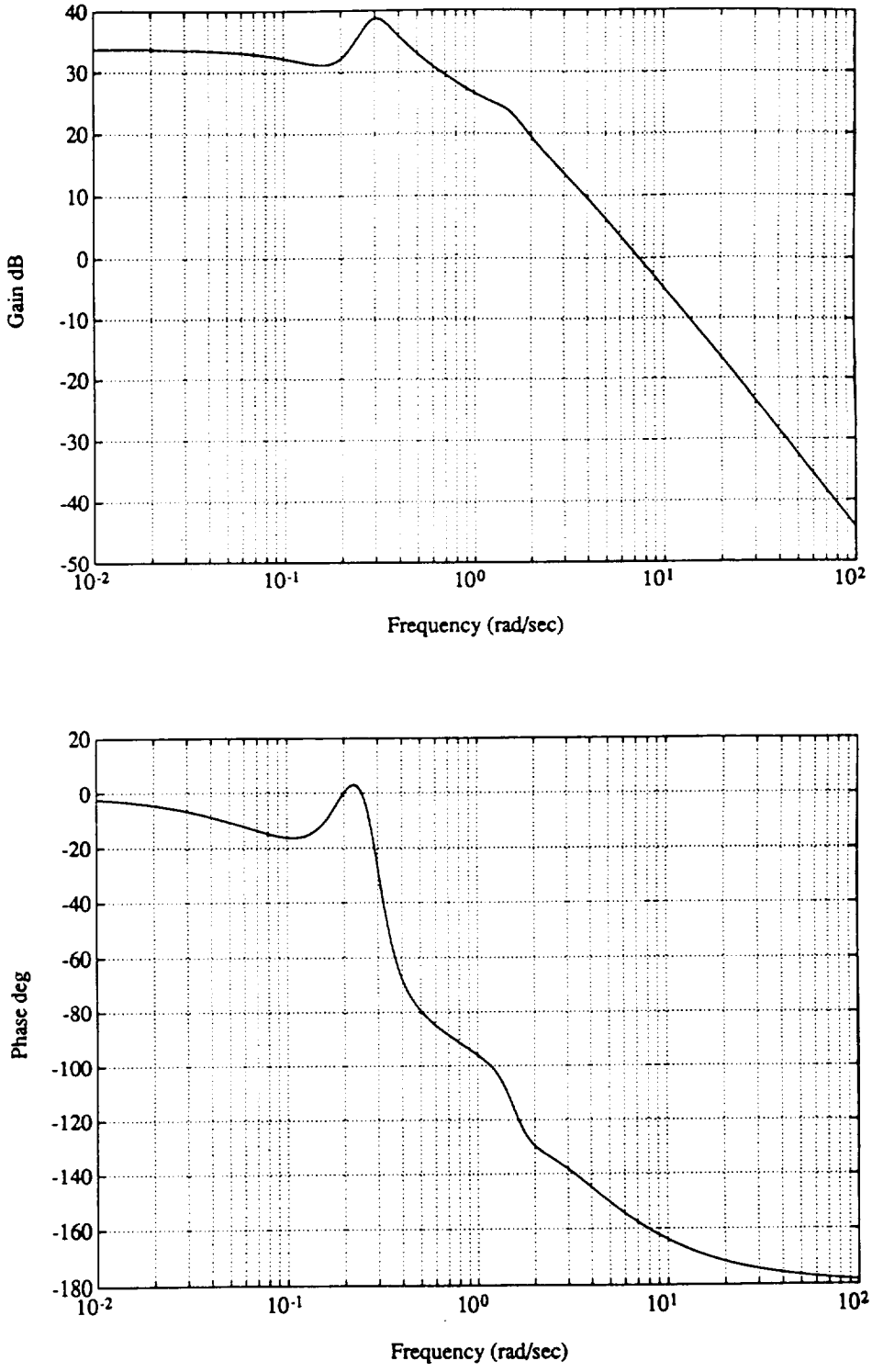

Figure F.1 Frequency Response of the Transfer Function Between Roll Attitude and Lateral Cyclic

Appendix E, it can be seen that the phase continues to decrease instead of asymptotically approaching -180.0 degrees as is predicted in this model.

The constant gain roll rate and roll attitude feedback to the lateral cyclic result in a simple feedback control law which can be represented by the equation

$$\delta_{lat} = - k_p\, p - k_\phi\, \phi$$

The roll attitude and roll rate feedback gains were determined by adding an additional zero into the forward path to account for the roll rate feedback. The design was then carried out using a classical control approach using the following loop transmission function:

$$G(s) = k_\phi\,(\tau s + 1)\,\frac{\phi(s)}{\delta_{lat}(s)}, \qquad \tau = \frac{k_p}{k_\phi}$$

The influences of the roll rate gain (k_p) and the roll attitude gain (k_ϕ) were determined using a root locus, which is presented in Figure F.2. The ratio of the roll rate gain to the roll attitude gain (τ) was fixed at different values and then the corresponding loci were plotted. Figure F.2 shows the root loci for no roll rate feedback and for a gain ratio (τ) of 0.1667. The loci show that feeding back the roll rate proportional to the roll attitude adds damping to the high frequency complex pair. The other eigenvalues are relatively insensitive to the roll feedback. At the selected gains, the natural frequency of the complex pair is just above five radians per second and the damping is approximately seventy percent. Figure F.3 presents the frequency response of the loop transmission function when the attitude feedback gain is 0.0667 inches/degree and the rate feedback gain is 0.4 inches/degree/second. The frequency response indicates that the system possesses approximately seventy five degrees of phase margin at the gain crossover frequency.

While the sensitivity of the open loop system is unity at all frequencies the sensitivity of the closed loop system is defined as:

$$S(s) = \frac{1}{1 + G(s)}$$

Figure F.4 presents the sensitivity of the closed loop roll attitude response and shows that the sensitivity of the roll response has been attenuated by an order of magnitude at frequencies below 0.5 radians per second but approaches unity at higher frequencies where feedback is not effective.

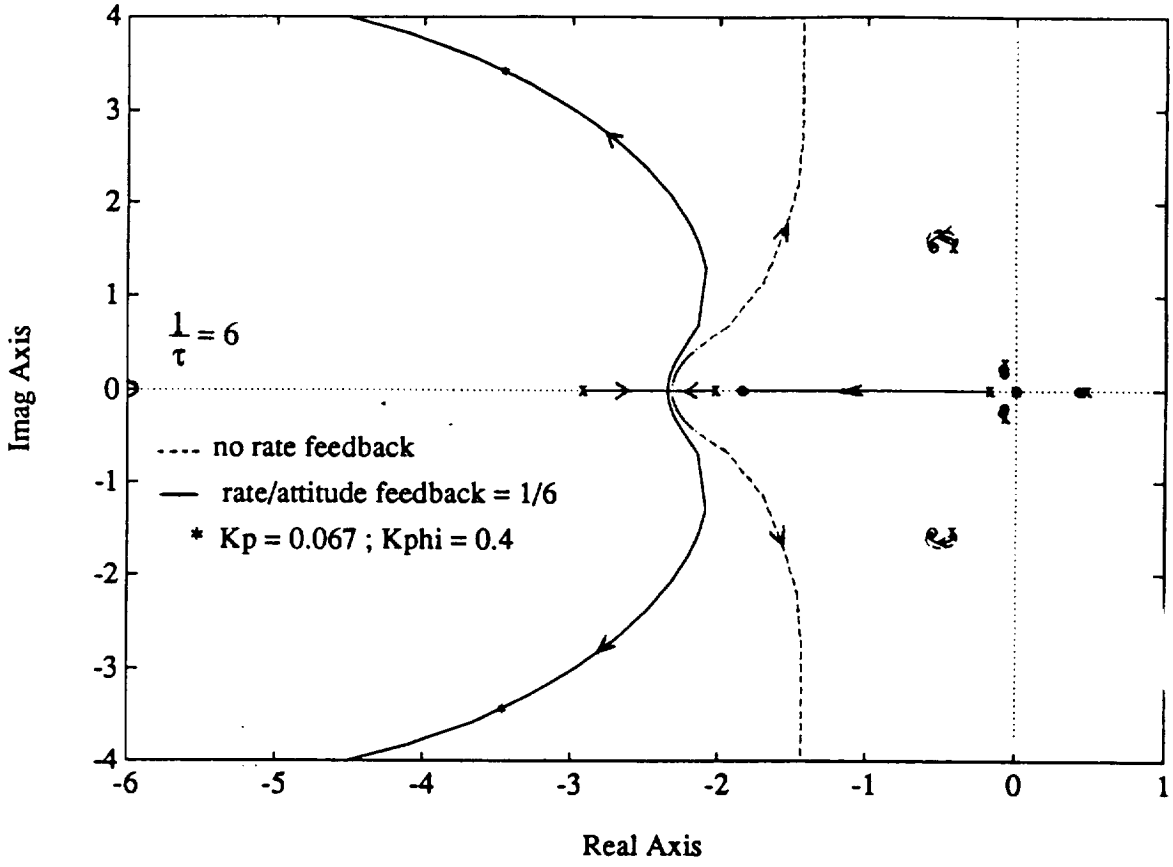

Figure F.2 Roll Feedback Root Loci

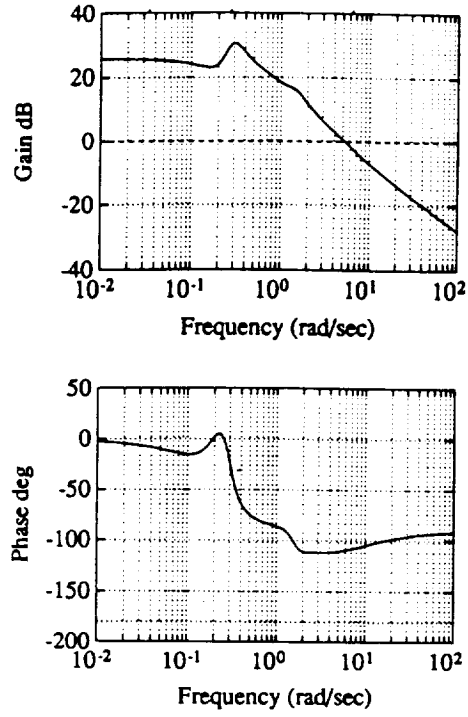

Figure F.3 Frequency Response of the Roll Loop Transmission ($k_p = 0.0667$, $k_\phi = 0.4$)

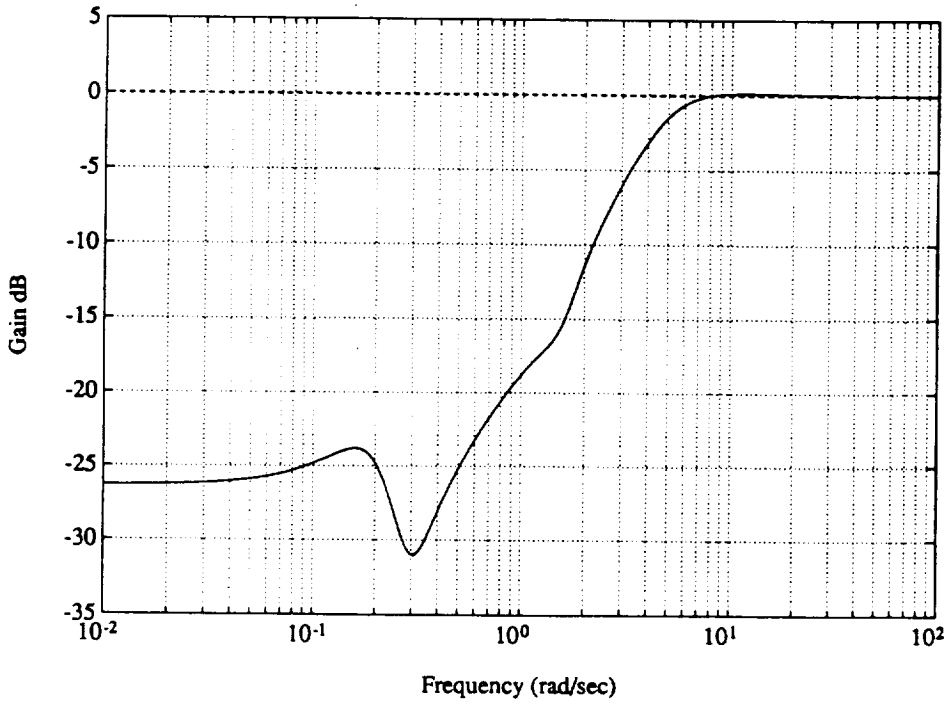

Figure F.4 Sensitivity of the Roll Attitude Response With Roll Loops Closed

With the roll loops closed, the yaw rate and the integral of the yaw rate were fed back to the pedals to reduce the sensitivity of the yaw response. The transfer function between the yaw rate and the pedals was again determined from the eight state model using Matlab's SS2TF function. To make sure that the yaw rate response was regulated about the origin, the integral of the yaw rate was fed back in addition to the yaw rate. The frequency response of the transfer function between the integral of the yaw rate and the pedals is presented in Figure F.5. At low frequencies, the plot has a slope of twenty dB/decade indicating the presence of the integrator that was added to provide high gain at low frequencies. The design procedure was identical to the roll loop design procedure.

The constant gain yaw rate and integral yaw rate feedback to the pedals is given by

$$\delta_{ped} = - k_r\, r - k_i \int r$$

The determination of the yaw rate and integral yaw rate feedback gains was achieved by adding an additional zero into the forward path to account for the yaw rate feedback. The design was then carried out using a classical control approach using the following loop transmission function:

$$G(s) = k_i\,(\tau s + 1)\,\frac{1}{s}\,\frac{r(s)}{\delta_{ped}(s)}, \quad \tau = \frac{k_r}{k_i}$$

The integrator was added to provide the integral of yaw rate. This requires an additional state equation to be added to the linear model to provide the integral of the yaw rate. The state equation added was simply

$$\dot{\int r} = r$$

The influences of the yaw rate gain (k_r) and the integral yaw rate gain (k_i) were determined using a root locus, which is presented in Figure F.6. The ratio (τ) of the yaw rate gain to the integral yaw rate gain was fixed at different values and then the corresponding loci were plotted. Figure F.6 shows the loci for gain ratios of zero and 0.2. The figure shows that the addition of the yaw rate feedback adds damping to the mid frequency complex pair causing them to coalesce at high enough values of the integral yaw rate gain. The real pole is also driven farther into the left half plane when yaw rate is fed back. The figure shows that the yaw feedback has a small effect on the roll complex pair and also adds damping to the low frequency complex pair. When the yaw rate feedback gain is equal to 0.2

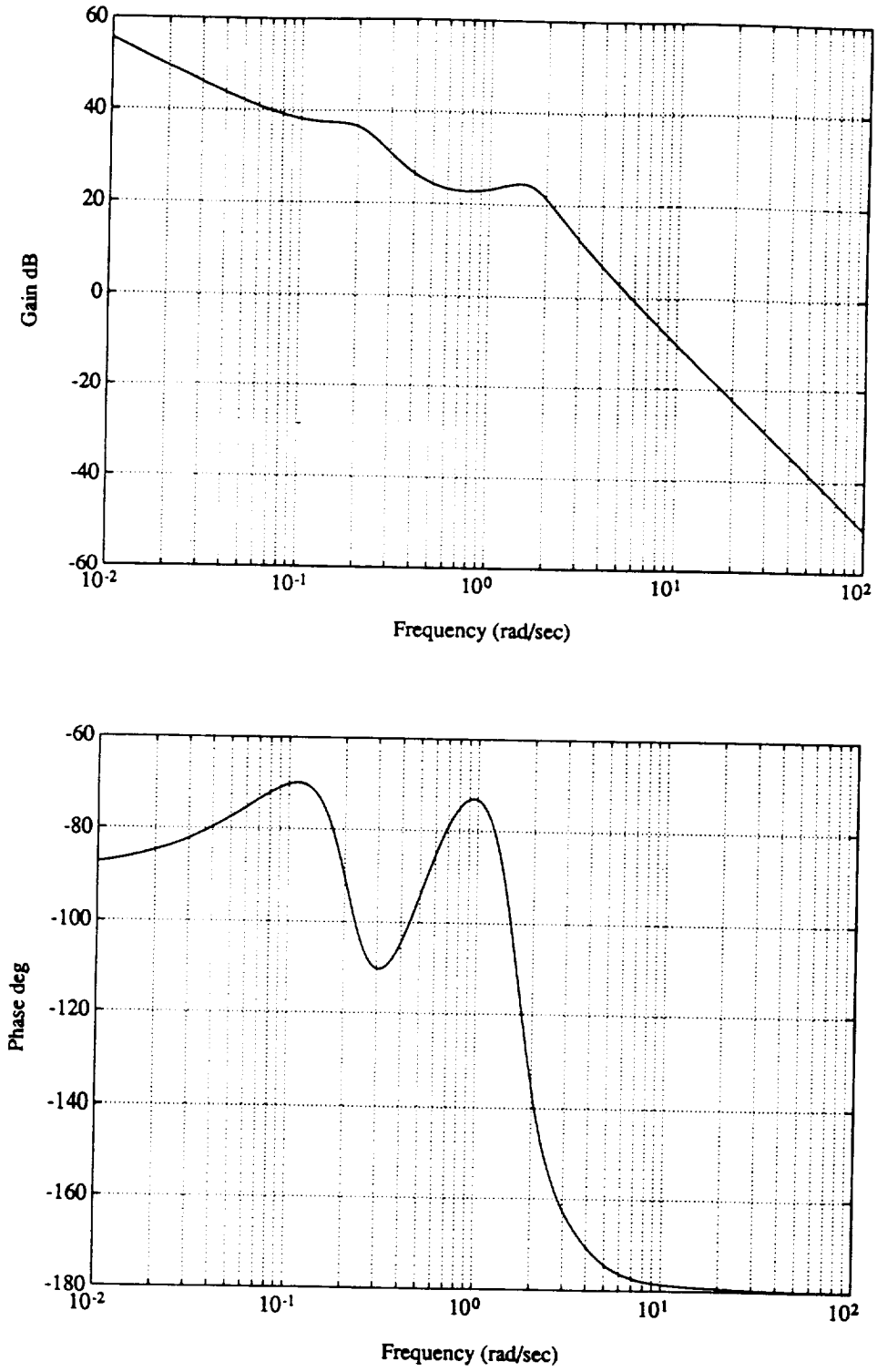

Figure F.5 Frequency Response of the Transfer Function Between Integral Yaw Rate and Pedals

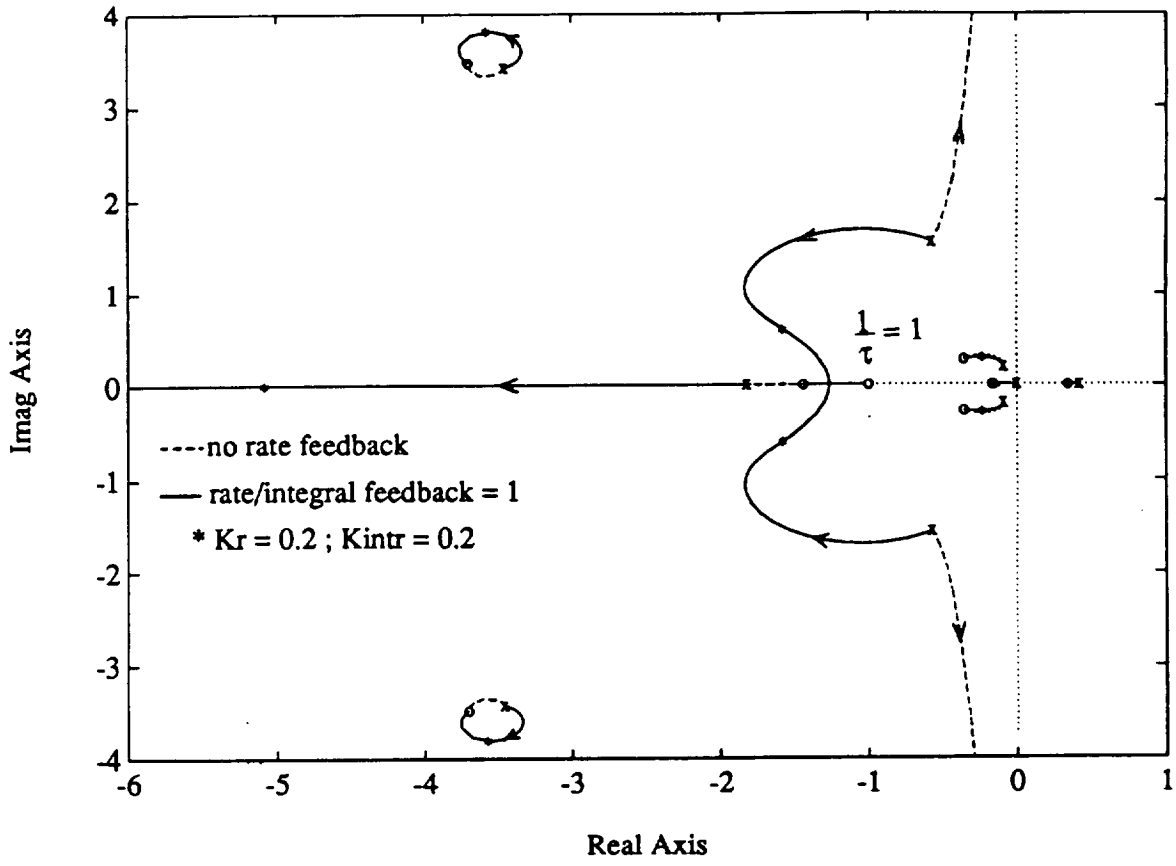

Figure F.6 Yaw Feedback Root Loci

inches/degree/second and the integral yaw rate gain is 0.2 inches/degree, the real pole is at -5.0 radians per second. Figure F.7 presents the frequency response of the corresponding loop transmission and shows that this loop possesses a phase margin in excess of eighty degrees at the gain crossover frequency. Figure F.8 presents the sensitivity of the integral of the yaw rate when the roll and yaw loops are closed. The sensitivity of the closed loop system is again defined as:

$$S(s) = \frac{1}{1 + G(s)}$$

Figure F.8 shows that at low frequencies the sensitivity approaches zero indicating that the steady state yaw rate response should be well regulated.

Once the roll and yaw loops were closed to desensitize the off axis responses to longitudinal commands, the pitch rate and pitch attitude were fed back to the longitudinal cyclic to stabilize the unstable pole and provide an adequate degree of stability. The transfer function between the pitch attitude and the longitudinal cyclic was also obtained from the eight state linear model using Matlab's SS2TF function. The frequency response of this transfer function is presented in Figure F.9. This figure shows that at frequencies below 0.1 radians per second, the pitch attitude is proportional to the longitudinal cyclic deflection but reaches a peak at 0.35 radians per second and then rolls off at a rate of forty dB/decade.

The constant gain pitch rate and pitch attitude feedback to the longitudinal cyclic is represented by the control law

$$\delta_{lon} = - k_q \, q - k_\theta \, \theta$$

The determination of the pitch rate and pitch attitude feedback gains was achieved by adding an additional zero into the forward path to account for the pitch rate feedback. The design was then carried out using a classical control approach using the following loop transmission function:

$$G(s) = k_\theta \, (\tau s + 1) \frac{\theta(s)}{\delta_{lon}(s)}, \quad \tau = \frac{k_q}{k_\theta}$$

The influences of the pitch rate gain (k_q) and the pitch attitude gain (k_θ) were determined using a root locus, which is presented in Figure F.10. The ratio (τ) of the pitch rate gain to

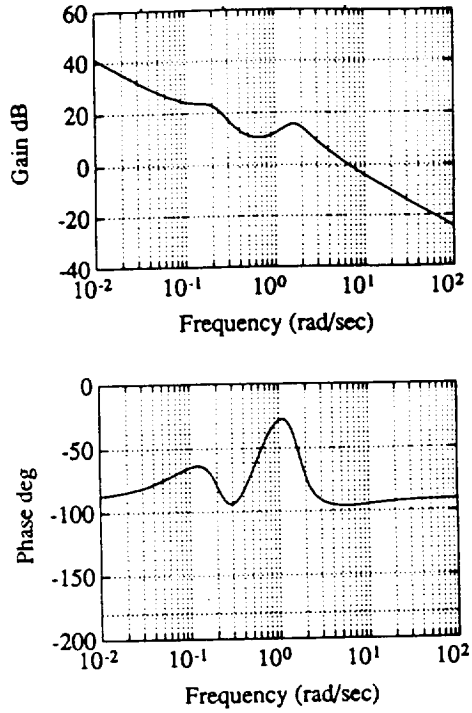

Figure F.7 Frequency Response of Yaw Loop Transmission ($k_r = 0.2$, $k_i = 0.2$)

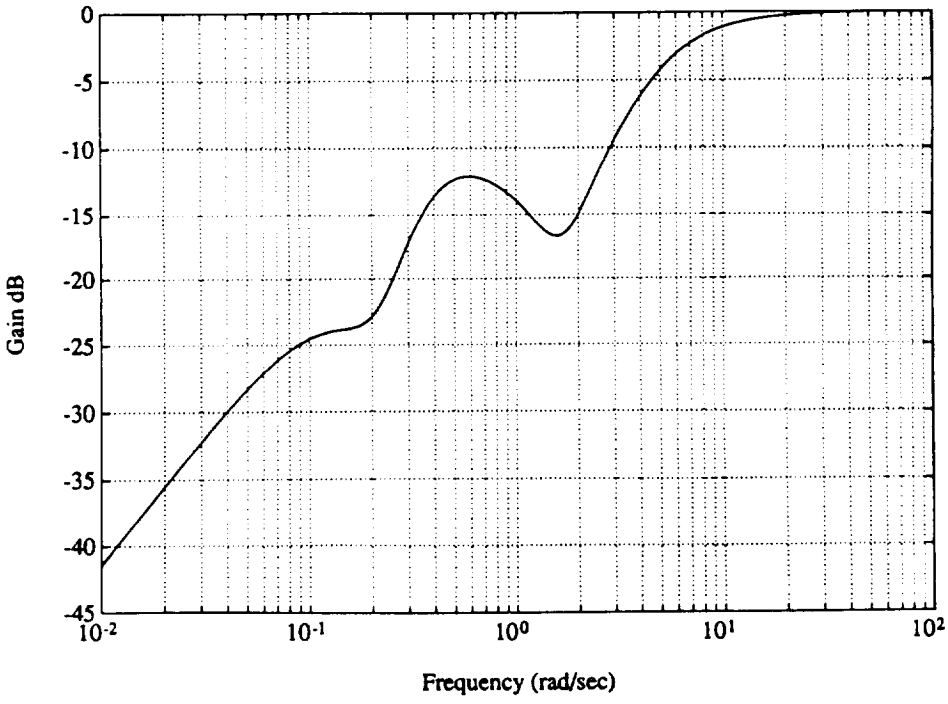

Figure F.8 Sensitivity of the Integral of Yaw Rate With the Roll and Yaw Loops Closed

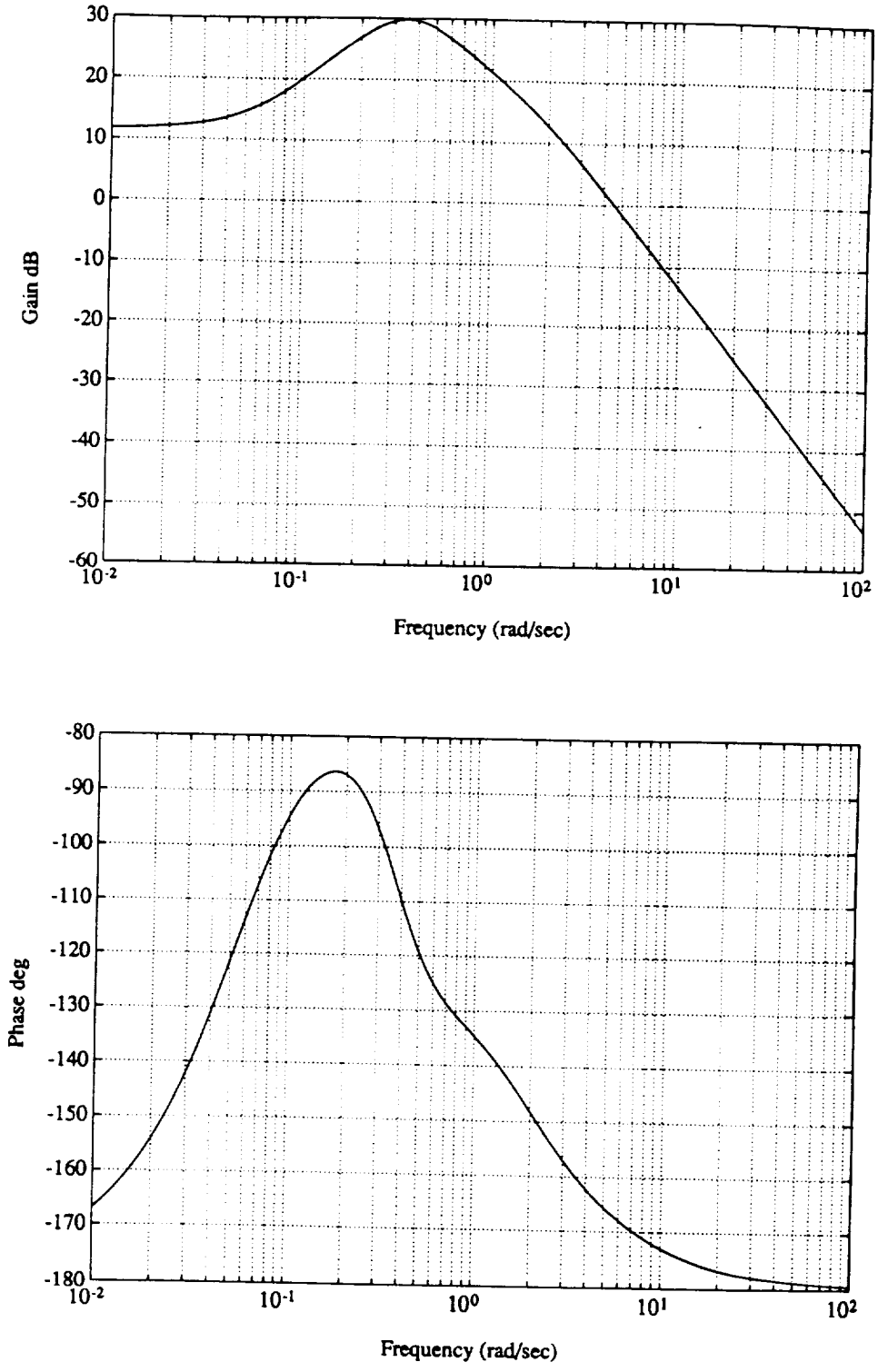

Figure F.9 Frequency Response of the Transfer Function Between Pitch Attitude and Longitudinal Cyclic

the pitch attitude gain was fixed at different values and then the corresponding loci were plotted. Figure F.10 shows the loci for gain ratios of zero and 0.333. The figure shows that the attitude feedback stabilizes the unstable pole as desired. The addition of the rate feedback increases the bandwidth of the mid frequency complex pair and increases the damping of the low frequency complex pair. The root loci also show that the roll complex pair is not affected by the pitch feedback. Figure F.11 presents the frequency response of the corresponding loop transmission and shows that, at low frequency, there is approximately seven dB of gain margin when the phase is -180 degrees. Figure F.12 presents a Nyquist plot of the pitch loop transmission including the compensation. Since there is one unstable pole in the open loop transfer function, the Nyquist stability criterion requires that for the closed loop transfer function to be stable, the plot of the pitch loop transmission must encircle the -1.0 point once in a counter-clockwise direction. The Nyquist plot presented in Figure F.12 confirms that with the pitch attitude and pitch rate feedback the -1.0 point is encircled once in a counter-clockwise direction indicating that the closed loop transfer function will be stable. The Nyquist plot also indicates that the closed loop system will have a gain margin of 7.2 dB at low frequency and a phase margin of 73.2 degrees at a frequency of 4.9 radians per second.

The entire feedback control law that stabilizes the aircraft's divergent longitudinal mode and also suppresses the lateral-directional response to longitudinal inputs is given by the following equations:

$$\delta_{lat} = -\ (0.0667\ \text{in/deg/sec})\ p\ -\ (0.4\ \text{in/deg})\ \phi$$

$$\delta_{ped} = -\ (0.2\ \text{in/deg/sec})\ r\ -\ (0.2\ \text{in/deg})\ \int r$$

$$\delta_{lon} = -\ (0.2\ \text{in/deg/sec})\ q\ -\ (0.6\ \text{in/deg})\ \theta$$

The eigenvalues of the closed loop system are presented in Table F.1. Note that there are nine eigenvalues instead of eight since the integral of the yaw rate was added to the model which increased the order of the system by one.

To evaluate the sensitivity reduction properties of the lateral-directional feedback, the roll attitude sensitivity function and the integral of yaw rate sensitivity function were computed and compared with the sensitivity functions determined during the design process. The sensitivity function is a transfer function between the variable of interest and an input (δ_i) which is injected at the output of the aircraft. The corresponding sensitivity

function (S(s)) is given by the expression:

$$S(s) = C(sI-(F-GK_{fb})^{-1})GK_{fb}C^T + I$$

C=[0 0 0 0 0 0 1 0 0] for roll attitude sensitivity

C=[0 0 0 0 0 0 0 0 1] for integral of yaw rate sensitivity

Figure F.13 presents the roll attitude sensitivity comparison which shows that the sensitivity of the roll response is degraded by closing the yaw and pitch loops after closing the roll loops. At low frequencies, the roll sensitivity is particularly degraded when compared to the sensitivity computed when only the roll loops were closed. However, the roll feedback still has a beneficial effect on the sensitivity by reducing it at frequencies below four radians per second. Figure F.14 presents the integral of yaw rate sensitivity comparison which shows that the yaw sensitivity is degraded by closing the pitch loop after closing the yaw loop. This figure shows that the sensitivity function is degraded by a fairly constant amount at low frequencies. This comparison also shows that, though the sensitivity is degraded by closing the proceeding loops, the yaw feedback still has a beneficial effect on the sensitivity at frequencies below two radians per second.

Table F.1 Eigenvalues of the Nine State Model of the Augmented Aircraft Trimmed at Eighty Knots with the Stabilator Ten Degrees Trailing Edge Down

Eigenvalues	Mode Characteristics
- 0.0294	Lateral Velocity
- 0.0743	Forward Velocity and Lateral Velocity
- 0.6091	Flight Path Angle and Lateral Velocity
- 1.3650	Yawing and Lateral Velocity
- 2.8083 ± 2.2768	Pitching
- 5.0679	Rolling and Yawing
- 3.6117 ± 3.8213	Rolling

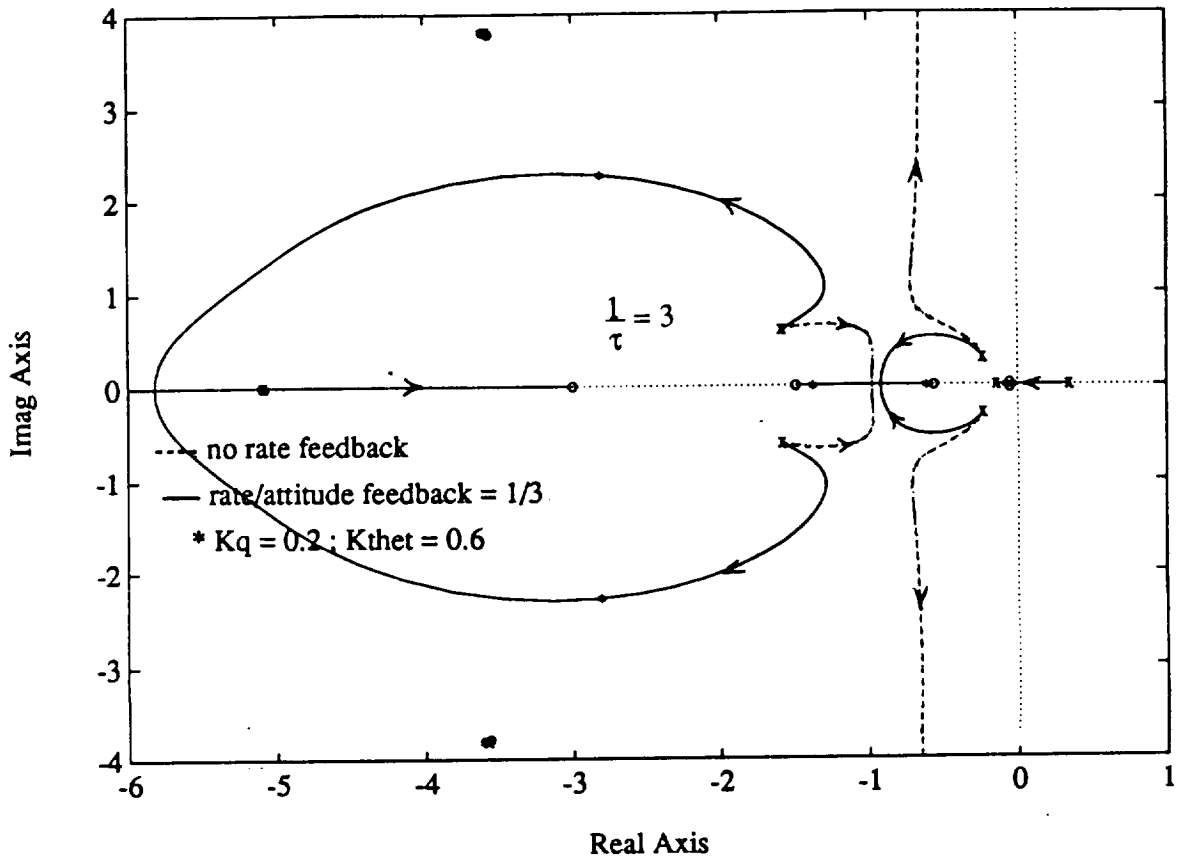

Figure F.10 Pitch Feedback Root Loci

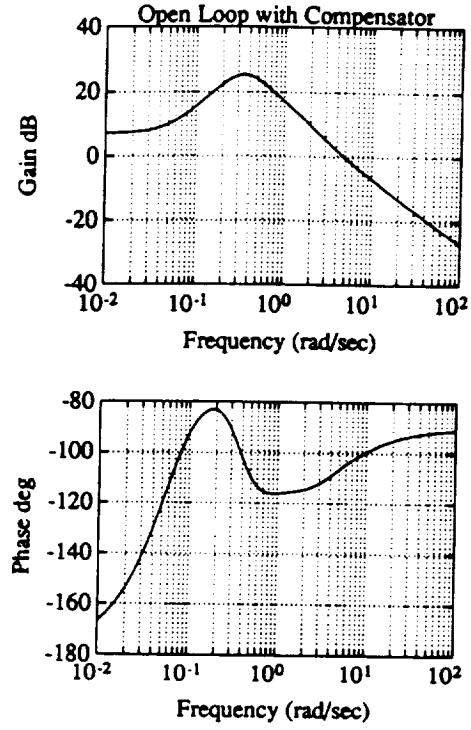

Figure F.11 Frequency Response of Pitch Loop Transmission ($k_q = 0.2$, $k_\theta = 0.6$)

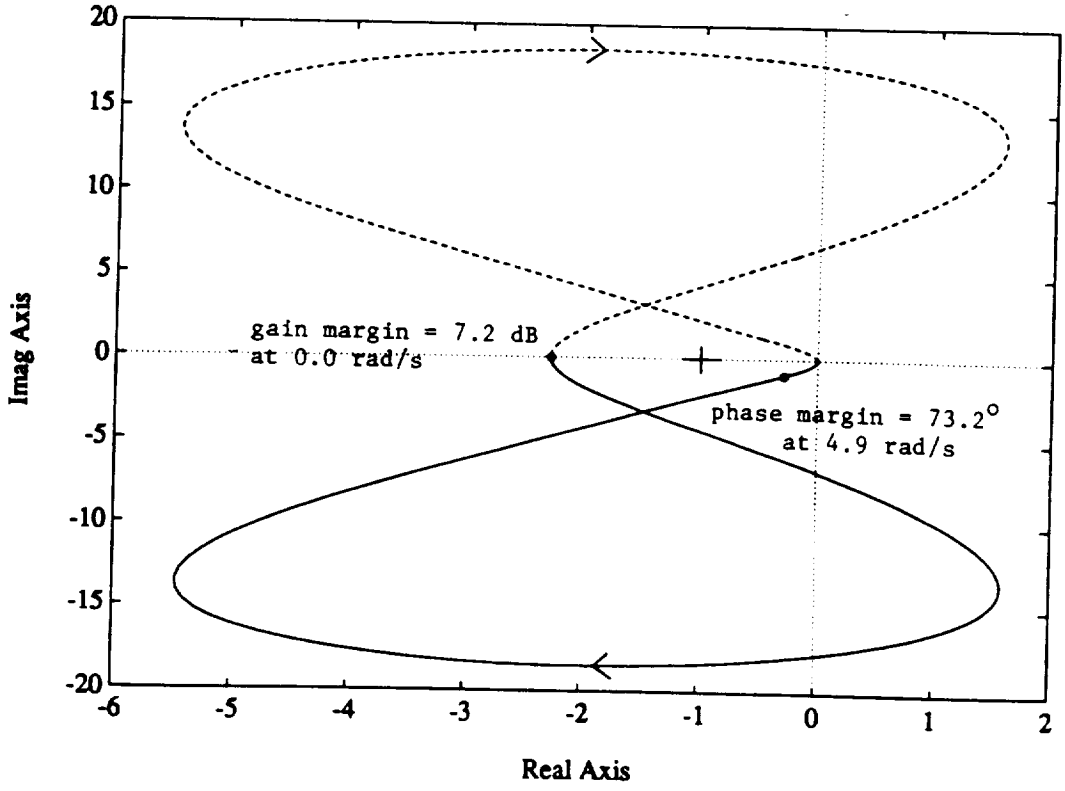

Figure F.12 Nyquist Plot of Pitch Loop Transmission ($k_q = 0.2$, $k_\theta = 0.6$)

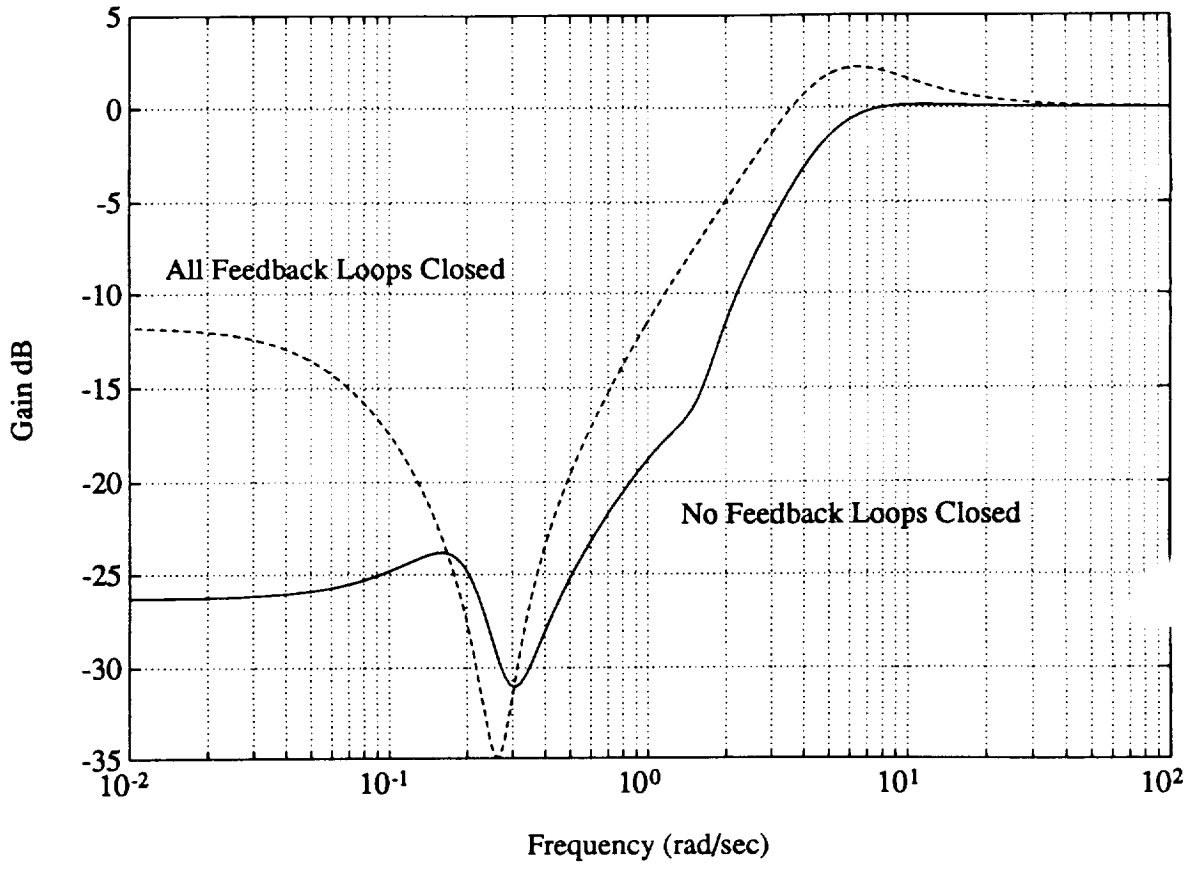

Figure F.13 Roll Sensitivities Before and After Closing Proceeding Feedback Loops

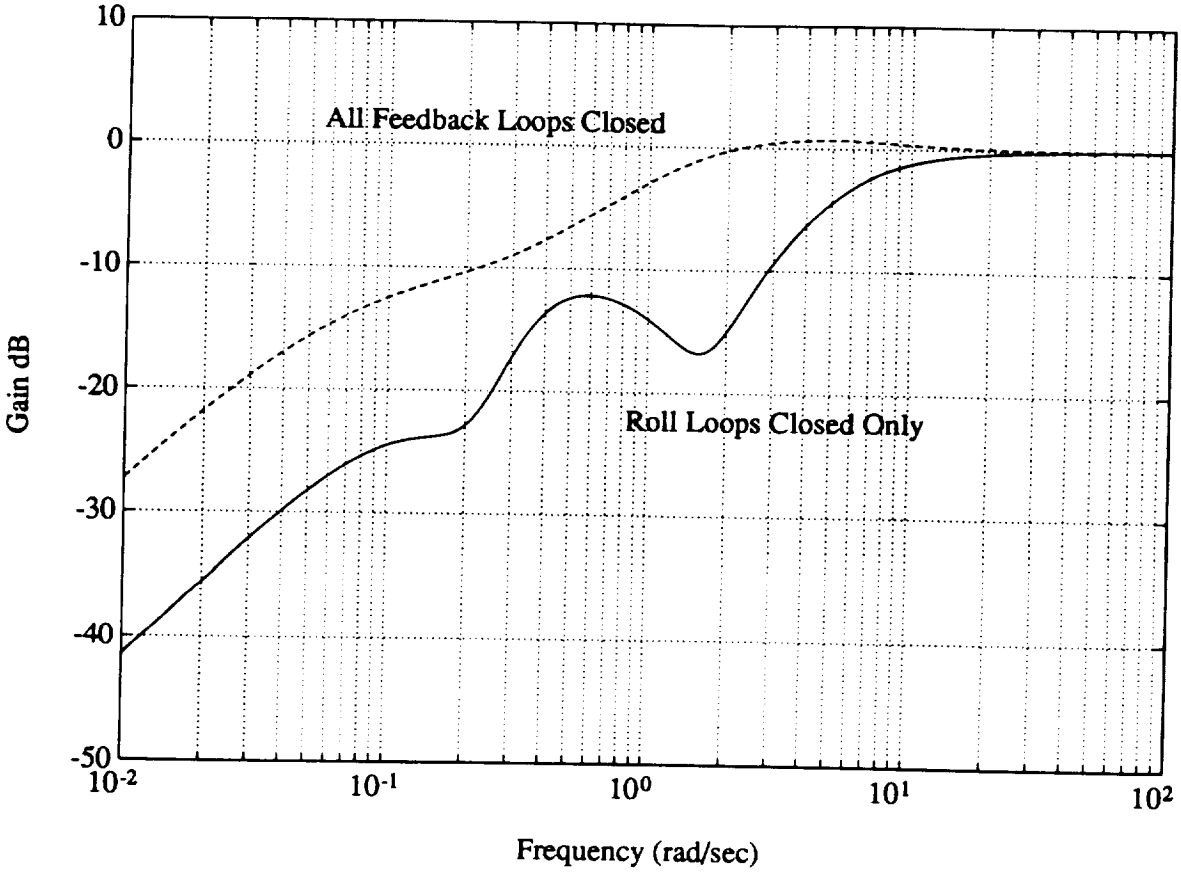

Figure F.14 Integral of Yaw Rate Sensitivities Before and After Closing Proceeding Feedback Loops

Appendix G Model of Desired Longitudinal Dynamics

The four state linear model of the desired dynamics is of the form:

$$\dot{x}_{m1} = F_{m11}\, x_{m1} + G_{m1}\, \delta_c$$

where the order of the longitudinal states (x_{m1}) and command inputs (δ_c) and the corresponding units are presented in Tables G.1 and G.2. The F_{m11} and G_{m1} matrices are presented following the states and controls.

Table G.1 Order and Corresponding Units of the States of the Four State Linear Model of the Desired Dynamics

Symbol	State	Units
u_m	Desired Forward Velocity	Feet per Second
γ_m	Desired Flight Path Angle	Degrees
q_m	Desired Pitch Rate	Degrees per Second
θ_m	Desired Pitch Attitude	Degrees

Table G.2 Order and Corresponding Units of the Inputs of the Four State Linear Model of the Desired Dynamics

Symbol	Control	Units
u_c	Commanded Forward Velocity	Feet per Second
γ_c	Commanded Flight Path Angle	Degrees
θ_c	Commanded Pitch Attitude	Degrees

```
Fm11 =

   -0.5000         0         0         0
         0   -5.0000         0         0
         0         0   -7.0000  -25.0000
         0         0    1.0000         0


Gm1 =

    0.5000         0         0
         0    5.0000         0
         0         0   25.0000
         0         0         0
```